Computational Study of Poppet Valves on Flow Fields

By

Prashant Mane

Submitted in Partial Fulfillment of the Requirements

For the Degree of

Master of Science in Engineering

in the

Mechanical Engineering
Program

YOUNGSTOWN STATE UNIVERSITY

Dec, 2013

COMPUTATIONAL STUDY OF POPPET VALVES ON FLOW FIELDS

Prashant V. Mane

I hereby release this thesis to the public. I understand that this thesis will be made available from the OhioLINK ETD Center and the Maag Library Circulation Desk for public access. I also authorize the University or other individuals to make copies of this thesis as needed for scholarly research.

Signature:

Prashant Mane, Student	Date

Approvals:

Dr. Ganesh Kudav, Thesis Advisor	Date

Mr. Param Adhikari, Thesis Co-Advisor	Date

Dr. Suresh Sharma, Committee Member	Date

Dr. Salvatore A. Sanders, Associate Dean of Graduate Studies	Date

ABSTRACT

Valves are critical components in a fluid flow network. Based on the type of fluid used, valves may suffer unforeseen wear and tear that might lead to an inadvertent failure. Major work in this thesis is focused on high pressure water valves that are used for descaling purposes. Controlling fluid flow at high pressures is not only challenging but also becomes time-wise critical. Failure of one such high pressure un-loader valves was studied first for the feasibility of my thesis work. A reverse flow operation was set in one such valve due to piping constraints established by industrial requirements. Experience and data recording showed that the premature failures of such valves by BOC Water Hydraulics were seen in months which lasted for years in standard operation. Computer simulation was being utilized to understand the fluid phenomena at such high pressures. The highly energized fluid from the descaling pump sets off a static pressure of 4300 psi at the valve inlet. It is responsible for continuous fluid flow rate of up to 208 gpm when the valve becomes fully open. Computational Fluid Dynamics (CFD) approaches are widely being utilized for fluid research in design optimizations. A *Standard Turbulence* model was used to understand the fluid flow variables using velocity/pressure contours for several possible valve opening positions. A very low pressure developed below the poppet seat of the valve suggests the onset of cavitation zones which may lead to leakage. Leakage at such a descaling pressure further accounts for cavitation and may which ultimately affect valve's overall performance resulting in cartridge replacement. Using CFD, the poppet valve assembly was modeled and simulated using ANSYS Fluent, commercially available CFD software. Low pressure below the atmospheric gage pressure in the valve body is found to be responsible for the initial onset of cavitation.

ACKNOWLEDGEMENTS

I would sincerely like to thank my original thesis advisor, Dr. Yogendra M. Panta who gave me the current thesis topic and completely laid out the research work for me. He is always very supportive of me and guided me throughout all thesis work and reviewed generously even after Dr. Ganesh Kudav became my formal advisor. I have learned much from him such as hard work, dedication, and enjoying what I am doing. It was my pleasure working under his supervision and gaining a lot of knowledge in the field of fluid dynamics. In addition, I would like to thank Dr. Ganesh Kudav who accepted to be my new thesis advisor. He helped me immensely in this very short period of time. Param Adhikari, serving as my thesis co-advisor, helped me in simulation and regular research discussions. I would also like to thank Dr. Suresh Sharma for being another thesis committee member. Moreover, I would like to thank my friends at YSU, Ravi, Munindra, as well as Dawn, for their valuable assistance while pursuing my studies. I would like to thank and pray for my late friend Amit Uniyal for his spiritual guidance to pursue higher studies. My special thanks to my friend, Lori Hogan, for her thorough moral support and positive energy during my graduate studies. Heartiest thanks to Bhupesh Brahmbhatt and his family for their love and support. Also I would like to acknowledge the support of Mr. Don Burks for his valuable guidance and thoughts in writing this thesis. I would like to thank Mr. Jonathan Szallai and Ms. Angela Messenger from writing center for proof reading thesis.

DEDICATION

I would like dedicate this thesis to my family and Indian friends for their encouragement and for their love and affection.

This thesis is especially dedicated to my grandmother, Mrs. Sushila Mane, father, Mr. Vijayrao Mane, uncle, Mr. Virendra Mane, aunt, Mrs. Geeta Mane, and brother, Vinayak Mane, for their sacrifice and their tremendous support when I needed them most. I would like to thank my cousin Priyank Pethe for his support. I would not be the person I am today if it was not for them pushing me to realize my full potential and supporting me in every step of my life.

Furthermore, multitudes of prayers and thanks to my late mother and grandfather for bestowing blessing over me. Thank you all for your immense love and ever-present inspiration on this journey.

TABLE OF CONTENTS

LIST OF FIGURES

LIST OF TABLES

Nomenclature

dF_{Bi}	Differential body force component
f	Face of a meshed cell
σ_{ii}	Normal viscous stress terms
$\dfrac{\partial \rho}{\partial t}$	Rate of change of density within the control volume
u, v, w	x-, y-, and z-components of the velocity, respectively
μ	Dynamic viscosity of the fluid
υ	Kinematic viscosity of the fluid
∇	Vector operator in Cartesian coordinates
ρ	Density of the fluid
$\nabla_{\Phi f}$	Gradient of Φ at face f
Γ_{Φ}	Diffusion coefficient for Φ
$\nabla_{\Phi f}$	gradient of Φ at faces f
Φ_f	value of Φ convected through the faces $, f$
τ_{ij}	Shear viscous stress terms
ΔP	Pressure Drop
$\vec{A}$	Surface area vector
A_f	area of faces, f
CAD	Computer-aided design
CFD	Computational Fluid Dynamics
D	Diameter of the pipe
DM	Design Modeler

ε	Turbulence dissipation rate
f	Friction factor
g	acceleration of gravity
G_b	Generation of turbulent kinetic energy due to buoyancy (b)
G_k	Generation of turbulent Kinetic energy (k) due to the mean velocity Gradient
g_x	gravitational force in x direction
g_y	gravitational force in y direction
g_z	gravitational force in z direction
h_L	Head loss
h_{Lmj}	Major head losses
h_{Lmn}	Minor head losses
k	Turbulence Kinetic energy
K_c	Cavitation Index
L_e	equivalent length of the pipe
N_{faces}	number of faces enclosing cell
P_∞	main flow pressure
P_1	Inlet pressure of the fluid
P_2	Outlet pressure of the fluid
P_v	Vapor pressure of the fluid
S_Φ	Source of Φ per unit volume
S_ε	User defined source term for ε
S_K	User defined source term for K
STD	Standard Turbulence Model
V	cell volume

$\vec{v}$	Velocity vector of fluid
V_∞	main flow velocity
V_1	Inlet velocity of the fluid
V_2	Outlet velocity of the fluid
VOF	volume-of-fluid technique
Y_M	Contribution of the fluctuating dilatation in compressible turbulence to the overall dissipation rate.
YSU	Youngstown State University
σ	Cavitation Index

Chapter 1

Introduction

Valves are mechanical devices that are specially designed to direct, start, stop, mix, or regulate the flow, pressure, or temperature of a process fluid. Valves can be designed to handle either liquid or gas applications. Mainly valves are used in industry for any process application where the most important thing is to provide a precise amount of flow into a system. Today's spectrum of available valves extends from simple water faucets to control valves equipped with microprocessors, which provide single loop control for the process. The most common types in use today are gate, plug, ball, butterfly, check, pressure-relief, and globe valves. Valves can be manufactured from several types of materials, including steel, iron, plastic, brass, bronze, or from a number of special alloys.

In ancient times before the development of simple irrigation systems, crop cultivation was always dependent on the mercy of the weather. The primary idea of the valve arose when farmers realized that fallen trees and debris could actually be a hindrance to the flow of water to their crops. In attempts to regulate the course of water, the concept of using an artificial barrier to divert the water to a nearby field was applied. An important element of this irrigation system was a removable wooden or stone barrier, which could be placed at the entrance of each irrigation channel. This is how the gate valve evolved; this apparatus could be a wedged between the walls of a canal to stop the flow or divert the flow to other channels, or when placed in a position between shut and fully open could regulate the amount of water entering the channel downstream (Skousen, 2007).

As early as 5000 BC, crude gate valves were found in a series of dikes designed as part of ancient irrigation system developed by the Egyptians along the banks of the Nile River.

Archaeologists have found that other ancient cultures in Babylon, China, Phoenicia, Mexico, and Peru also used similar irrigation systems. Valve design changed very little until the Renaissance period when modern hydraulics engineering principles began to evolve. In attempt to improve the performance of canal locks, Leonardo da Vinci analyzed the stresses that would occur at different lock gates with varying heights of water on the either side of the gate. These early studies of the concept of pressure drop helped determine the basis for modern fluid dynamics, which is essential for understanding a calculation of the performance of the valve (Skousen, 2007).

In 1717, Englishman Thomas Newcomen invented an atmospheric engine which used low pressure steam to drive a piston. As Newcomen improved his machine, he introduced a simple iron plug valve which was used to regulate the flow of steam to piston- the first known application of the throttling valve. Watt's upgraded Newcomen's steam engine by making it double acting engine. Watt's engine introduced steam to both sides of the piston, driving both the upstroke and down stroke simultaneously. Critical to Watt's steam engine were self-acting valves, which were used to introduce and vent steam from both sides of the piston. These valves were vastly fundamental in the success of steam engines, which ushered in the industrial age. Furthermore, Corliss's steam engine was designed with sophisticated self –acting control valves, which were similar in design and standard of the modern age.

The discovery of crude oil as a plentiful and inexpensive source for power in the early nineteenth century urged the creation of refineries. With flourishing refineries, all other process industries soon followed and thus the development of chemical, petrochemical, pulp and paper, food and beverage processing plants created the need for hundreds of

sophisticated valves in those various industries. Electricity as a source of power lead to the creation of coal fired, hydroelectric, and nuclear power plants, which involved the use of valves in not only simple water and steam applications, but also severe applications that involved high pressure drops and subsequent cavitation, flashing, and choking (Skousen, 2007).

1.1 The classification of the valve
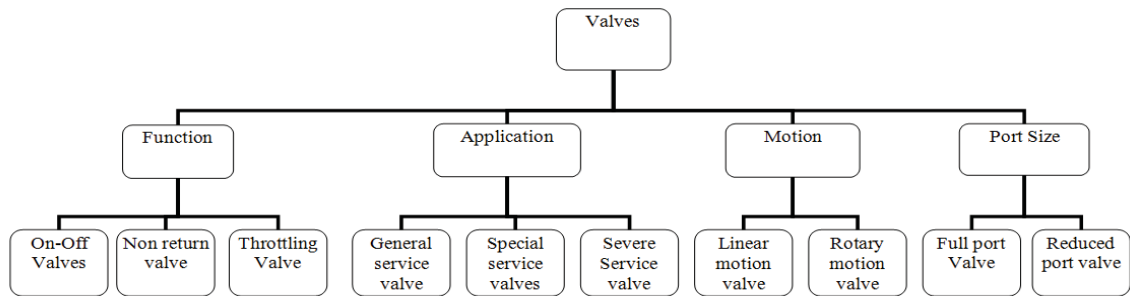
Figure 1.1 Classifications of Valves

A) According to the function- Design and function in handling process fluids valves can be categorized in to three areas.

On-off valves handle the fluid and allow or block the flow of fluids. Non return valves allow the flow in one direction only. Similarly, Throttling valves allow regulation of the flow at any point between fully open or fully closed.

ON /OFF VALVES

On/ off valves are also referred to as block valves; these are used to start and stop the flow of the liquid in the process as required. Common types of on/ off valves are the gate,

plug, ball, pressure relief, and tank bottom valves. Most of the on /off valves are hand operated but can be automated with the addition of the actuator to it.

Major application of on/off valves

1. To divert the flow around an area where preventive maintenance is to be performed so as to prevent and protect from possible safety hazards.

2. Helpful in mixing applications where a number of fluids are combined for a predetermined amount of time and when exact measurements are not required.

3. Pressure relief valves are self-actuated on/off valves that open when preset temperature is achieved. Such valves are further divided in two subdivisions: relief valves and safety valves.

Relief valves are used to guard against the over pressurization of a system, whereas safety valves are used for gas applications in which over pressurization of a system is presenting a threat to safety or process hazards and must be vented**.**

Non return valves allow the flow of the fluids in one desired direction and are designed in such a way that flow or pressure is restricted mechanically from occurring. All check valves are non-return valves and are basically used to prevent backflow which could potentially damage equipment. They are used to protect the pump in liquid operations or the compressor in gas applications from backflow when the pump or compressor is shutdown. They are likewise used in the process system with varying pressure, which must be kept separate.

Throttling valves are used to regulate the flow, temperature or pressure of the system. These valves can be moved to any desired position within the range of stroke of the valve and hold the position, including the fully open or fully closed position. Although many throttling valve designs are provided with a hand-operated wheel or lever, some are equipped with actuators which provide greater thrust and position capability as well as automatic controls. A pressure regulator is a throttling valve that can vary the valve position to maintain constant pressure downstream. If the pressure builds downstream, the regulator closes slightly to decrease said pressure. If the pressure decreases downstream, the regulator opens to build the required pressure.

B) Classification according to the Application-

General service valves are versatile valve designs that can be used for numerous applications without modifications. Special service valves are designed especially for specific applications. Severe service valves are controllers which are highly engineered to avoid the side effects of difficult applications.

General service valves are designed for commonplace applications that have lower pressure ratings that lie between the American National Standards Institute Class 150 and 600, with a moderate temperature rating of -50 to 65 degrees Fahrenheit, that include noncorrosive fluids and common pressure drops that do not result in cavitation or flashing. These valves have some degree of interchangeability and flexibility built in to the design to allow use in a wider range of applications. Their bodies are made of carbon or stainless steel.

Special service valves are custom-engineered, designed for single application, that are outside normal process applications. Due to unique design and engineering, these devices will only operate at certain functional parameters and service conditions for a particular application. They can resist demanding temperature, high pressure, or a corrosive medium.

Severe service valves are specially equipped with special features to handle volatile applications, such as high pressure drops that result in severe cavitation, flashing, choking, or high noise levels. Such valves may be transformed by engineering modification so as to reduce the effects of the applications.

C) Classification according to the motion

Linear motion valves are built with a sliding stem design that pushes the closure element into an open or closed position. The closure element is used to describe any internal device that is used to open, close, or regulate the flow. Gate, globe, pinch, diaphragm, split-body, three ways, and angle valves all fit into these classifications. Linear valves are known for their simple design, easy maintenance, and versatility with more size, wide range of pressure, and more design options than other motion classifications.

Rotary motion valves use a closure element that rotates through a quarter-turn or 45 degree range to open or block the flow. Rotary valves are usually smaller in size and weigh less than comparable linear valves in size-for-size applications; they are limited to certain pressure drops and very prone to cavitation and flashing problems. The design of the rotary valves has become more sophisticated and now they are widely used in many severe service applications.

D) Classification according to port size

Full port valves are used in process applications; most valves are designed to restrict the flow to some extent by allowing the flow area of the closure element to be smaller than that of the inner diameter of the pipeline. On the other hand, some gate and ball valves can be designed so that internal flow passage ways are large enough to pass flow without a significant restriction. Such valves are called full-port valves, because the internal flow is equal to the full area of the inlet port. Full port valves are used primarily with on/off blocking devices, where the flow must be stopped or diverted. Full port valves additionally allow for the utilization of the "pig" in the pipeline. The "pig" is a self-driving mechanism designed to scour the inside of the pipeline and to remove any process build up or scale.

Reduced port valves are ones in which the closure elements restrict the flow. The flow area of that port of the closure element is less than the area of the inside diameter of the pipeline. For example, the seat in the linear globe valve or a sleeve passageway in plug valves would have the same flow area as the inside of the inlet and outlet port of the valve body. This restriction allows the valve to take a pressure drop as the flow moves through the closure element, allowing for partial pressure recovery after the flow moves past the restriction. The primary purpose of the reduced-port valve is to control the flow through reduced flow or via throttling, which is defined as regulating the closure element to provide varying levels of flow at a certain opening of the valve (Skousen, 2007).
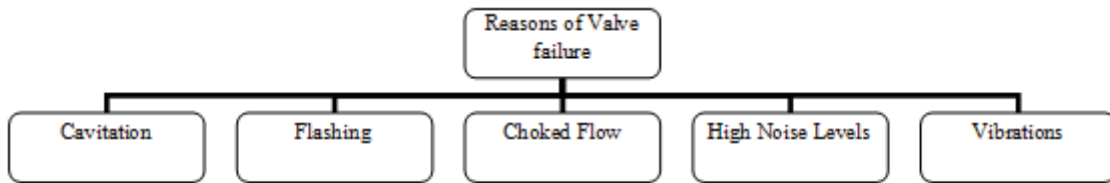
1.2 CAVITATION

Figure 1.2 Reasons for Failure of Valves

There are a few basic reasons for valve failure (Figure 1.2), but our main focus will be on cavitation effects.

Flow moves through the valve due to a pressure difference between the upstream and downstream pressures, which is called the pressure drop (ΔP). A high pressure drop through a valve creates a number of problems, such as cavitation, flashing, choked flow, high noise levels and vibration. Such problems can provide immediate consequences like erosion or cavitation damage to the body and trim, malfunction or poor performance of the valve itself, wandering calibration of the attached instrumentation, piping fatigue, or hearing damage to nearby workers. Valves in high pressure drop applications require extensive trims, more frequent maintenance, large spare part inventories, and piping supports. Such measures drive up the engineering and the maintenance costs.

Cavitation is a phenomenon that occurs only in liquid services. It was first discovered as a problem in the early 1900s, when naval engineers noticed that high speed boat propellers generated vapor bubbles. These bubbles lessened the speed of the ship, as well as caused physical damage to the propeller of the ship.

Whenever the ambient pressure drops below the vapor pressure of liquid, vapor bubbles are created. In fluid process applications, when fluid accelerates to pass through the narrow restrictions at the Vena Contracta, the pressure may drop below the vapor pressure of the fluid. This causes vapor bubbles' formation. As the flow continues to pass the Vena Contracta, the velocity decreases as the flow area expands and pressure builds up again. The resulting pressure recovery increases the pressure of the fluid above the vapor pressure. As the vapor bubble is formed in the Vena Contracta, it travels downstream until the pressure recovery causes the bubble to implode. This two-step process of the bubble formation in the Vena Contracta, and its subsequent implosion downstream, is called cavitation. Cavitation is a phase that is characterized by a liquid-vapor-liquid process, all contained within a small area of the valve within microseconds. Although minor cavitation damage can be considered normal for some applications because it can be dealt with routine maintenance, major cavitation would cause replacement of process equipment.
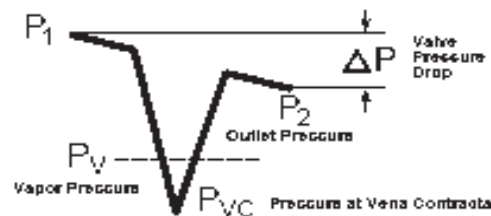

Figure 1.3 Flow curve showing pressure drop falling below the vapor pressure (Skousen, 2007).

Conditions that present cavitation effects (Skousen, 1997) are as follows:

1)   The fluid must remain a liquid both upstream and downstream from the valve.

2)   The liquid must not be at a saturated state when it enters the valve or the pressure drop will create residual vapor downstream from the valve.

3)   The pressure drop at the Vena Contracta must drop below the vapor pressure of the process fluid.

4)   The outlet pressure must recover at a level above the vapor pressure of the liquid.

5)   The liquid must contain some entrained gases or impurities, which acts as a "host" for the formation of the vapor bubble. This host is sometimes called the nuclei. The nuclei are contained in the process fluid as either microscopic particulates or dissolved gases; the chances of forming vapor bubbles are very likely.

The creation and implosion of the cavitation bubble involves five stages-

1)   The liquid's pressure drops below the vapor pressure as velocity increases through the valve's restriction.

2)   The liquid expands into vapor around the nuclei host, which may be any entrained gas.

3)   The bubble grows until the flow moves away from the Vena Contracta, and the increasing pressure recovery inhibits the growth of the bubble.

4)   As the flow moves away from the Vena Contracta, the area expands – slowing velocity and increasing pressure. The pressure increase collapses or implodes the bubble vapor back to a liquid.

5)   If the bubble is near the valve's surface, the force of implosion is directed toward the surface wall, causing material failure.

The bubbles created by the cavitation are much smaller and more powerful than bubbles caused by normal boiling. These bubbles release energy that can be heard as noise in the valve or in the downstream piping. The noise generated in the early stage of cavitation is described as a cracking noise, while extensive cavitation is a steady hiss. The most permanent damage caused by cavitation is the physical damage of the interior of the valve created by the imploding bubbles. As the bubbles expand in the Vena Contracta, they move in to the down-stream portion of the valve and then implode as the pressure recovery occurs. If the bubbles are near a metal surface, such as a body wall, they have a tendency to release the energy of implosion toward the wall. This occurs when unequal pressure is exerted upon the bubble.

With cavitation, the real damage occurs in the phase of the process where the bubble implodes. This energy is released towards the metal surface and can tear away minute pieces of metal, especially if the pressure intensity reaches or passes the tensile strength of the valve material. These shockwaves have been reported to be as high as 100,000psi (6900 bar). The valve parts damaged by cavitation have a pitted appearance or feel like a sandblasted surface. The cavitation damage in appearance is far different than flashing or erosion damage as it appears smooth. The long-term cavitation effect is it may attack material's coating, film or oxide, which will open up the base material to chemical or corrosive attack. Soft materials, such as aluminum are easily prone to cavitation by the cavitation bubble and quickly tear away. Hardened materials are better able to withstand the effects of cavitation, and only after a period of time will they fatigue and begin to wear. There is no such material that has been developed that can resist cavitation indefinitely. Even the hardest of material will eventually wear away against the effect of cavitation. Another serious side effect of cavitation is decreased performance of valves

and reduced efficiency in the process system. When cavitation occurs, the valve's ability to convert entire pressure drop to mass flow rate is diminished. In other words, cavitation can cause less flow through the valve.

Cavitation can be controlled or eliminated by one of the three basic methods: first, by modifying the system; second, by making certain body parts out of hard or hardened materials; or third, by installing special devices in the valve that are designed to keep cavitation away from the valve's surface.

Industrial Parameters for Cavitation (Skousen, 2007)

1) Cavitation Index- $K_c = \Delta P /P_1-P_v$

2) Cavitation Index- $\sigma = P_2-P_v/P_1-P_2$

Where P_1 is inlet pressure, P_2 is outlet pressure, P_v is vapor pressure of liquid and K_c & σ are cavitation index.

The Cavitation indices are used to predict the possibility of cavitation in process equipment, including valves. The ability to predict cavitation is important to the design and application. The flow curve cavitation index K_C shows the effects of cavitation on the linear relationship between flow rates and the square root of pressure drop. It assumes that a valve can function without cavitation at any pressure drop less than a pressure drop calculated with index K_C.

σ is cavitation index used its ratio of forces resisting cavitation to force promoting cavitation. σ becomes larger, less cavitation occurs inside the valve. σ becomes smaller, cavitation damage increases in the valve.

Thesis Organization

The materials presented in this thesis are organized in a manner that starts with the physical model showing fluid domain in poppet valve and CFD simulations discussed in Chapter 2. Chapter 3 is a discussion of the mathematical models employed during the numerical simulation section of the thesis. This chapter on the mathematical models includes the basic governing equations for the physics of fluid flow and turbulence characteristics. These equations include Continuity, Navier-Stokes, and the k-ε turbulence model. In Chapter 4, the methodology and techniques for numerical simulation in the CFD software, ANSYS Fluent, are presented. Results from computational simulation are reported in Chapter 5, which is followed by concluding remarks and recommendations for future work in Chapter 6.

Chapter 2

Physical Modeling

In the previous chapter, we discussed various valves used in industries. In this chapter, aspects of physical modeling are presented. Industrial systems comprise of individual units that perform together in harmony to accomplish the desired production activity. Poppet valves are one of the seating valves which are of primary importance in the area of high pressure hydraulics. It offers numerous advantages over spool valves. Positive sealing is achieved within good machining tolerances. Self-cleaning, contaminant resistant, low flow resistance, and robustness make them ideal for high pressure raw water operation.

Mainly valves are designed to have only line contact. However, true line contacts are impractical and valves with contact over an annular area are more resistant to damage. Poppets are generally conical shaped, but spherical or truncated conical shapes are also used. The study of flow variable and their characteristics for self-acting port valves in reciprocating pumps is the main focus in this study. These valves are completely operated by pressure forces exerted by fluid itself. In this scenario, the relationship between the flow, pressure, and thus, induced force on these valves is critical to their operation. Particularly, when the pressure drop is low or limited, a fluid design of poppet valve geometric profiles and pressure ports can lead to delays in opening and closure, resulting in increased cavitation and noise.

In process industry, such valve processes are continuously optimized further to operate more efficiently to achieve closer to its mechanical limits. Besides the instrumental

process control measures to maintain safe plant operation, the last stage of protection of a process apparatus against excess pressure is often made possible through the use of a mechanically self-actuated device.
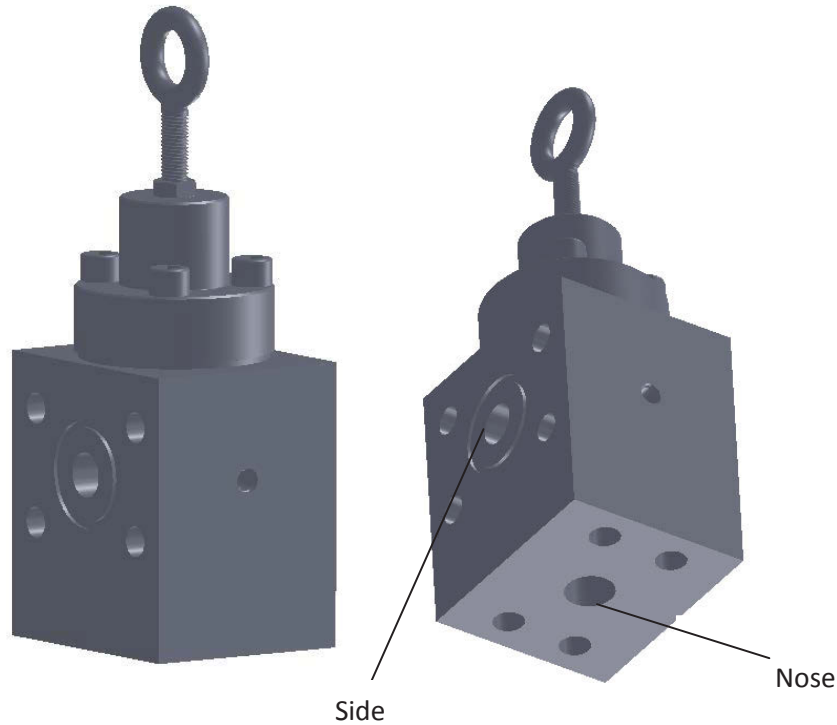

Figure 2.1 A valve housing showing Nose and Side (picture: Courtesy of BOC Water Hydraulics, Salem, Ohio)

The preliminary estimation of the fluid flow rate and the flow forces is essential to know for the design of hydraulic valves. If the design is based on experiments, test rigs and test procedures must be developed, and many prototypes have to be built and tested. The use of computers in simulations is completely inevitable to manufacture inexpensive products. The cost of possible experimentation exceeds the time and labor. The literature is full of many CFD approaches to understand the high pressure hydraulics used in valves for design optimization. CFD simulation is an alternative and useful tool, which avoids the construction and testing of many prototype valve during the initial and intermediate

phases of the design process. Most times, however, and depending on the complexity of the valve, 3D (three-dimensional) models with large amounts of cells and high computational cost are needed. Moreover, if the unsteady behavior of fluid flow in the valve is to be studied, transient CFD models with deforming meshes with varying boundary conditions are needed to set up, adding yet more computational memory, time, and cost. A unsteady or transient behavior of fluid has been studied in commercial proportional valves with a full description of all geometric features and their corresponding effects on the flow field and on overall performance. The experimental data of flow rate from the manufacturer were tallied with numerical results from the CFD. The study shows that the compensation techniques based on spool profiling effectively balances the flow force at different levels of valve openings (Amirante, Moscatelli & Catalano, 2007). The same research group developed a methodology to evaluate flow forces on an open center direction control valve (Amirante, Del Vescove, & Lippolis, 2006). Validation and comparison of experimental results were done using computer numerical simulation for contra push check valve. It was found that the k–e model agreed well with the experimental data at different positions of the valve (Han, Zheng Ming & Yu Yi, 2011). Axisymmetric modeling was done in ANSYS Fluent and particular regions of interest have been modeled using ANSYS.

Structured mesh was used to reach a mesh independent consistent solution. Analytical and experimental results were compared. A methodology has been presented for the development of a scaled down model to estimate the fluid flow and the flow forces in hydraulic valves (Jose, Mario & Thomas, 2008). Numerical and experimental validation has been done for a safety valve model working at up to 600 bar (8702 psi) using ANSYS CFX (Beune, Kuerten & Schmidt, 2011). A 2D axisymmetric modeling was done to

capture and trace the gross phenomena at operating zones for a pressure regulating spool valve that uses air (Chattopadhyay, Kundu, Saha & Gangopadhyay, 2012). Recent studies in velocity field analysis in an experimental cavitating mixing layer show that the turbulence-cavitation relationship inside a mixing layer was due to a mutual interaction between large and small scales of the flow in presence of two phase flow (Aeschlimann, Barre & Djeridi, 2011).

A local manufacturing company specialized in hydraulic flow solutions for industrial needs is being faced with failed valves while it engineered to operate in reverse flow conditions due to piping constraints of industrial architecture. A premature valve failure started to appear sooner than expected, approximately in a few months. It previously worked for years without any problems in normal flow conditions. The variation of fluid flow properties in reverse flow condition is interesting to see how it has not provided the same working efficiency.

The initial conditions that led to this premature failure of the valve from years to months are:

In Shut position (poppet closed): Flow = 0 gpm, Inlet pressure developed by pump in series prior to the valve = 4300 psi

In Open position (poppet fully open): Flow= 208 gpm, Pressure = 150 psi (Estimated)

The study has thus been very important for understanding the dynamics of fluid flow and the characteristics suited for a particular geometry.
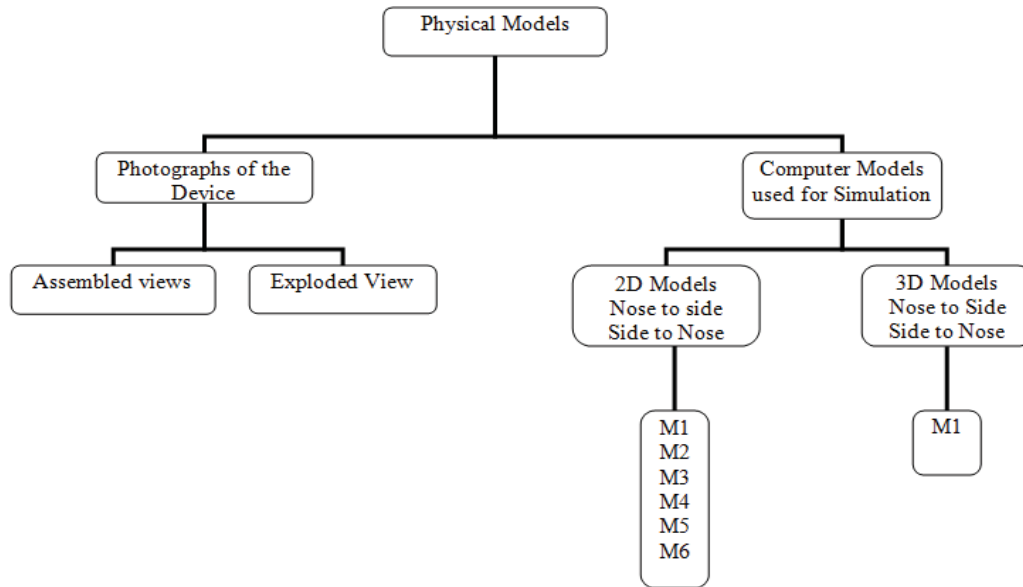

Figure 2.2 Description of Physical Models

Model No.	opening in inch
M1	1 inch
M2	0.3 inch
M3	0.2 inch
M4	0.1 inch
M5	0.0125 inch
M6	0.00625 inch

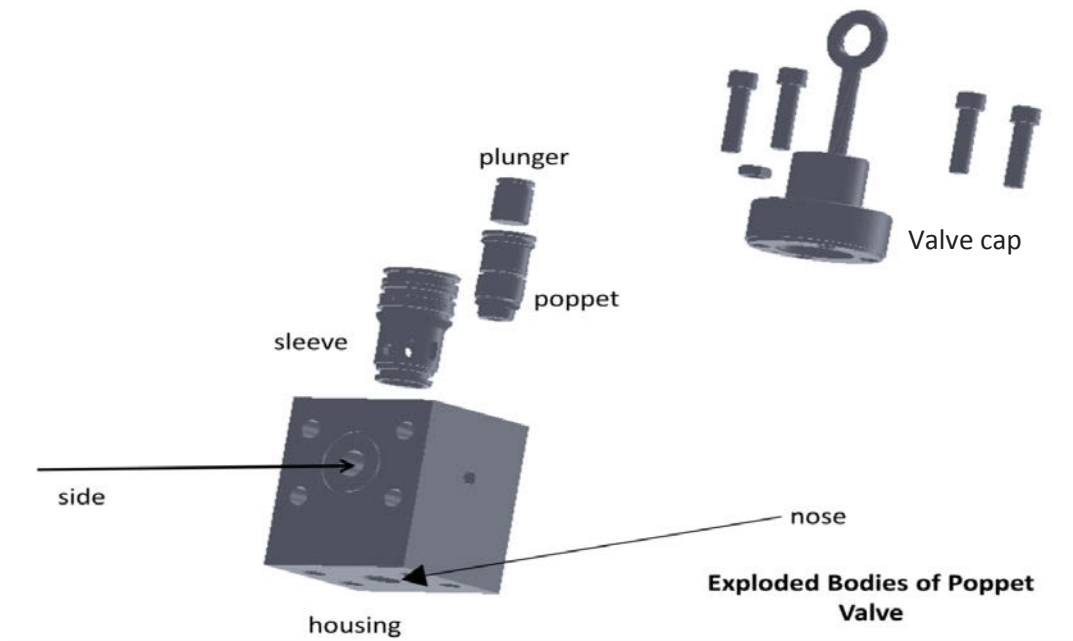Table 2.1 Model numbers and Opening size used in 2D/3D computer models

plunger

poppet

Valve cap

sleeve

side

nose

Exploded Bodies of Poppet Valve

housing

Figure 2.3 Exploded view of the valve. (Picture: Courtesy of BOC Hydraulics, Salem, Ohio)
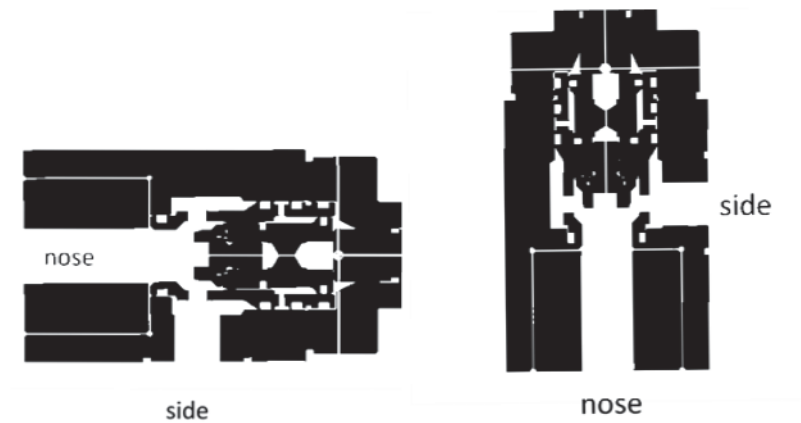
nose

side

side

nose

Figure 2.4 Sectional views at mid-section of the housing shown in Figure 2.3

The physical model of the valve housing is shown in the Figure 2.3. Here, nose and side are the main lines from which the fluid either enters or exits. The standard flow operation of the valve is usually from nose to side. The valve failed under side to nose flow operation in this particular case. The exploded view in Figure 2.3 shows the valve

components including the valve housing. As shown in the figure, a stationary sleeve is concentric to the moving poppet. The eye bolt is used to set the maximum opening position of the poppet while in operation. This will, in turn, change the flow resistance while in operation and ultimately determine whether the flow is choked or not.
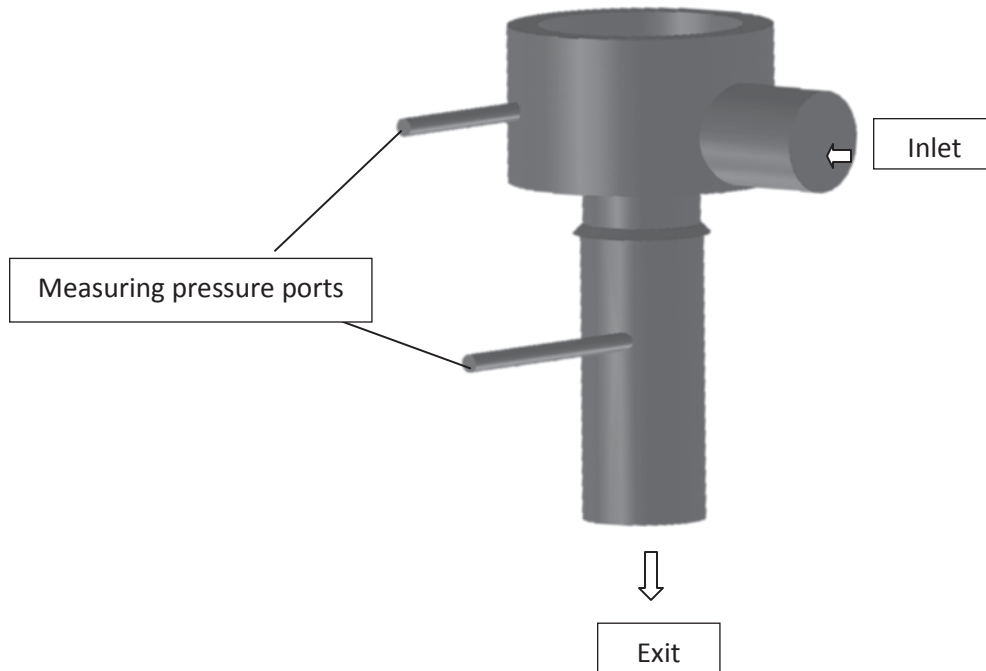
Figure 2.5 a simplified 3D fluid domain of the valve.

A full three-dimensional model as shown was simplified from Figure 2.3 [Figure2.5]. The current simplification of fluid domain is used to understand the fluid flow phenomenon for the fluid flow variables during the reverse flow operation in comparison to the standard flow condition (side to nose v/s nose to side). Based on the aforementioned literature review, only the low pressure was observed which may be one of the actual causes for the initiation of cavitation. Water, with its properties at standard room conditions of temperature and pressure, was used in fluid domain for fluid flow simulation. The enhanced wall function feature of ANSYS Fluent was applied to model

the wall conditions at no-slip boundary conditions. Convergence criteria was set at least $10E^{-3}$, usually $10E^{-6}$.

2.1 2D modeling
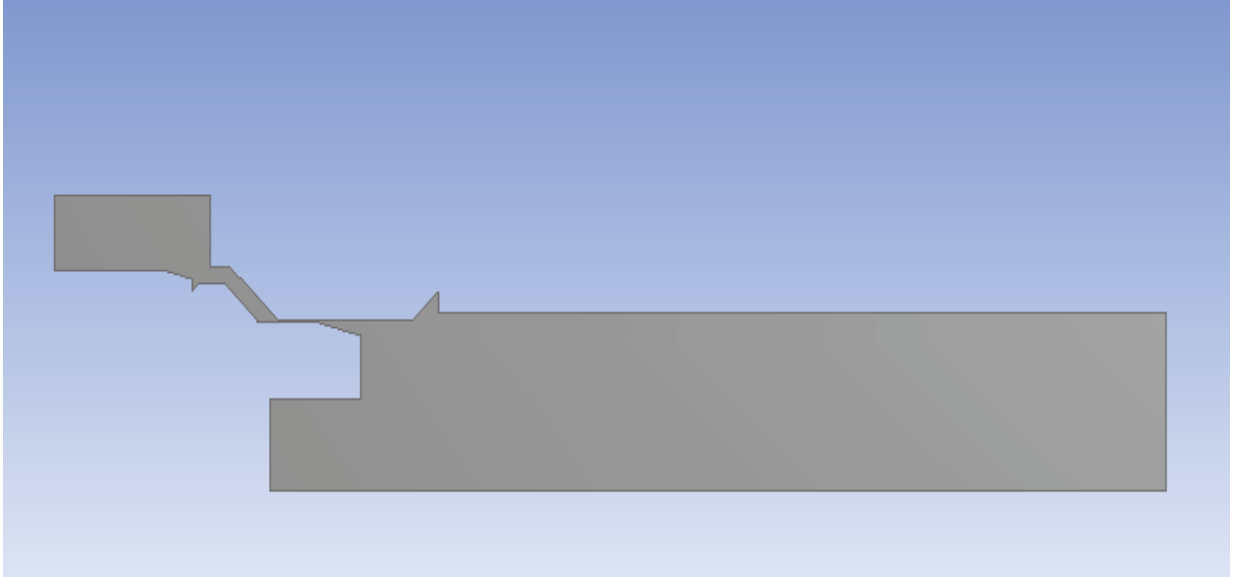
Figure 2.6 Opening of 0.1 inch in 2D -M4 [ANSYS Fluent 14]

The design of the various sides' opening (exit for standard operation) was done in ANSYS Fluent packed Design Modeler (DM), a preprocessing geometric modeling software in CFD. After the completion of the Geometry of fluid domain, the next important step is meshing, which was done using ANSYS Fluent packed Meshing Adds-on.

Details of "Mesh"	
Method	None
⊟ **Patch Conforming Options**	
Triangle Surface Mesher	Program Controlled
⊞ **Advanced**	
⊞ **Defeaturing**	
⊟ **Statistics**	
☐ Nodes	211386
☐ Elements	210292
Mesh Metric	Orthogonal Quality ▼
☐ Min	0.705075681888853
☐ Max	1
☐ Average	0.998870109093075
☐ Standard Deviation	5.97346908295593E-03

Figure 2.7 Mesh details for the fluid domain of the valve displayed by ANSYS Fluent 14.0.

 This Meshing Criteria shown in Figure 2.7 is from the simulation of the opening 0.0125 inch. The appropriate meshing scheme of uniform quad/tri and meshing operation were used. The Orthogonal quality obtained in meshing process was 0.70 (good quality mesh) and well under acceptance criteria. The next step under the meshing tool was defining the named creation for fluid domain and control surfaces such as side, nose, and axis surfaces using a further physics set up as (boundary conditions) in ANSYS Fluent.

The Physics of the Fluid flow was selected as Turbulent K- ∈ model available in ANSYS Fluent. The boundary conditions are set as Pressure inlet for the nose and set pressure was 4300 psi. The side part is pressure outlet and set pressure was 0 psi. The convergence criteria for this simulation were set as $10E^{-3}$ for continuity, X-momentum-momentum, and K-∈.
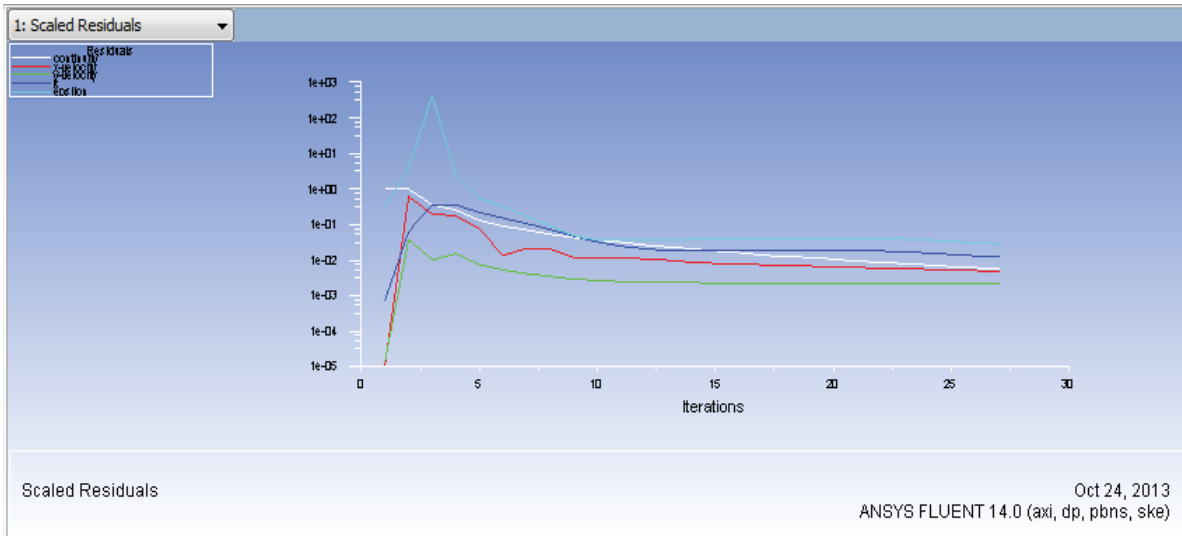
Figure 2.8 Scaled Residuals showing convergence vs. iterations for continuity, X-momentum, Y- momentum, K and Epsilon displayed by ANSYS Fluent 14.0.

Once the convergence was satisfied, the next step is to visualize flow contours, plots and animations. The contours located in graphics animation gave fluid variables such as velocity and pressure contours of the fluid flow. Vectors give the direction of the velocity vectors. The report section of the results gives various flow reports including mass flow rate report and various other needed reports of the simulation performed.

3D Modeling

The 3D modeling was done for only one model, M1, which is the full opening. The Model was generated in Solid Works and then imported in ANSYS Fluent. After that, the same procedural steps were followed as described in 2D modeling for simulating the model using ANSYS Fluent.

Here we conclude the topic of physical modeling and in the next chapter we discuss the mathematical modeling.

Chapter 3

Mathematical Modeling

In this chapter, the mathematical modeling of the valve is presented. The mathematical modeling for the fluid domain in the valve consists of sets of governing equations for the physics of the fluid flow that are used for a closed form solution and are also embedded with ANSYS Fluent to analyze and describe the physical phenomenon in a given fluid domain. The basic governing equation for the fluid domain of the valve is given as follows.

A)   Continuity equation

B)   Navier-Stokes equations

C)   Transport equations

D)   Energy equation

The content of this chapter includes the introduction and description of governing equations for the fluid domain of the valve in order to analyze the fluid flow in the domain. A mathematical model is utilized in order to model the fluid flow variables. Basic governing equations embedded in ANSYS Fluent are used to simulate the fluid flow in the fluid valve domain. A turbulent model was used in order to account for the turbulent nature of the fluid in the domain. The standard k-ε turbulence model was assumed as the most common and widely accepted model for the turbulent nature of flow simulations in CFD.

The appropriate assumptions with governing equations used for fluid flow inside the valve body are

- Turbulent flow.

- Incompressible flow.

- Steady flow.

Physics of Fluid Flow

3.1 Continuity equation

The law of conservation of mass for fluid flow states that the rate of mass leaving a control volume is equal to the rate of mass entering the control volume. In other words, mass is always conserved in a control volume. Continuity equation can be expressed mathematically (Pritchard & Leylegian, 2011).

$$\frac{\partial \rho}{\partial t} + \nabla . \rho \vec{V} = 0 \qquad (3.1)$$

Where

$$\frac{\partial \rho}{\partial t} \equiv \text{Rate of change of density within the control volume}$$

$\nabla = $ Vector operator for Cartesian-coordinates $= \hat{\imath}\frac{\partial}{\partial x} + \hat{\jmath}\frac{\partial}{\partial y} + \hat{k}\frac{\partial}{\partial z}$

$\vec{V} = $ Velocity vector of fluid $= u\,\hat{\imath} + v\hat{\jmath} + w\hat{k}$

$\vec{\nabla} = \hat{\imath}\frac{\partial}{\partial x} + \hat{\jmath}\frac{\partial}{\partial y} + \hat{k}\frac{\partial}{\partial z}$

$\nabla . \rho \vec{V} = $ net flow across boundaries of the control volume

For steady and incompressible flow, the continuity equation reduces to:

$$\nabla . \vec{V} = 0 \tag{3.2}$$

For steady and incompressible flow, 2D continuity equation can be expressed as

$$\nabla . \vec{V} = \frac{\partial u}{\partial x} + \frac{\partial v}{\partial y} = 0 \tag{3.3}$$

For steady and incompressible flow, 3D continuity equation can be expressed as

$$\nabla . \vec{V} = \frac{\partial u}{\partial x} + \frac{\partial v}{\partial y} + \frac{\partial w}{\partial z} = 0 \tag{3.4}$$

3.2 Navier-Stokes Equations

The viscous stresses and the rate of angular deformation, or in other words, the rate of shearing strain, are directly proportional to one another for a Newtonian fluid. Since water is considered to be an incompressible Newtonian fluid, it is possible to express the viscous stresses in terms of velocity gradients. (Pritchard & Leylegian, 2011)

$$\Gamma \propto \frac{\partial u}{\partial y}$$

$$\Gamma = \mu \frac{\partial u}{\partial y} \tag{3.5}$$

Where,

$$\mu = Dynamic\ or\ absolute\ viscosity\ of\ the\ fluid$$

$$\frac{\partial u}{\partial y} = Rate\ of\ shearing\ strain$$

26

It should also be noted that the kinematic viscosity, υ, can be substituted for μ, the ratio of the dynamic viscosity of the fluid by its density, ρ.

The kinematic viscosity equation is expressed as (Pritchard & Leylegian, 2011)

$$\upsilon = \frac{\mu}{\rho} \tag{3.6}$$

the reduced form, and more recognizable form of the Navier-Stokes equations, (Ansys Fluent Documentation 14)

$$\rho \frac{Du}{Dt} = \rho \left(\frac{\partial u}{\partial t} + u \frac{\partial u}{\partial x} + v \frac{\partial u}{\partial y} + w \frac{\partial u}{\partial z} \right) = \rho g_x - \frac{\partial p}{\partial x} + \mu \left(\frac{\partial^2 u}{\partial x^2} + \frac{\partial^2 u}{\partial y^2} + \frac{\partial^2 u}{\partial z^2} \right) \tag{3.7}$$

$$\rho \frac{Dv}{Dt} = \rho \left(\frac{\partial v}{\partial t} + u \frac{\partial v}{\partial x} + v \frac{\partial v}{\partial y} + w \frac{\partial v}{\partial z} \right) = \rho g_y - \frac{\partial p}{\partial y} + \mu \left(\frac{\partial^2 v}{\partial x^2} + \frac{\partial^2 v}{\partial y^2} + \frac{\partial^2 v}{\partial z^2} \right) \tag{3.8}$$

$$\rho \frac{Dw}{Dt} = \rho \left(\frac{\partial w}{\partial t} + u \frac{\partial w}{\partial x} + v \frac{\partial w}{\partial y} + w \frac{\partial w}{\partial z} \right) = \rho g_z - \frac{\partial p}{\partial z} + \mu \left(\frac{\partial^2 w}{\partial x^2} + \frac{\partial^2 w}{\partial y^2} + \frac{\partial^2 w}{\partial z^2} \right) \tag{3.9}$$

Taking into account the assumptions stated earlier, the equations can be reduced further. With either, only two-dimensional or three dimensional flow was considered. The simplified Navier-Stokes equations can be expressed for 2D and 3D analyses. For steady and incompressible flow, 2D Navier-stokes equations (g_x=0, g_y=0)

$$\rho \frac{Du}{Dt} = \rho \left(u \frac{\partial u}{\partial x} + v \frac{\partial u}{\partial y} \right) = -\frac{\partial p}{\partial x} + \mu \left(\frac{\partial^2 u}{\partial x^2} + \frac{\partial^2 u}{\partial y^2} \right) \tag{3.10}$$

$$\rho \frac{Dv}{Dt} = \rho \left(u \frac{\partial v}{\partial x} + v \frac{\partial v}{\partial y} \right) = -\frac{\partial p}{\partial y} + \mu \left(\frac{\partial^2 v}{\partial x^2} + \frac{\partial^2 v}{\partial y^2} \right) \tag{3.11}$$

$$0 = \rho g_z - \frac{\partial p}{\partial z} \tag{3.12}$$

$$p = \rho g_z \tag{3.13}$$

Similarly, steady and incompressible flow, 3D Navier-stokes equations (g_x=0, g_y=0,g_z=g)

$$\rho\frac{Du}{Dt} = \rho\left(u\frac{\partial u}{\partial x} + v\frac{\partial u}{\partial y} + w\frac{\partial u}{\partial z}\right) = -\frac{\partial p}{\partial x} + \mu\left(\frac{\partial^2 u}{\partial x^2} + \frac{\partial^2 u}{\partial y^2} + \frac{\partial^2 u}{\partial z^2}\right) \tag{3.14}$$

$$\rho\frac{Dv}{Dt} = \rho\left(u\frac{\partial v}{\partial x} + v\frac{\partial v}{\partial y} + w\frac{\partial v}{\partial z}\right) = -\frac{\partial p}{\partial y} + \mu\left(\frac{\partial^2 v}{\partial x^2} + \frac{\partial^2 v}{\partial y^2} + \frac{\partial^2 v}{\partial z^2}\right) \tag{3.15}$$

$$\rho\frac{Dw}{Dt} = \rho\left(u\frac{\partial w}{\partial x} + v\frac{\partial w}{\partial y} + w\frac{\partial w}{\partial z}\right) = \rho g - \frac{\partial p}{\partial z} + \mu\left(\frac{\partial^2 w}{\partial x^2} + \frac{\partial^2 w}{\partial y^2} + \frac{\partial^2 w}{\partial z^2}\right) \tag{3.16}$$

3.3 Transport Equations

The two equation models of turbulent flow transport in a fluid domain with turbulent energy (k) and its dissipation rate (ε) are the most simple and robust (Fluent). The transport equations allow for the turbulent velocity and length scales to be determined independently from one another. The k-ε model is the most simple and robust of the two equation models and is known to be the most widely used and accepted turbulent model to investigate fluid flows and heat transfer in varieties of fluid flow problems.

The model consists of the turbulent kinetic energy, k, and the rate of dissipation, ε for a fluid domain. The turbulent kinetic energy and dissipation rate are displayed, respectively, as shown by two equations 3.17 and 3.18. (Reference ANSYS Fluent Documentation)

$$k: \quad \frac{\partial}{\partial t}(\rho k) + \frac{\partial}{\partial x_i}(\rho k u_i) = \frac{\partial}{\partial x_j}\left[\left(\mu + \frac{\mu_t}{\sigma_k}\right)\frac{\partial k}{\partial x_j}\right] + G_k + G_b - \rho\varepsilon - Y_M + S_k \tag{3.17}$$

$$\varepsilon: \quad \frac{\partial}{\partial t}(\rho\varepsilon) + \frac{\partial}{\partial x_i}(\rho\varepsilon u_i) = \frac{\partial}{\partial x_j}\left[\left(\varepsilon\mu + \frac{\mu_t}{\sigma_\varepsilon}\right)\frac{\partial\varepsilon}{\partial x_j}\right] + C_{1\varepsilon}\frac{\varepsilon}{k}(G_k + C_{3\varepsilon}G_b) - C_{2\varepsilon}\rho\frac{\varepsilon^2}{k} + S_\varepsilon$$

$$\tag{3.18}$$

Where,

$G_k \equiv$ Generation of turbulent kinetic energy (k) due to the mean velocity gradient

$G_b \equiv$ Generation of turbulent kinetic energy due to buoyancy (b)

$Y_M \equiv$ Contribution of the fluctuating dilatation in compressible turbulence to the

overall dissipation rate

$S_k \equiv$ User defined source term for k.

$S_\varepsilon \equiv$ User defined source term for ε.

The turbulent viscosity μ_t, can be expressed as (reference ANSYS Fluent Documentation)

$$\mu_t = \rho\, C_\mu \frac{k^2}{\varepsilon} \tag{3.19}$$

The arbitrary constants in the above two equations have the following default values in ANSYS Fluent: $C_{1\varepsilon} = 1.44$, $C_{2\varepsilon} = 1.92$, $C_\mu = 0.09$, $\sigma_k = 1.00$, $\sigma_\varepsilon = 1.30$. As explained in the ANSYS Fluent Documentation, the default values listed above have been determined experimentally, using water and air as the fluid for analysis.

3.4 Energy Equation-

The energy equations (Pritchard & Leylegian, 2011) for the flow domain originating at 1 ending at 2 are

$$\frac{P_1}{\rho} + \frac{V_1{}^2}{2} + gZ_1 = \frac{P_2}{\rho} + \frac{V_2{}^2}{2} + gZ_2 + h_L \qquad (3.20)$$

$$h_L = h_{Lmj} + h_{Lmn}$$

$$h_{Lmj} = f \frac{L}{D} V^2$$

$$h_{Lmn} = K \frac{V^2}{2g}$$

This is the energy equation mostly used in fluid mechanics to determine the pressure difference between any two points in a fluid domain, when head loss h_L is provided. The h_L is the sum of both major and the minor losses. The minor losses result from entrances, fittings, area changes and so on. The major losses occur due to frictional effects in a fully developed flow.

3.5 CAVITATION -

Cavitation is when fluid pressure at any point in a system drops to the vapor pressure and boiling occurs. Cavitation damages equipment and degrades performance. Boiling causes formation of vapor bubbles inside the system. The vapor bubbles grow and then collapse, producing shock waves, noise and dynamic effects that leads to decrease in overall performance and sometimes failure of the equipment. In Figure 3.1, damage is shown due to cavitation to a propeller. The cavitation damage to propeller occurs because the spinning propeller creates low pressures near the tips of the blades where the velocity is high.

Figure 3.1 Cavitation damage to a propeller (Elger, Williams, Crowe & Roberson, 2012)

Cavitation degrades materials because of the high pressure associated with the collapse of vapor bubbles. Experimental studies have shown that very high intermittent pressure, as high as 800 Mpa(115,000 psi), develops in the vicinity of the bubbles when they collapse. The considerable damage occurs when the bubbles collapse close to boundaries such as pipe walls, pump impellers, valve casings and dam slipway floors. (Elger, Williams, Crowe & Roberson, 2012)
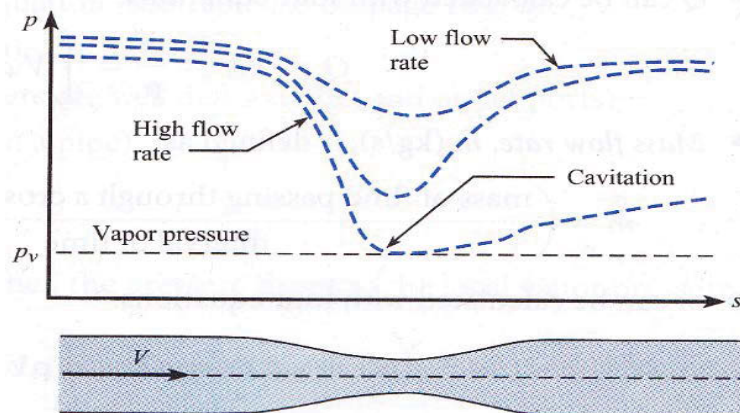
Figure 3.2 Flow through pipe restriction, variation of pressure for three different flow rates (Elger, Williams, Crowe & Roberson, 2012).

Cavitation occurs as a result of a very high pressure drop. As water flows through a pipe restriction as shown in the figure, the velocity increases according to the continuity equation and pressure drop is dictated by the Bernoulli equations. When we have low flow rates, there is a relatively small drop in pressure at the restriction, so the water remains well above the vapor pressure, and boiling does not occur. However, as the flow rates increase, the pressure at the restriction becomes lower until a flow rate is reached where the pressure equals the vapor pressure as shown in the Figure 3.2. At that point, the liquids boil to form bubbles and cavitation occurs. The beginning of cavitation can also be affected by the pressure of contaminant gases, turbulence, and by viscous effects.
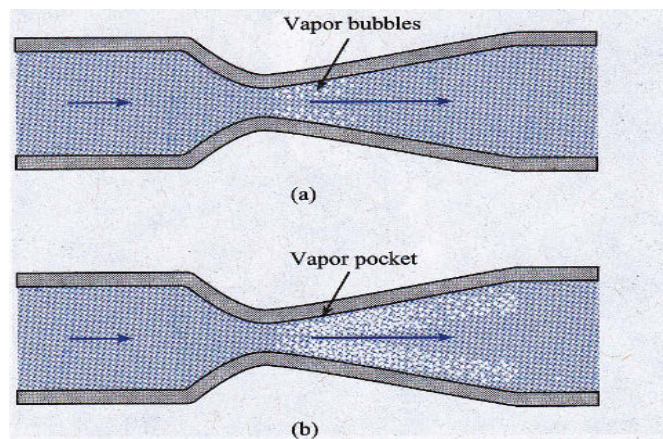
Figure 3.3 Formation of vapor bubbles in the process of cavitation (Elger, Williams, Crowe & Roberson, 2012).

The vapor bubbles formation at a restriction is shown in the Figure 3.3. The vapor bubbles form and then collapse as they proceed in the high pressure regime and are swept downstream with the flow. As the flow velocity is increased and low pressure, which is still the vapor pressure, the zone of bubble formation is extended, as shown in Figure 3.3.

Here, the entire vapor pocket may extensively grow and collapse as a big unit and can produce serious vibration problems.

CHAPTER 4

Numerical Methodology

Numerical approach is a very unique method while solving for both algorithm and mathematical modeling in fluid mechanics. Numerical modeling and simulation is a technique that allows for highly complex, mathematical equations to be solved. To solve the fluid flow problem, the software should have the ability to analyze the problem, set up the problem in the form of an algorithm, and have the ability to solve and give results with minimal errors. ANSYS Fluent is the software which is used to solve complex fluid mechanics problems. The software was built to model and analyze many types of laminar and turbulent fluid flows. The software has different packages and add-ons that allow the user to model various geometries with different mathematical models. ANSYS Fluent is the software which uses a finite volume method approach for solving the equations. ANSYS Fluent has its own geometric modeling software known as ANSYS Design Modeler. The software is user-friendly and allows users to use third party design software like AUTOCAD or SOLIDWORKS and it allows importing of external geometry created in this software to ANSYS fluent. Another important criterion to achieve accurate results is by applying the best possible meshing technique to the geometry so as to get fine mesh. The processing and post-processing of the meshed object were performed in ANSYS Fluent. The algorithms and programs that were used in the study of flow through fluid domain are discussed in other sections as followed.

ANSYS Fluent is equipped with several add-ons that enable the user to model and analyze complex fluid flows. The software also has the ability to couple the effects of heat transfer with fluid flow. ANSYS Fluent couples the equations of flow theory with

mathematical models in order to solve highly complex fluid flows. ANSYS Fluent consists of two different flow solvers, each with their own strengths and weaknesses. The two flow solvers used in ANSYS Fluent are the pressure-based and density-based solvers.

4.1 CFD Methodology

The set up and running of a successful simulation requires a procedural set up of the fluid flow problem, and it consists of a few sequential steps in series that need to be completed. The procedure is shown as below.

CFD Analysis-
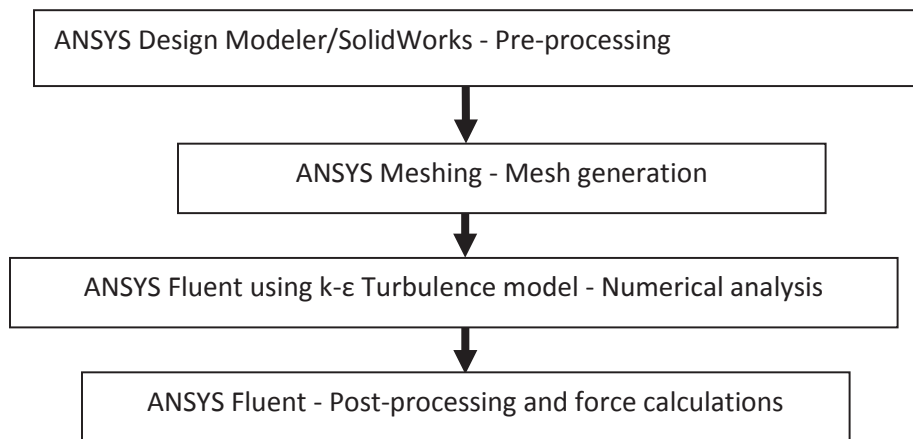
Figure 4.1 Fluent Process flow diagrams (Tu, Yeoh & Liu, 2008)

1. **Creation of Geometry**
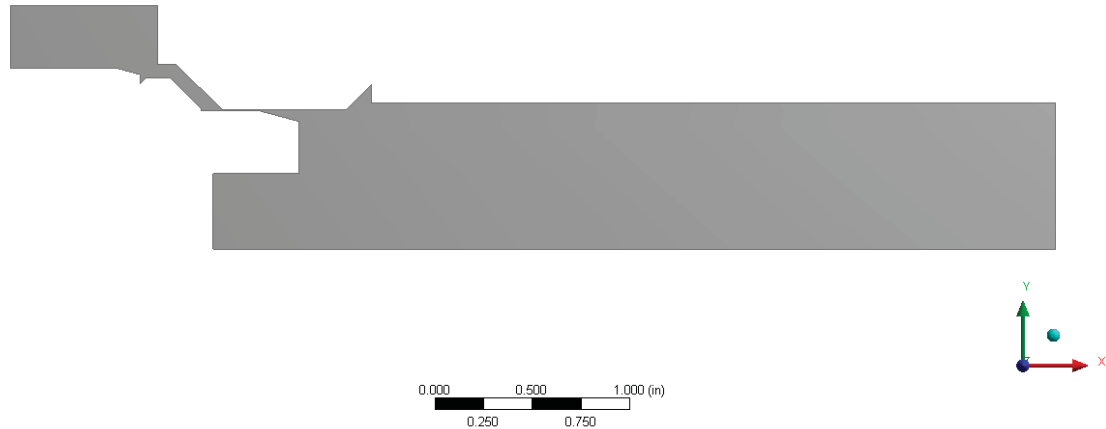
Figure 4.2 Geometry creations in ANSYS Fluent 14.0

This is the pre-processing step that is the creation of the geometry in ANSYS Design Modeler or with the help of any other design software like CAD or SOLIDWORKS. For the scope of this thesis, the 2D geometry was done in Design Modeler and the 3D geometry in SOLIDWORKS. This completes the first step in any CFD analyses. It is the definition and creation of the flow region (computational fluid Domain) for the CFD calculations.

2. **Mesh Generation**
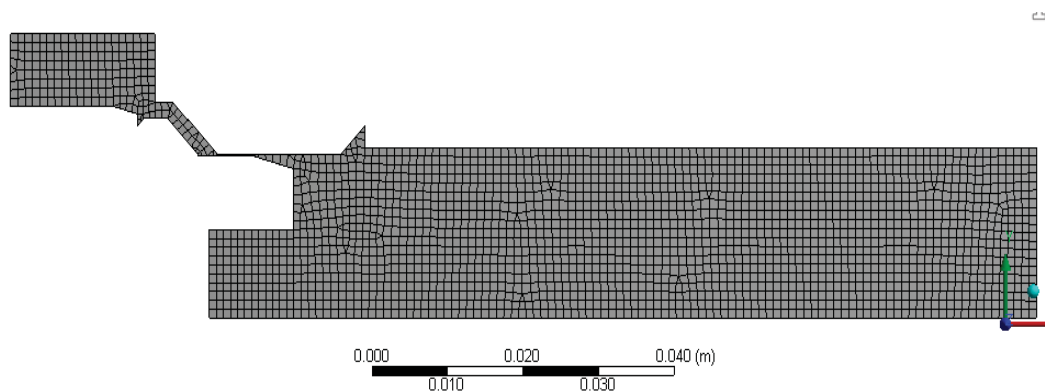
Figure 4.3 Meshing operations In ANSYS Fluent 14.0

The second step is the mesh generation. It constitutes one of the most important steps during the pre-processing stage after the definition of the domain geometry. CFD requires the subdivision of the domain into a number of smaller, non-overlapping subdomains in order to solve the flow physics within the geometry that has been created. This results in generation of the mesh cells. The mesh add-on can open from the main ANSYS Fluent set up tool bar. The geometry is meshed first with the automatic method and then refinement was applied to it. The mesh is then generated; results of meshing had nodes-20811, elements-19970 with orthogonal quality of 0.72.   The accuracy of the CFD solutions is governed by the number of cells in the mesh within the computational domain. The more the number of cells in the fluid domain, the more accurate solution can be achieved. However, the accuracy of the solution is strongly dependent on the imposed limitations dominated by computational costs and calculation turnover times.

3. **Selection of physics and fluid Properties**
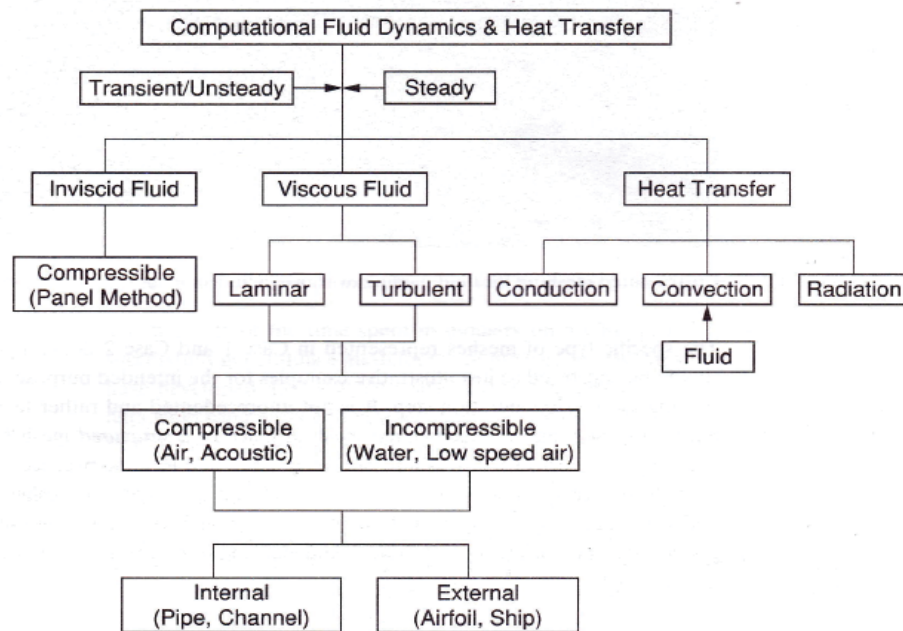
Figure 4.4 Flow physics (Tu, Yeoh & Liu, 2008)

Many CFD problems may require complex physical flow processes like combustion, radiation, cavitation etc. Processes like combustion and radiation have high tendencies to influence the local and global heat transport, which consequently affects the overall fluid dynamics of the flow domain. CFD user has to clearly underline the type of the flow physics so as to get accurate results from the simulation. Shown above is the flow chart of the various physics in CFD.

This is the perfect way to start the solution for the given CFD problem, by initially stating the fluid flow system, whether it is transient/steady or unsteady solutions. The user has to define which class of the fluids is being used, whether it is inviscid or viscous. After that, we have to specify whether the flow is laminar or turbulent and transport for heat is contributing or not. If there is heat transfer, then the mode of heat transfer needs to be specified, such as conduction, radiation, or convection.

4. **Defining the Boundary conditions**
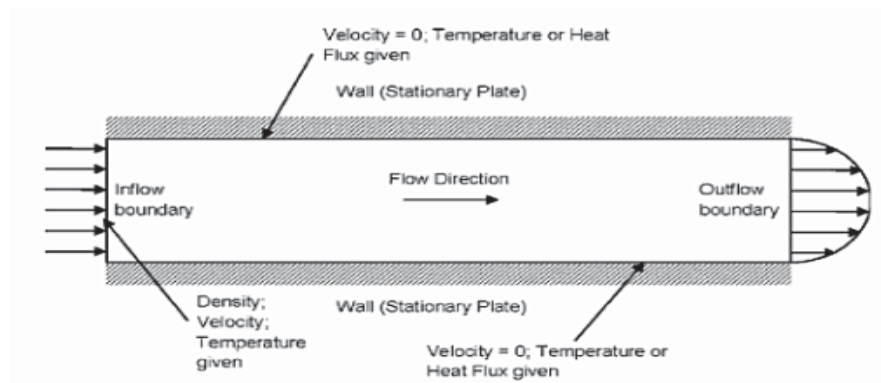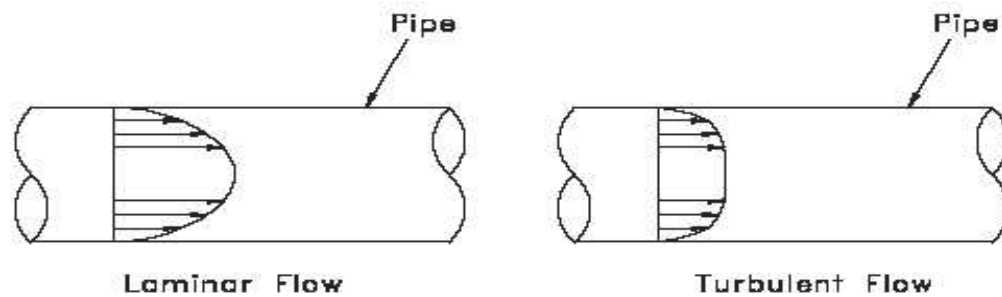
Figure 4.5 shows boundary conditions for an internal flow (Tu, Yeoh & Liu, 2008)

This step in the pre-processing deals with the specification of the boundary condition for the impending simulations. This helps to specify the solver, which is the inlet and the outlet boundaries, within the flow domain; also suitable fluid flow boundary conditions are required to accommodate the fluid behavior entering and leaving the flow domain.

5. Run the Simulation
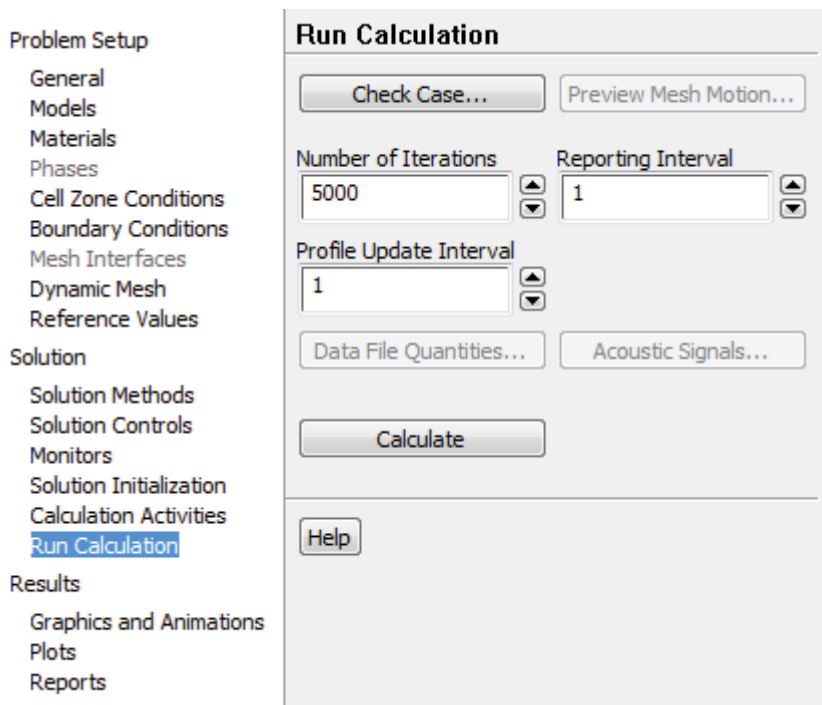
Figure 4.6 Solution and setup in ANSYS Fluent 14.0

The other important step is the set up physics of the problem that is done actually by Fluent. Here, the user has to define the type of solver to be used and whether it is pressure based or density based. The type of material and the material properties are to be specified so as to solve the problem using those properties of the fluid flowing in the domain. The type of flow which is used for simulation has to be specified, whether laminar flow or turbulent flow. The 2D model simulations to be performed are axisymmetric or planar, so the computational time can be reduced.

4.2 CFD Solver

The appropriate selection of the solver is the most important step for more accurate results when compared with experimental results. The user must specify the type of solver, pressure or density based, and whether the flow is steady or unsteady. For this study, the solver chosen was the pressure based solver and the flow was considered as a steady flow so as to obtain more realistic and accurate results from the simulations. [ANSYS Fluent 14.0 Documentation]

$$\frac{\partial}{\partial t} \int_V \rho \phi \, dV + \oint_A \rho \phi \mathbf{V} \cdot d\mathbf{A} = \oint_A \Gamma_\phi \nabla \phi \cdot d\mathbf{A} + \int_V S_\phi \, dV$$
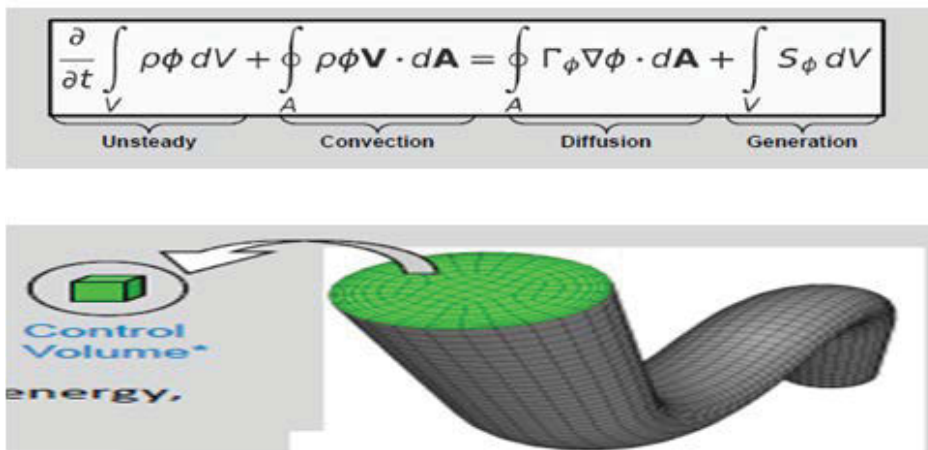
<div align="center">Unsteady   Convection   Diffusion   Generation</div>

Figure 4.7 Finite volume method [ANSYS Fluent 14.0 documentation]

ANSYS CFD solver is based on the finite volume method where the domain is discretized into a finite set of control volumes. General conservation (transport) equations for mass, energy, species etc. are solved within this set of control volumes. Partial differential equations are discretized into a system of algebraic equations. Then, all algebraic equations are solved numerically to render the solution field. Fluent control volumes are cell centered, i.e. they correspond directly with the mesh.

Pressure-Based Segregated Algorithm-

The pressure-based solver in ANSYS Fluent is used for the most incompressible flows, whereas the density-based solver is used for compressible flows. The pressure-based solver uses an algorithm to solve for the governing equation in sequential order. The solution to the governing equations is by an iterative method.
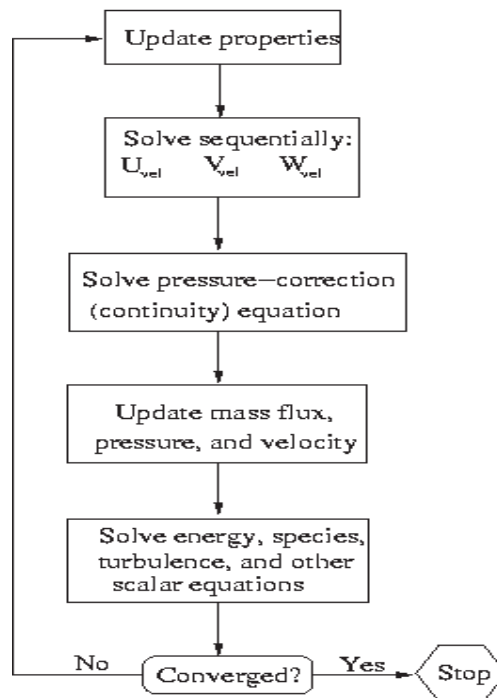
Figure 4.8 Pressure based algorithm [ANSYS Fluent 14.0 documentation]

Most of the CFD problems are usually a large set of nonlinear algebraic equations. Thomas's algorithm is particularly economical in obtaining the solution for one-dimensional steady state heat conduction problems. For multidimensional situations, it only leaves the options of the iterative method. In this method, one guesses the solution and uses the equations to systematically improve the solution until it reaches some level of convergence. This is usually the case in major CFD problems. The initial guess is used to solve for the momentum equation, and after that, it is used to solve for the

$$\oint \rho \phi \vec{v} \cdot d\vec{A} = \oint \Gamma_\phi \nabla \phi \cdot d\vec{A} + \int_V S_\phi dV \qquad (4.1)$$

Where,

$\rho \equiv$ density

$\vec{v} \equiv$ velocity vector

$\vec{A} \equiv$ surface area vector

$\Gamma_\phi \equiv$ diffusion coefficient for ϕ

$\nabla \phi \equiv$ gradient of ϕ

$S_\phi \equiv$ source of ϕ per unit volume

pressure correction as given by the governing equations. Once the solution to the pressure correction equation is consistently solved, the output is used to solve for the velocity field, mass fluxes, and pressure sequentially. These solutions are then used to solve for any other remaining scalar quantities such as turbulence and energy.

Species transport was not included in the scope of this thesis as the fluid is considered pure- free of any chemical or other carrying species. Finally, the convergence criteria are checked, and if the solutions have met the criteria, the iterative process is stopped and the solution is converged. If not, the solution is put back into the iterative loop and the process repeated.

Discretization Technique

Fluent uses a discretization technique to turn a general scalar equation into an algebraic equation, which enables the equations to be solved numerically. The governing equations are integrated about each of the volumes created during the meshing process. In doing so, the discrete equations satisfy the laws of mass conservation. Equation 4.1, shown below, describes the discretization process for an arbitrary control volume; Equation 4.1 can be simplified for a fluid flow through a surface area. This simplified equation, is shown in Equation 4.2. (ANSYS Fluent Documentation 14.0)

$$\sum_f^{Nfaces} \rho_f \vec{v}_f \phi_f \cdot \vec{A}_f = \sum_f^{Nfaces} \Gamma_\phi \nabla \phi_f \cdot \vec{A}_f + S_\phi V \qquad (4.2)$$

Where,

$N_{faces} \equiv$ number of faces enclosing cell

$\phi_f \equiv$ value of ϕ convected through face of f

$\rho_f \vec{v}_f \cdot \vec{A}_f \equiv$ mass flux through the face, f

$\vec{A}_f \equiv$ area of face, f

$\nabla \phi_f \equiv$ gradient of ϕ at face f

$V \equiv$ cell volume

Fluent, by default, stores the individual values of ϕ at the center of each of the volumes. In order to solve this problem, the face values are determined by interpolation. The interpolation method involves the use of the values from the center of the volume via an upwind scheme.

There are two upwind schemes that can be used for this interpolation process: a first order and second order. The first order upwind scheme assumes the cell-center values to be equal to the average value of the cell. In other words, $\phi_f = \phi$. The second order upwind scheme is used when a higher level of accuracy is preferred. The second order scheme, to determine the face values, uses a multidimensional linear reconstruction approach to achieve this higher level of accuracy. It involves the use of a Taylor Series expansion of the volume-centered solution about the centroid of each mesh element. The second order upwind scheme was used in the analysis of the flow through fluid domain in 2D and 3D models (Yatsco, 2011).

Convergence Criteria

The application of a numerical modeling technique requires ways to measure the validity and accuracy of the simulated solution. The way in which ANSYS Fluent determines whether or not a solution is valid is by way of convergence criteria. The convergence criteria that were found in ANSYS Fluent depend on what type of model is chosen. Each model contains its own residuals that ANSYS Fluent monitors in order to determine a converged solution. These residuals, depending on the type of model selected, involve x- and y- components of velocities, k and ε that include continuity, turbulence, and energy.

As stated earlier in the chapter, ANSYS Fluent uses an iterative process to achieve the best solution. The error between the previous and current solution are determined after iteration simultaneously. A converged solution depends on the error between the two solutions. It should be noted that an absolute converged solution, one where the error between the current and previous solution is zero, is very hard to obtain. Also, it is not always practical to achieve an absolute converged solution. The default settings for the residuals in ANSYS Fluent were 10^{-3}. These default settings are good for some simpler problems, but for most complicated problems, smaller error settings are required for better accuracy and good convergence. As a result, the residuals for the simulations here were set to have convergence criteria of at least 10^{-6} units and in some cases 10^{-9} units for the respective fluid parameters (Yatsco, 2011).

4.3 Validation of the Software

The ANSYS Fluent software has been used in several research applications dealing with hydraulic poppet valves. One such computational study was performed on the hydraulic

poppet valve by a research group from Ferdowsi University of Mashhad, Iran. In that study, the flow cavitation in a poppet valve, which is a typical hydraulic element in fluid power engineering systems, was numerically simulated. In this case, the working fluid was oil. Cavitation was commonly classified by a cavitation number (Mohammad & Hossein, 2008).

$$\sigma = \frac{(P_\infty - P_V)}{\left(\frac{1}{2}\rho V^2_\infty\right)}$$
(4.1)

Where P_v is the vapor pressure, ρ is the liquid density, and P_∞ and V_∞ are the main flow pressure and velocity respectively.

In that study, the incipient cavitation for an oil hydraulic flow in poppet valve with an axisymmetric configuration was simulated. Numerical results were compared with those of the available experiments where the two results for flow behavior were discussed in difference and similarities. The effects of the poppet angle at a constant poppet base and displacement were then investigated in order to improve the valve performance with regards to reduction of the cavitation.

In the study, the advection of the cavity interface was simulated based on volume-of-fluid (VOF) technique along with a cavitation model for mass transfer between the two phases of liquid and vapor. All simulations were performed for ISO-VG46 machine oil, a liquid commonly used in industrial hydraulic systems, with kinematic viscosity as $73E^{-6}$ m^2/s and density as 900 kg/m3 at a temperature of 30 ℃. The computation domain selected for that simulation was 15mm x12mm with a mesh resolution that had 10 cells per one millimeter.
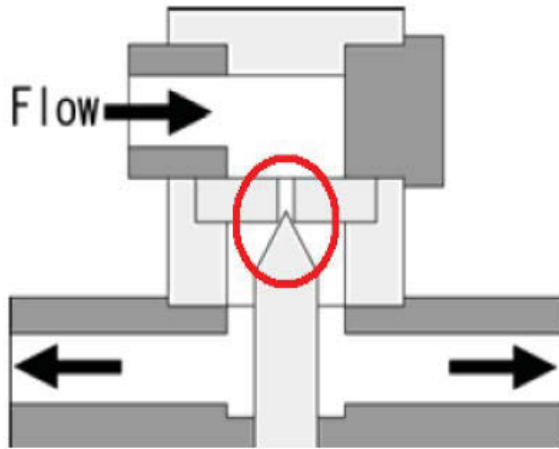
Figure 4.9 Schematic of a poppet valve (Kikui, Shotaro, Washio, Seiichi, Takahashi & Satoshi, 2006).

Figure 4.10 shows cavitation formation observed in the experiment and predicted in the model. The cavitation starts as a sudden appearance of a small bubble on the edge of the valve seat where the flow separation occurs. The cavitation phenomenon is seen in 6.7 ms after the start of the flow into the valve for the poppet displacement of 0.5 mm and flow rate that increased linearly from 2 to 40 cm^3/s in 66.7ms. A reduced pressure region close to the valve seat was observed from the simulations (6.7 ms), indicating the location where the cavitation occurs. When pressure all around the separation zone decreased below that of the vapor pressure, a full cavity region was formed. Therefore, the use of the model in this condition was justified. At 66.7 ms time elapsed, the oil flowed into the valve; both experiment and model predicted a cavity all around the valve seat, which caused serious failure in its performance. Pressure distributions and flow streamlines are also shown in the numerical images of Figure 4.10. In the region where the cavity was seen, the pressure is reduced to that of the vapor pressure and the flow streamlines are disturbed as seen in the figure.
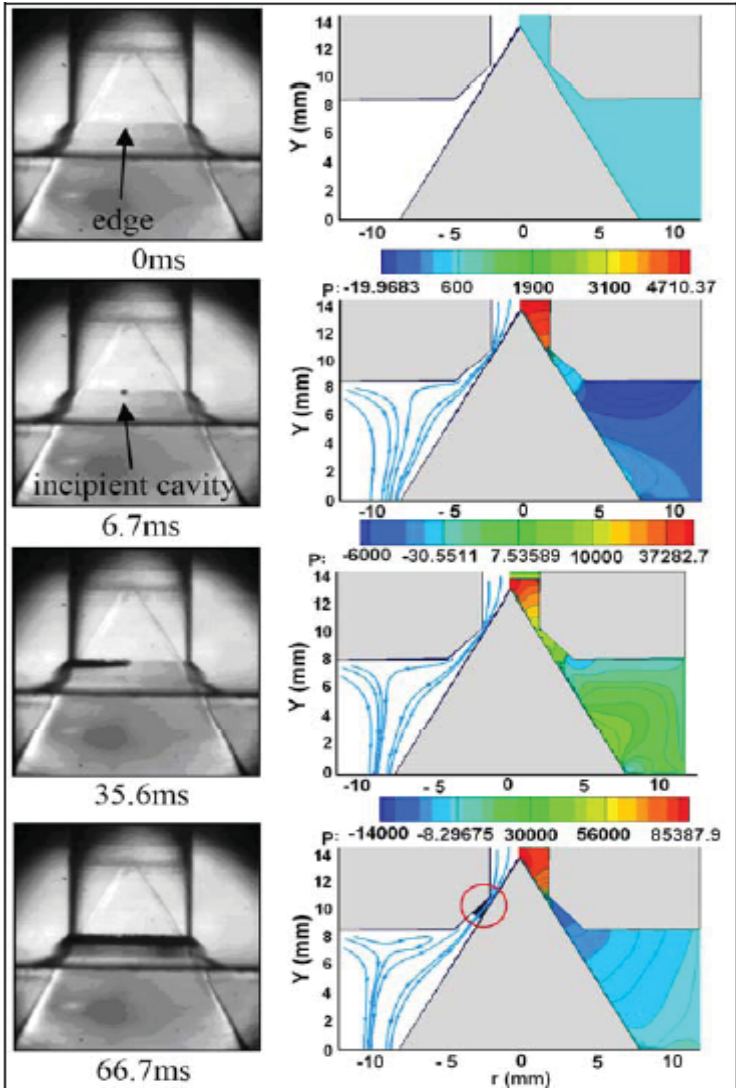
Figure 4.10 Inception of cavitation from experiement (Kikui, Shotaro, Washio, Seiichi, Takahashi & Satoshi, 2006) and numerical model of poppet valve. The pressure distribution and flow streamlines in numerical model.

Figure 4.11 Shows a close up view of the separation point where cavitation starts. The pressure distribution along with flow streamlines and velocity vectors are displayed in the figure. The figure that was shown was in transient flow; as a result, the pressure changes from one time to the next were significant. Therefore, the pressure contours in each images of Figure 4.11 were different. The minimum pressure has been observed at the

47

beginning of the flow (6.7 ms) as well as at the end of the valve channel. The absolute value of the minimum pressure is decreased and its location was gradually nearing the poppet minimum cross-sectional area as time passed. When cavitation occurs, the value of the minimum pressure falls below that of the vapor pressure and its location is fixed at the valve minimum cross-sectional area. From this, it was certain ANSYS Fluent is capable of predicting the phenomenon of cavitation in the poppet valve (Mohammad & Hossein, 2008).
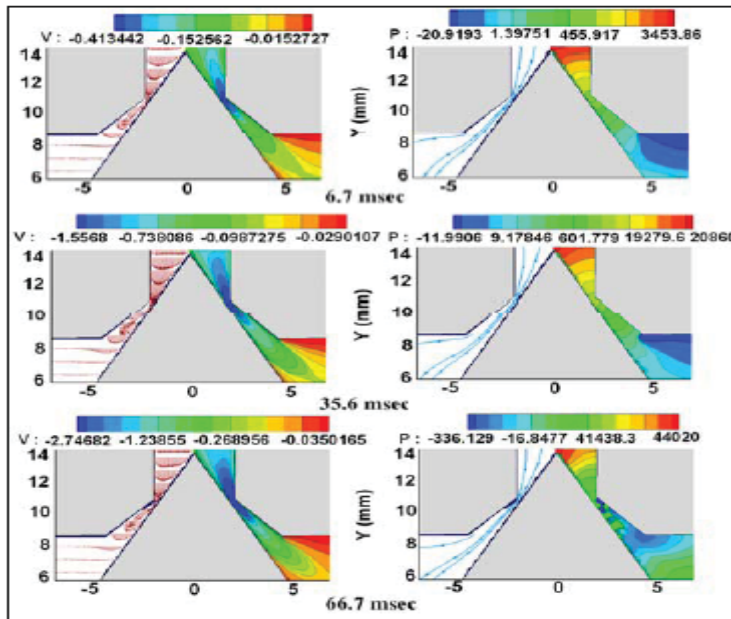
Figure 4.11 Close up view of separation point in the poppet valve, the left side shows velocity distribution and contours and right side pressure distribution and streamlines (Mohammad & Hossein, 2008).
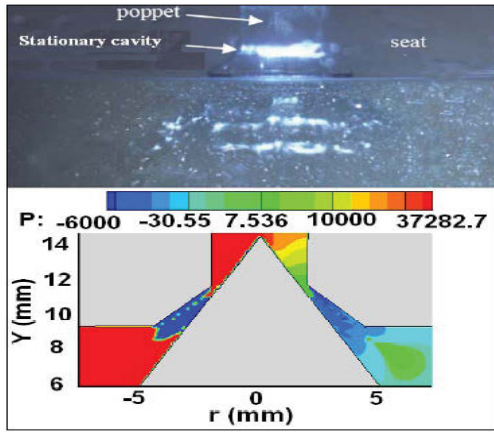
Figure 4.12 Experimental photographs (Kikui, Shotaro, Washio, Seiichi, Takahashi & Satoshi, 2006).
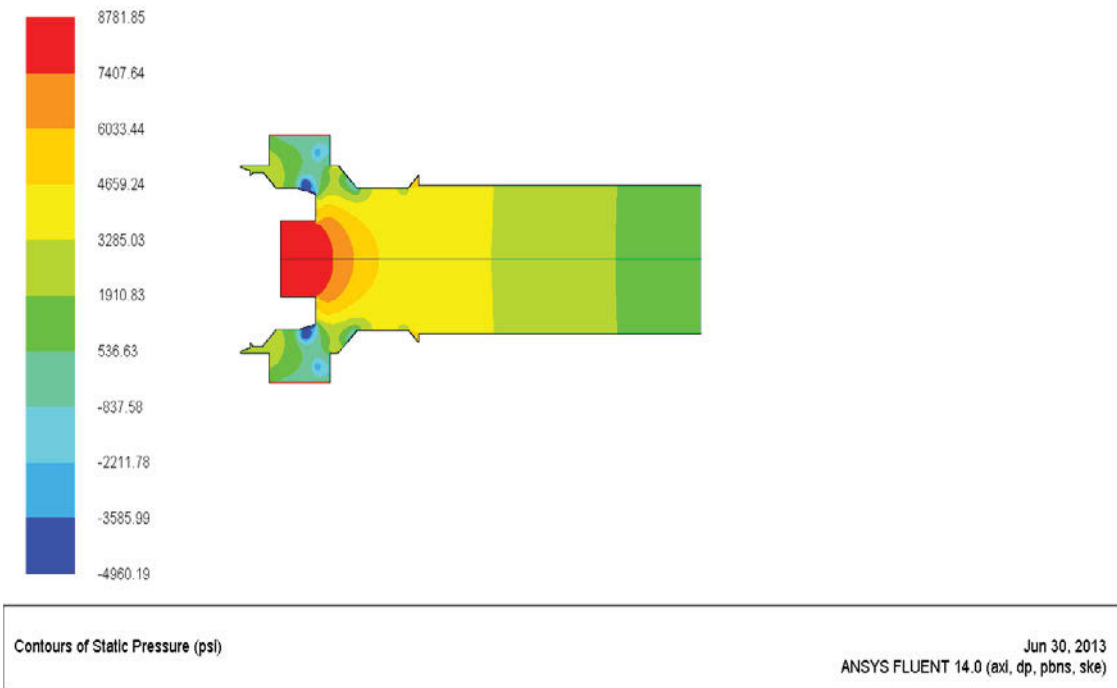
Figure 4.13 Static pressure contours for one inch opening (This Study).
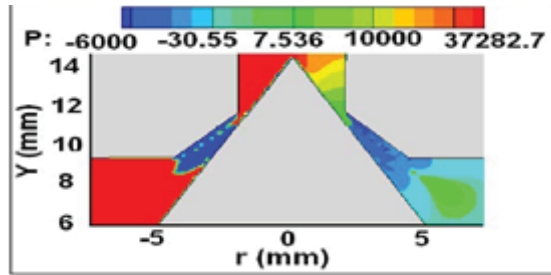
Figure 4.14 Experimental photographs (Kikui, Shotaro, Washio, Seiichi, Takahashi & Satoshi, 2006)

The results obtained from the simulation show us that cavitation effects are prominent in both of the cases. There is a high pressure drop in both models of about -4960.19 psi and, in the supplemental case, -6000 psi. As per the definition of cavitation, it occurs when the fluid pressure at any point in the domain drops below the vapor pressure. These results and supplemental results that are pressure contours clearly suggest that pressure drop below the vapor pressure is a major cause of cavitation. Thus, the validation of the ANSYS Fluent is completed as well as results which are reasonably supported by the supplemental work which was done by another research group.

Chapter 5

RESULTS AND DISCUSSION

In previous chapters of this research we talked about valves, classification of valves, and cavitation. In the second chapter, we talked about physical modeling, where physical models were developed. I had described fluid domain with its two opening. At first, flow was allowed from nose to side and in the second scenario, from side to nose. Various models were introduced into this research, mainly models M1 to M6, for various openings in inches. In Chapter 3, we talked about the fluid equations. These equations are the fundamental equations used for solving fluid flow problems. In Chapter 4, we talked about the use of ANSYS Fluent software in this research.

From those simulations and by using graphics and animations adds-on, contours for velocity and pressure were obtained. This gives us a general idea when looking for cavitation; pressure contour would indicate the lowest pressure, which should be less than the vapor pressure of the water. The same add-on gives us velocity contours which provide us with velocity magnitudes in the fluid domain by giving us values and velocity distribution. Also, we determine the velocity vectors from the graphics and animations add-on which provide us pictorial views of the velocity profile.

TWO DIMENSIONAL STUDIES

Various sets of boundary conditions were imposed in order to study the change in flow field variables during the fluid flow in the valve restriction.

For the two-dimensional study, six models with various opening were chosen, namely model no. M1 to M6

The inlet boundary condition applied at each nose to side and side to nose was 4300 psi. 0 psi was set at the outlet. Operating conditions were set at 14.69 psi, 58.018 F. The continuity, components of velocities, turbulent kinetic energy, and turbulent energy dissipation were set to satisfy the 10E-03 residuals.

Full Opening (1 inch) Model no. M1

The flow opening is set to 1 inch from the point of contact where the sealing is done.

The contours of static pressures are shown in Figure 5.1 and Figure 5.2
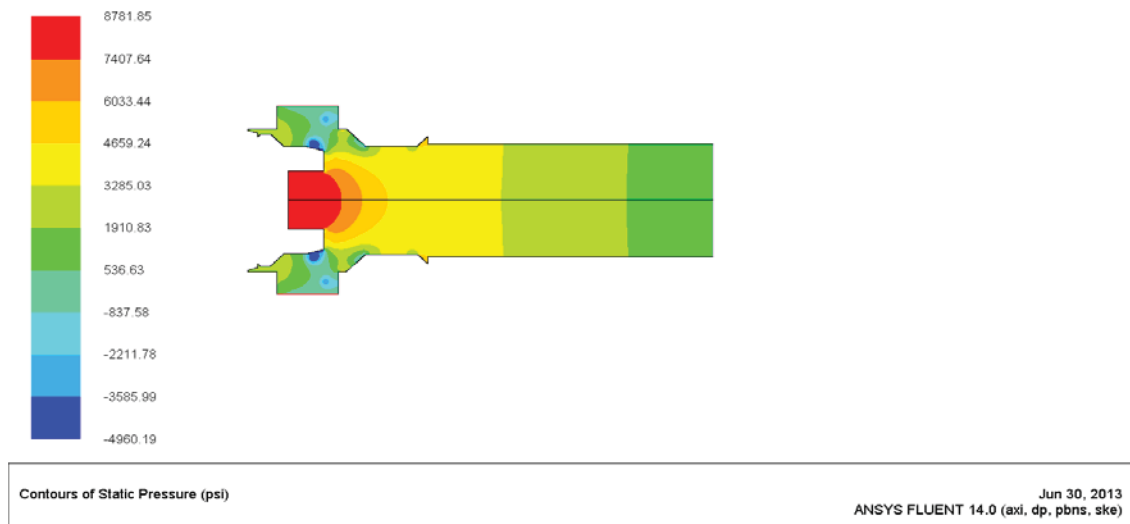
Figure 5.1 Contour of static pressure for Boundary condition 1 in nose to side flow
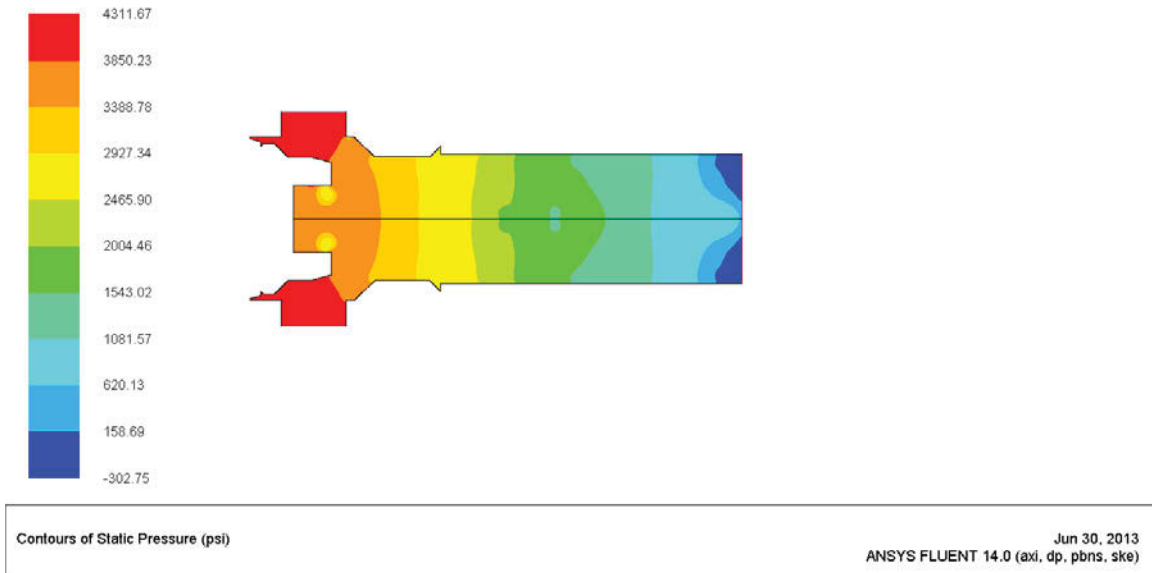
Figure 5.2 Contour of static pressure for Boundary condition 1 in side to nose flow

The lowest pressure developed in nose to side flow is lower than the side to nose flow. Even though the pressure was 4300 psi at nose (inlet) of the valve the highest static pressure observed was 8781.75 psi just below the poppet. The lowest static pressure observed was -4960.19 psi. The resulting static pressure below the poppet generates a pressure based force that helps in fast opening of the poppet. When the pressure was applied form side to nose scenario, the highest static pressure was found to be 4311.67 psi and the lowest was about -302.75 psi. We would observe severe cavitation in case of nose to side.

Opening (0.3 inch) Model no. M2

Static Pressure contour
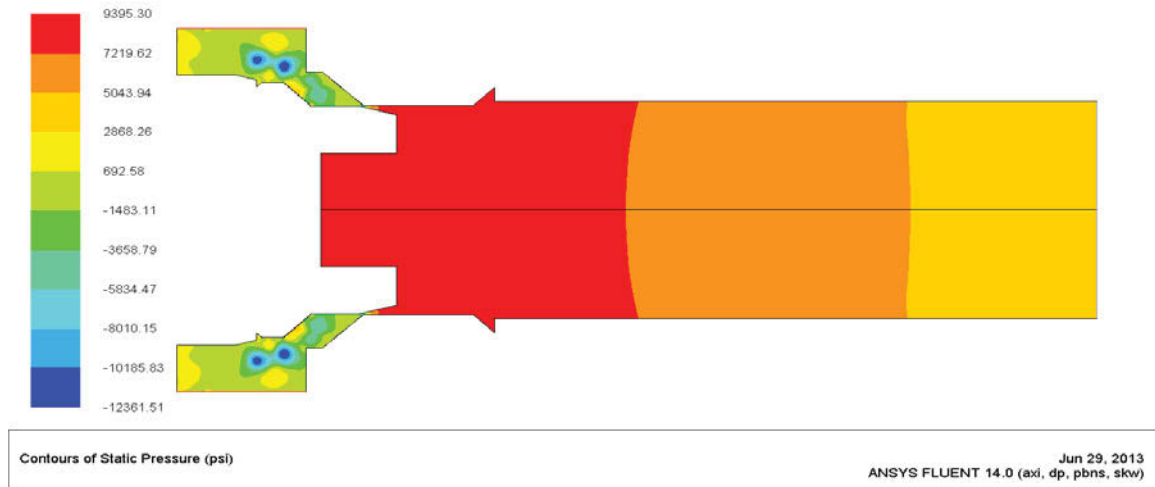
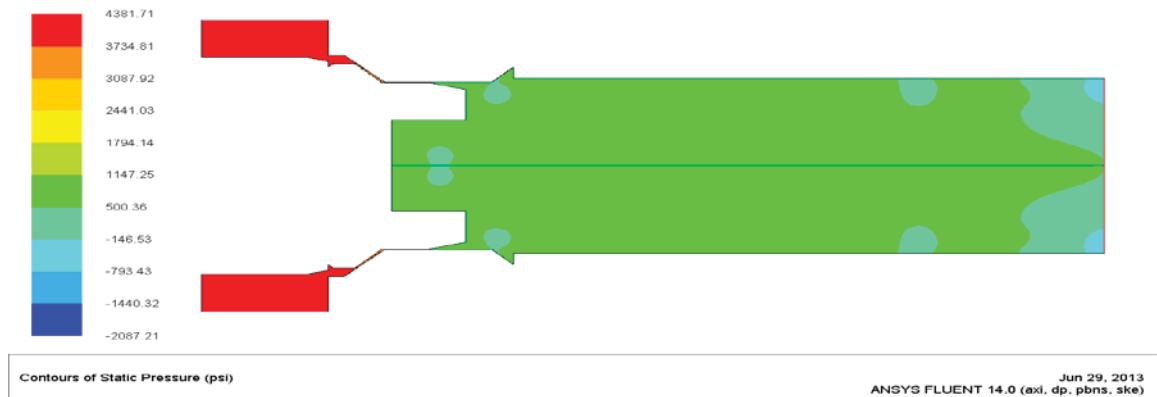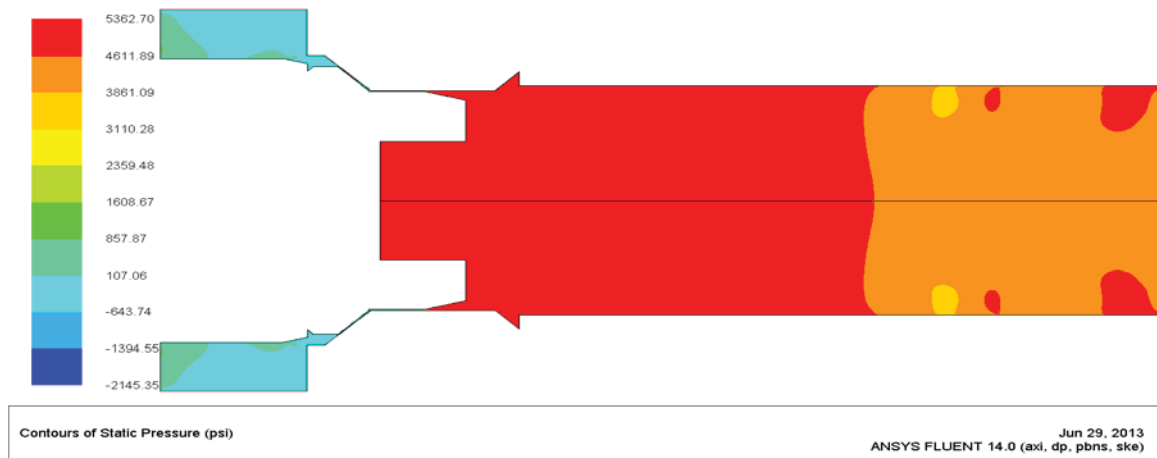Figure 5.3 Contours of Static pressure for opening 0.3 inch nose to side
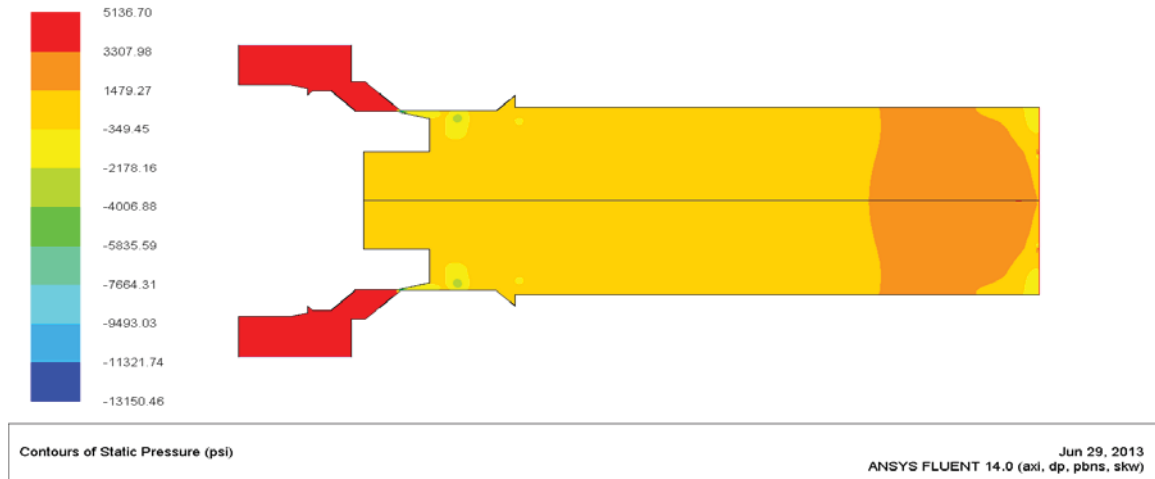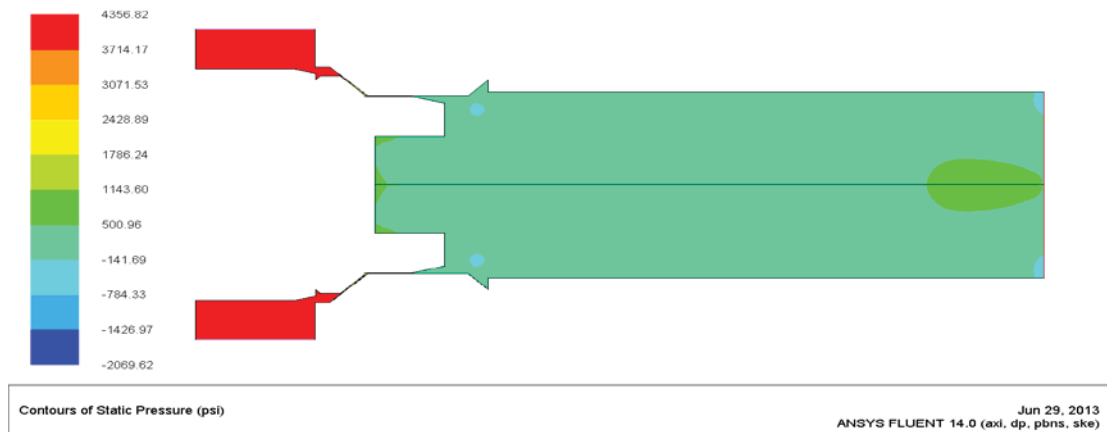

Figure 5.4 Contours of Static pressure for opening 0.3 inch side to nose

Even though the pressure was 4300 psi at the nose (inlet) of the valve, the highest static pressure observed was 9395.30 psi, just below the poppet. The lowest static pressure observed was -12361.51 psi. The resulting static pressure below the poppet generates a pressure based force that helps in fast opening of the poppet. When the flow was applied

from side to nose, the highest static pressure was observed to be 5136.70 psi and the lowest was about -13150.46 psi. In both cases, we would see severe cavitation because the fluid pressure drops far below the vapor pressure of water which is 0.363 psi at 70º F (Elger, Williams, Crowe & Roberson, 2012).

<u>Opening 0.2 inch Model no. M3</u>

Static pressure contours
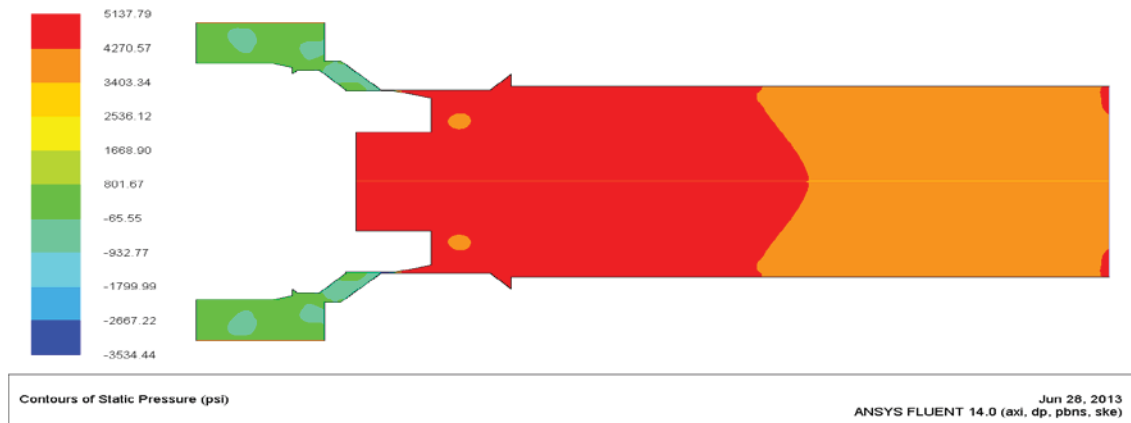
Figure 5.5 Contours of Static pressure for opening 0.2 inch nose to side
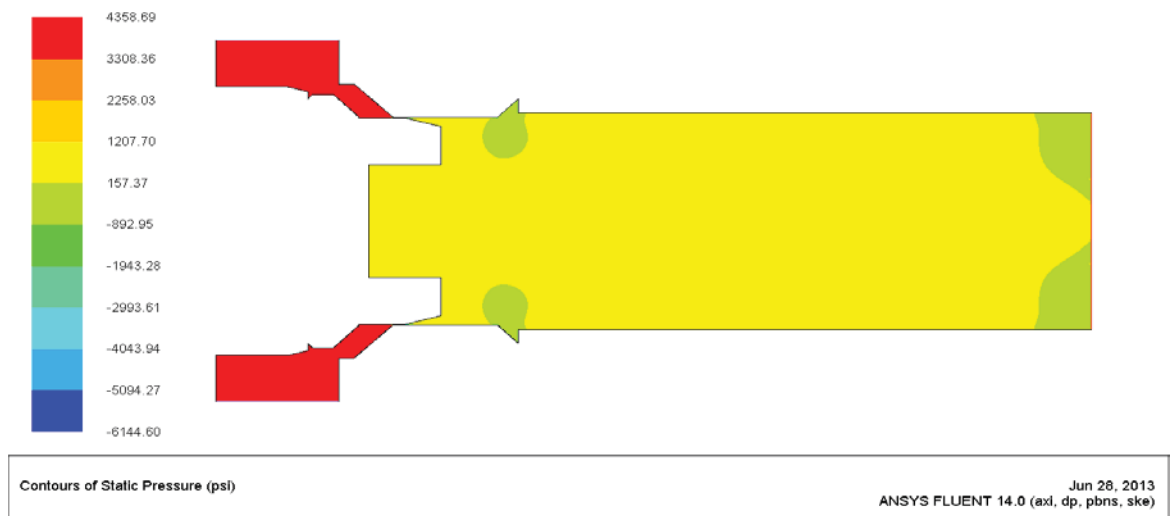
Figure 5.6 Contours of Static pressure for opening 0.2 inch side to nose

The highest static pressure was observed in nose to side flow which was about 5137.79 psi and in side to nose flow was 4358.69 psi. The lowest static pressure was visualized in side to nose scenario which was -6144.60 psi and in nose to side was -3534.44 psi. In this case, both nose to side and side to nose would have cavitation effects.

Opening 0.1 inch Model no. M4

Static pressure contours
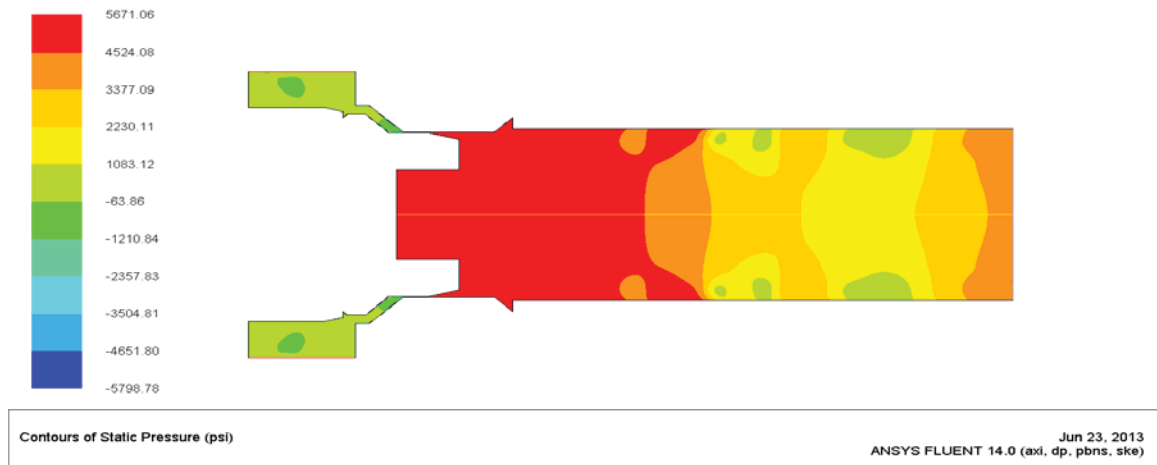
Figure 5.7 Contours of Static pressure for opening 0.1 inch nose to side
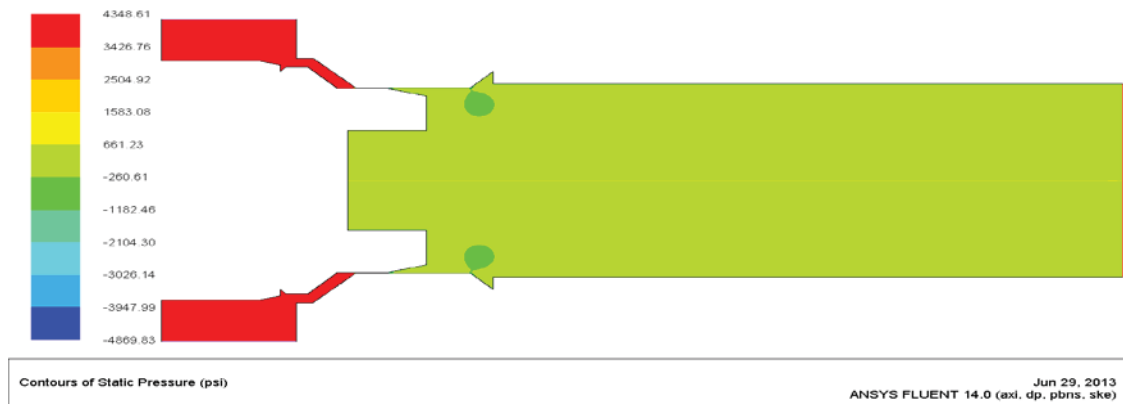
Figure 5.8 Contours of Static pressure for opening 0.1 inch side to nose

The highest static pressure was observed in nose to side scenario which was 5671.08 psi and side to nose was 4348.61 psi. The lowest static pressure was found in nose to side -5798.78 psi and side to nose as about -4869.83 psi. It is evident by looking at both cases that we can say cavitation effects would be prominent.

opening 0.0125 inch Model no. M5

Static Pressure contours
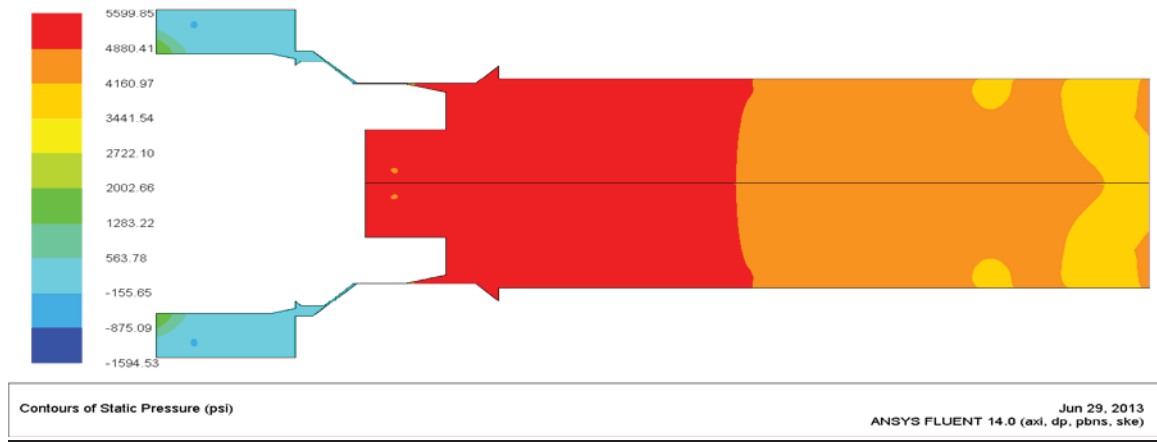
Figure 5.9 Contours of Static pressure for opening 0.0125 inch nose to side

Figure 5.10 Contours of Static pressure for opening 0.0125 inch side to nose

Even though the pressure was 4300 psi at the nose (inlet) of the valve the highest static pressure observed was 5599.85 psi just below the poppet. The lowest static pressure observed was -1594.53 psi. The resulting static pressure below the poppet generates a pressure based force that helps in fast opening of the poppet. When the flow was applied from side to nose, the highest static pressure was observed to be 4381.71 psi and the lowest was about -2087.21psi. Both cases would be immensely affected by cavitation.

Opeining 0.00625 inch Model no. M6

Figure 5.11 contours of static pressure for opening 0.00625 inch nose to side

Figure 5.12 contours of Static pressure for opening 0.00625 inch side to nose

Even though the pressure was 4300 psi at the nose (inlet) of the valve, the highest static pressure observed was 5362.70 psi just below the poppet. The lowest static pressure observed was -2145.55 psi. The resulting static pressure below the poppet generates a pressure based force that helps in fast opening of the poppet. When the flow was applied from side to nose, the highest static pressure was observed to be 4356.82 psi and lowest was about -2069.62psi. As in both cases, the liquid pressure drops below the vapor pressure of the liquid and the cavitation effects would be visualized.

THREE DIMENSIONAL STUDIES

Similarly to the 2D study, various sets of boundary conditions were imposed for the 3D study in order to study the change in the flow fields variables during the fluid flow in the valve restriction. For the three-dimensional study, six models with various openings were chosen, namely model no. M1 to M6. Here only M1 is presented because other models are still under investigation and it is premature to present their results.
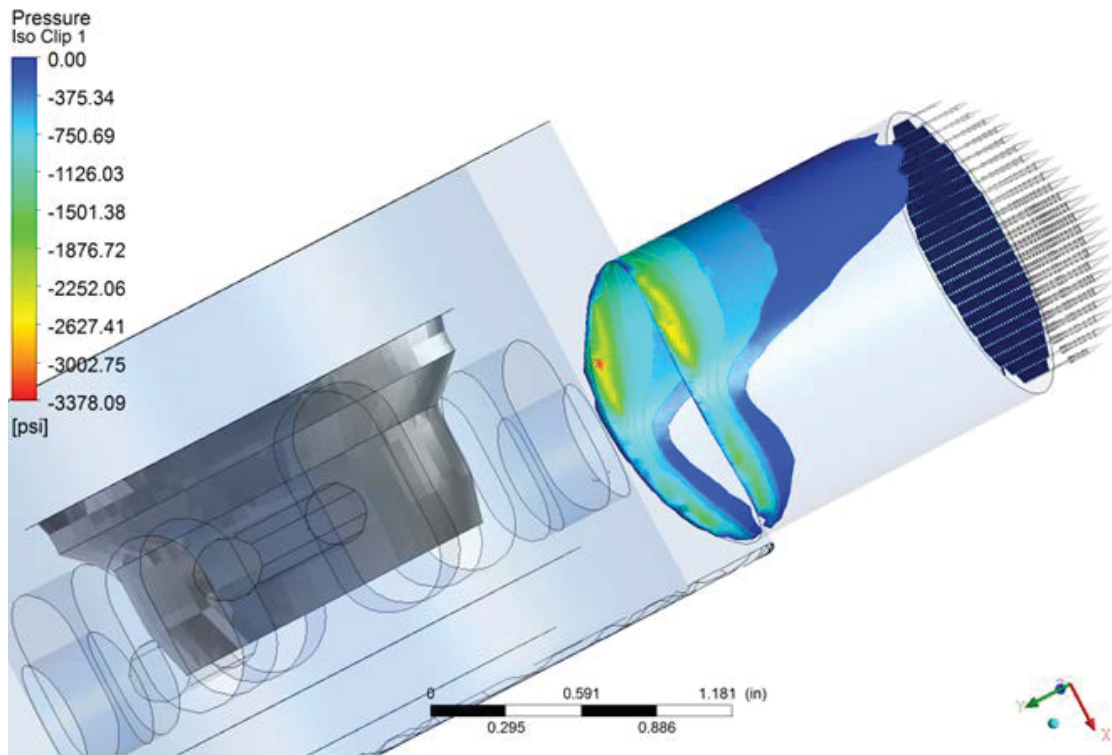
Figure 5.13 3D Static pressure capped below 0 psi in nose to side flow
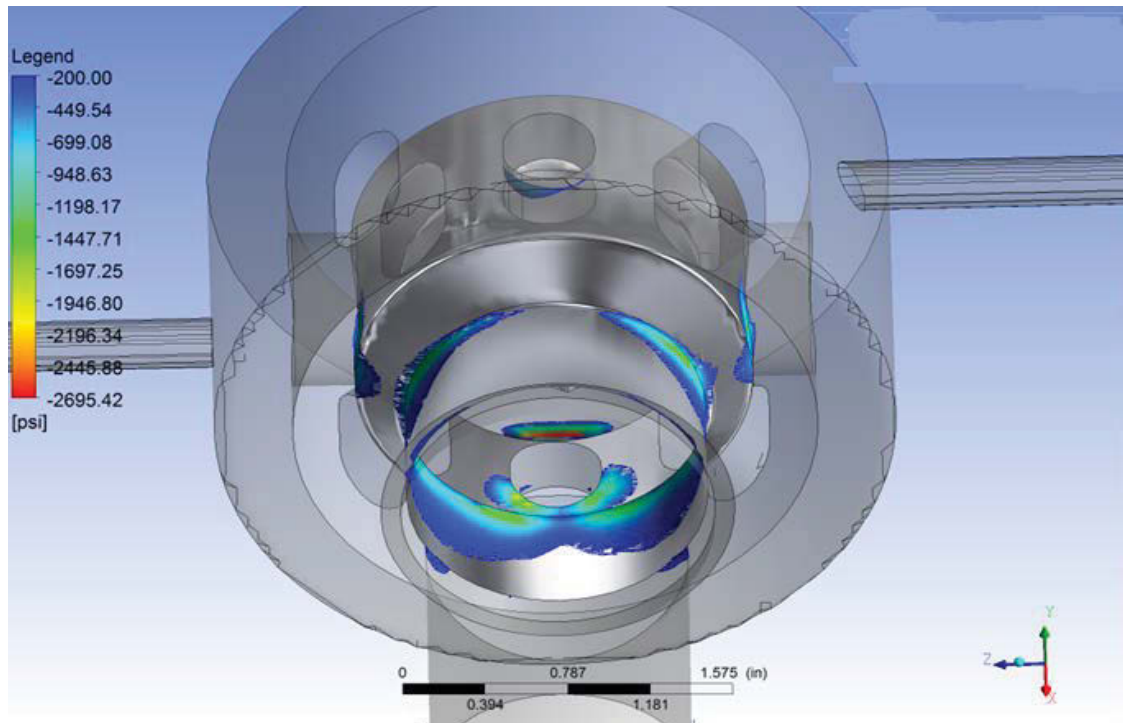
Figure 5.14 3D Static pressure capped below -200 psi in side to nose flow
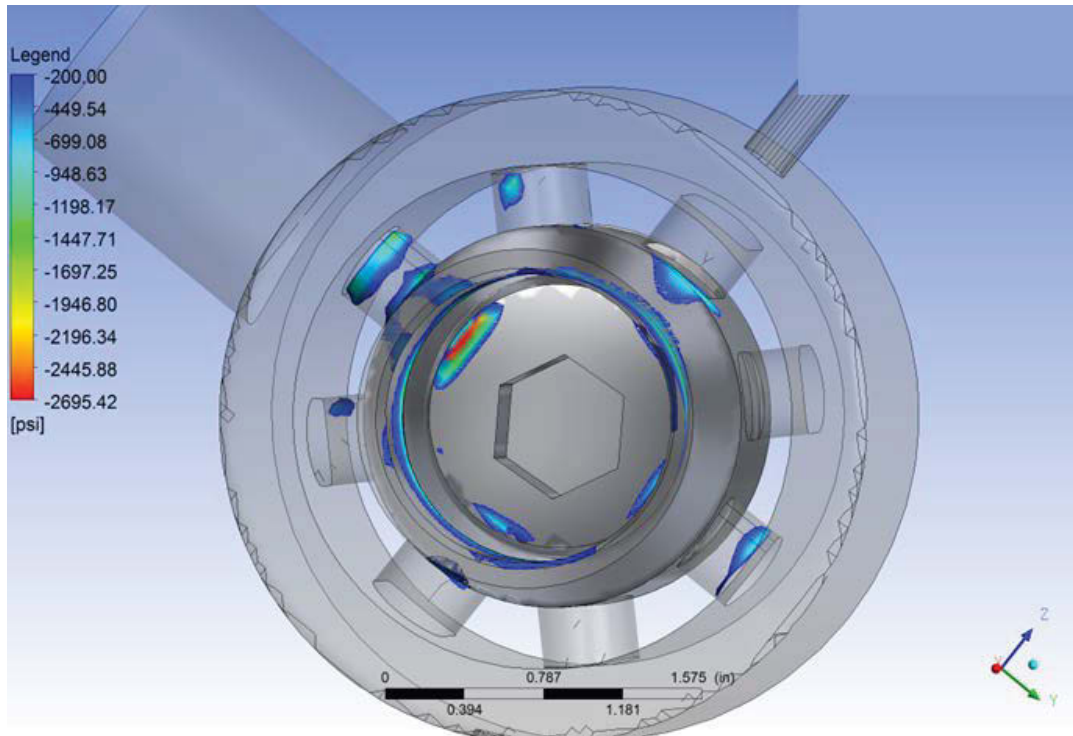
Figure 5.15 3D Static pressure capped below -200 psi in side to nose flow

In the 3D model, the nose to side case has the lowest static pressure of -3378.09, and side

to nose was found about -2695.42 psi. The effects of cavitation are also seen in both

cases.

Table no. 5.1 Pressure v/s. opening of the valve for Model No. M1-M6 in 2D

Opening	Nose -Side		Side-Nose	
inch	high pressure(psi)	low pressure(psi)	high pressure(psi)	low pressure(psi)
1	8781.75	-4960.19	4311.67	-302.75
0.3	9395.3	-12361.51	5136.7	-13150.46
0.2	5137.79	-3534.44	4358.69	-6144.6
0.1	5671.06	-5798.78	4348.61	-4869.83
0.0125	5599.85	-1594.53	4381.71	-2087.21
0.00625	5362.7	-2145.55	4356.82	-2069.62

In all cases, low pressure is seen to be lower than the vapor pressure of the fluid which is

0.363 psi. The effects of cavitation are prominent and severe in some cases.
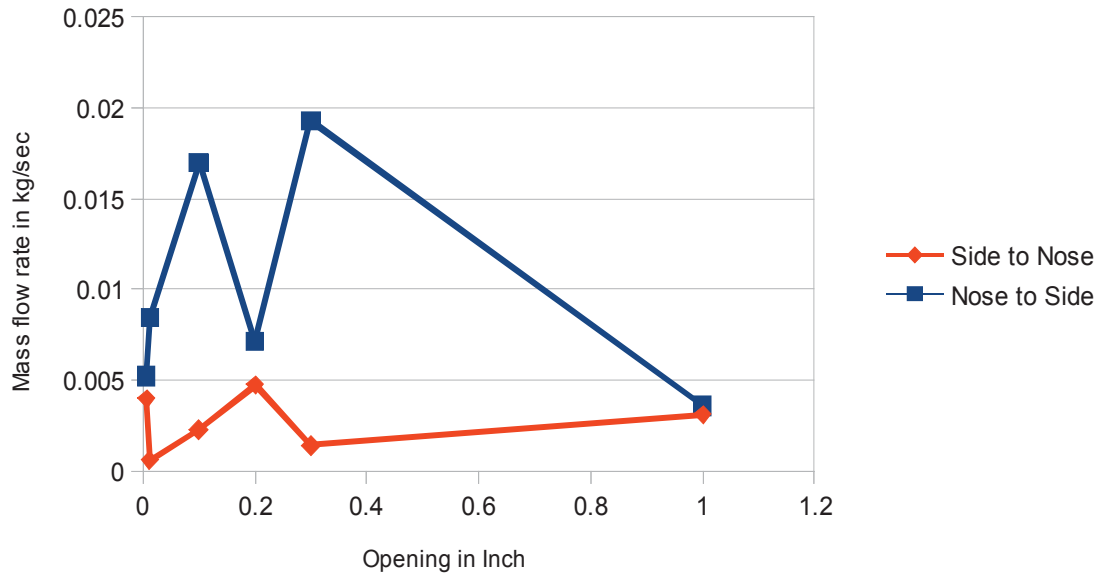
Figure 5.16 Mass flow rate v/s Opening in inch for both nose to side and side to nose

As seen from the figure for Mass flow rate v/s Opening in inch , it is observed that there is a significant drop in the mass flow rate when the flow is allowed from nose to side. Also, it is seen that there is an increase in the mass flow rate in the case when the flow is allowed from side to nose. There might be several reasons for increases or decreases in the mass flow rate. Turbulence, minimum area of the flow, and lastly, boundary conditions are responsible for variation in mass flow rate.

Chapter 6 Conclusions and Recommendations for Future Work

As presented in previous chapters, physical modeling, mathematical modeling, numerical methodology, and results were discussed.

The axisymmetric modeling predicted the low pressure zones in the flow path.

The 2D models were simulated for six different models having various openings. The results from static pressure contours suggest that low pressure zones in each simulation were observed and non-uniformity of the results suggest that residual criteria, computational memory, and convergence criteria play an important role.

As seen, 3D results give more insight and accurate results in comparison to 2D. Future research work should be done with 3D models and comparative study with the experimentation. There is still some work that needs to be done in order to figure out the cavitation effects. That being said, our 2D models were reasonably in agreement with the experiments and were validated with previous reported work. In the appendix, there are more visuals that will clarify how the pressure distribution and velocity profiles are playing a role in possibly creating cavitation in these high pressure valves.

References

Aeschlimann, V., Barre, S., & Djeridi, H. (2011). Velocity field analysis in an experimental cavitating mixing layer. *Physics of Fluid 23*, 55-105.

Amirante, R., Moscatelli, P., & Catalano, L. (2007). Evaluation of the flow forces on a direct (single stage) proportional valve by means of a computational fluid dynamic analysis. *Energy Convers Manage, 48*, 942-53.

Amirante R., Del Vescove G., & Lippolis A. (2006). Evaluation of the flow forces on an open centre directional control valve by means of a computational fluid dynamic analysis. *Energy Convers Manage , 47*, 1748–60.

Amirante, R., Del Vescove G., & Lippolis A. (2006). Flow forces analysis of open center hydraulic directional control valve sliding spool. *Energy Convers Manage, 47*, 114–31.

ANSYS Fluent v.14 [Computer software]. (2013). Available from ANSYS: http://www.ansys.com/Products/Simulation+Technology/Fluid+Dynamics/Fluid+ Dynamics+Products/ANSYS+Fluent/

Beune, Kuerten, & Schmidt. (2011). Numerical calculation and experimental validation of safety valve flows at pressures up to 600 bar. *ALCHE Journal*, *57*(12), 3285-3298. doi: 10.1002/aic.12534

BOC Water Hydraulics. (n.d.). BOC Water Hydraulics Inc. *BOC Water Hydraulics.* Retrieved from www.bocwater hydraulics.com.

Chattopadhyay, H., Kundu, A., Saha, B. K., & Gangopadhyay, T. (2012). Analysis of flow structure inside a spool type pressure regulating valve. *Energy Conversion and Management, 53*, 196–204.

Elger, D., Williams, B., Crowe, C., & Roberson, J. (2012).*Engineering fluid mechanics*. (10th ed.). NJ: John Wiley & Sons Inc.

Kikui, Shotaro, Washio, Seiichi, Takahashi, & Satoshi (2006). Observation of cavitation in oil hydraulic poppet valve. In *Proceedings of the Sixth International Symposium on Cavitation*. Wageningen, The Netherlands.

Mohammad, P., & Hossein, M. (2008). A computational study of cavitation in a hydraulic poppet valve. In *Proceedings of Fifth International Conference on Transport Phenomenon in Multiphase Systems*. Bialystok, Poland.

Passandideh_Fard, M., & Roohi, E. (2008). Transient simulation of cavitating flows using a modified volume-of-fluid (VOF) technique. *Journal of Fluids Engineering.*

Pritchard, P., & Leylegian, J. (2011). *Fox and McDonald's introduction to fluid mechanics*. (8th ed.). NJ: John Wiley & Sons Inc.

Singhal, N. H., Athavale, A. K., Li, M., & Jiang, Y. (2002). Mathematical basis and validation of the full cavitation model. *Journal of Fluids Engineering*, *124*, 1-8.

Skousen, P. (2007). *Valve handbook*. New York, NY: McGraw Hill.

Takahashi, S., Washio, S., Umeura, K., & Okazaki, A. (2003). Experimental study on cavitation starting at and flow characteristics close to the point of separation. In *Proceedings of the 5th International Symposium on Cavitation*. Osaka, Japan.

Tu, J., Yeoh, G. H., & Liu, C. (2008). *Computational fluid dynamics*. Burlington, MA: Elsevier.

Valdés, J.R., Miana, M.J., Núñez, J.L., & Pütz, T. (2008). Reduced order model for estimation of fluid flow and flow forces in hydraulic proportional valves. *Energy Conversion and Management, 49*, 1517–1529.

Valve Manufacturers Association of America. (n.d.). The Valve Manufacturers Association of America. *The Valve Manufacturers Association of America.* Retrieved from www.vma.org.

Wiesche, S. (2005). Numerical simulation of cavitation effects behind obstacles and in an automotive fuel jet pump. *Heat Mass Transfer*, *41*, 615-624.

Xu, H., Guang, Z.M., & Qi, Y.Y. (2011). Hydrodynamic characterization and optimization of Contra-push check valve by numerical simulation. *Annals of Nuclear Energy* 38, 1427–1437.

Yatsco, M. (2011). *Numerical analysis and wind tunnel validation of wind deflectors for rooftop solar panel racks* (Master's thesis) Youngstown State University, Youngstown, OH.

Appendix

A1. Annual shipment of various valve in millions from 2004-2013 (Source: www.vma.org)

	2003	2004	2005	2006	2007	2008	2009	2010	2011	2012
Pressure-Relief Valves	183.0	184.2	201.2	213.0	219.5	230.5	219.0	222.9	226.0	239.5
Automated Valves	1000.0	1006.3	1083.8	1147.0	1181.4	1240.5	1182.5	1219.1	1231.5	1300.0
Plug Valves	210.0	211.3	231.4	244.5	251.0	263.6	250.4	256.0	260.0	275.5
Industrial Butterfly Valves	295.0	296.9	329.1	348.0	358.5	376.4	357.6	361.0	366.5	388.5
Ball Valves	565.0	568.6	633.9	670.0	670.0	690.0	724.5	688.3	706.8	717.5	760.5
Gate, Globe and Check Valves	466.5	469.5	512.0	540.0	556.0	583.9	554.6	567.9	576.5	611.0

A2. End user industry share of market, (Source: www.vma.org)

	Chemical	Water & Sewage	Power Generation & Co-Generation	Petroleum Production	Petroleum Refining	Pulp & Paper	Oil & Gas Trans.	Commercial Const.	Food & Beverage	Gas Distribution	Iron & Steel	Other
2012	17.1	16.8	13.3	12.4	11.7	6.7	5.8	4.5	2.4	2.5	2.0	4.8
2013	17.2	16.2	14.5	12	11.9	6.5	5.9	4.4	2.4	2.4	2.0	4.5
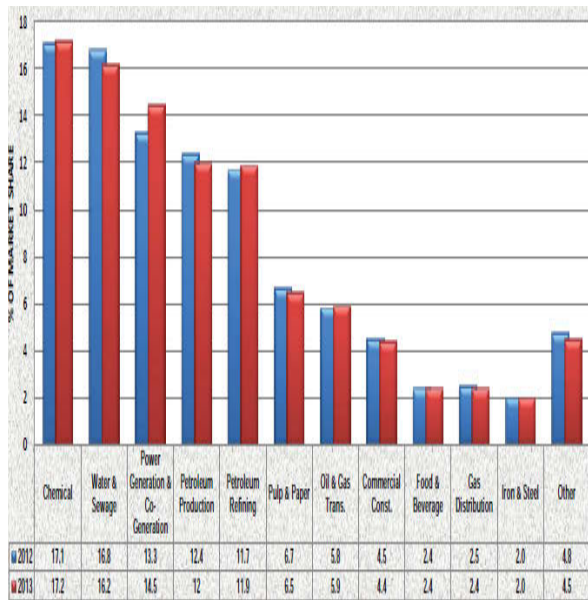
A3 Figure dynamic pressure contours for 1 inch opening nose to side

Full Opening 1 inch

Nose to Side
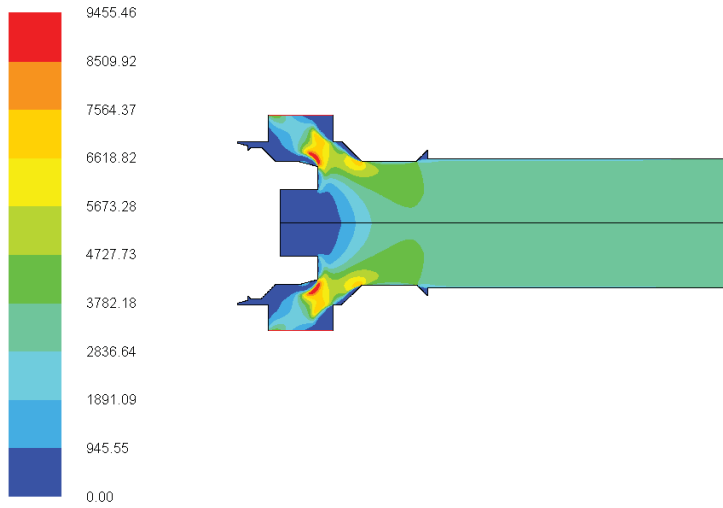
Contours of Dynamic Pressure (psi)

Jun 30, 2013
ANSYS FLUENT 14.0 (axi, dp, pbns, ske)

A4 Figure Total pressure contours for 1 inch opening nose to side
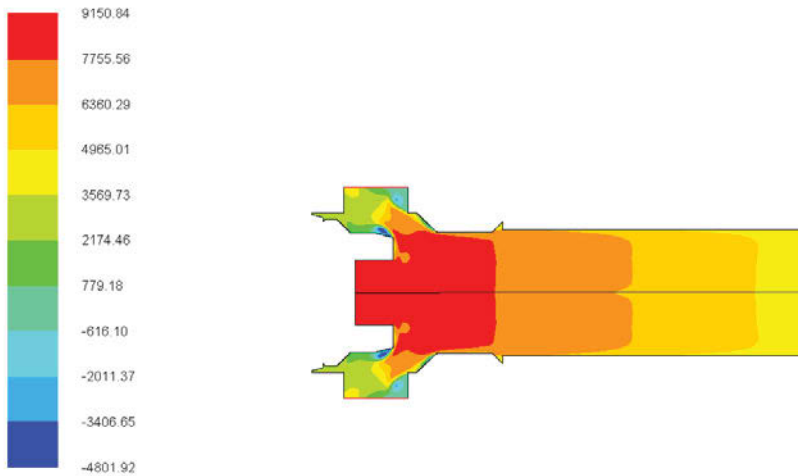
Contours of Total Pressure (psi)
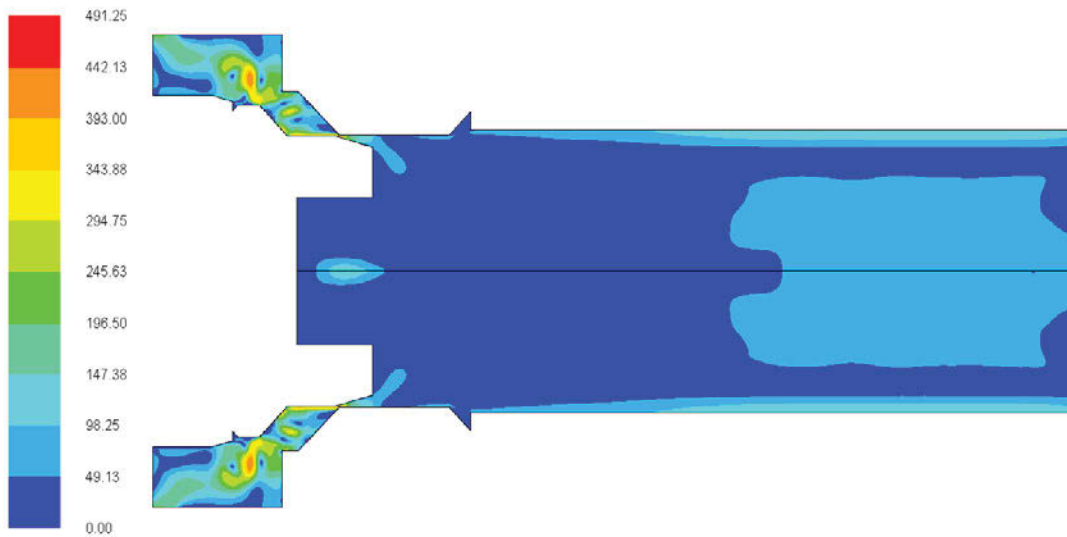
Sep 04, 2013
ANSYS FLUENT 14.0 (axi, dp, pbns, ske)

A5 Figure Contours for Velocity Magnitude for 1 inch opening nose to side
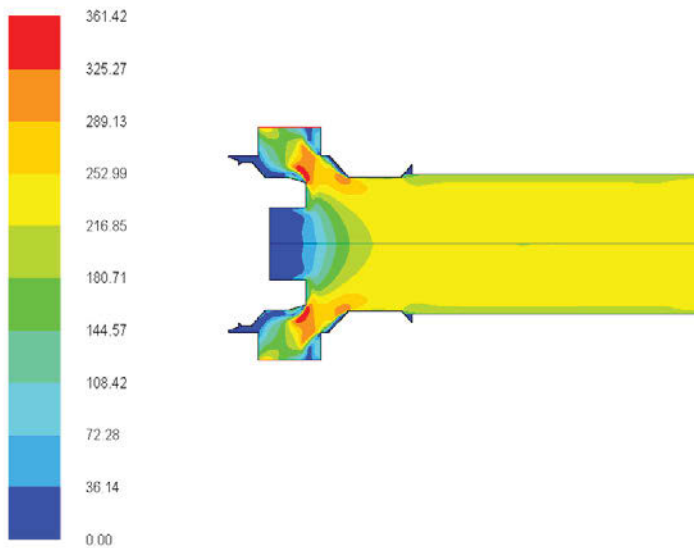
Contours of Velocity Magnitude (m/s)
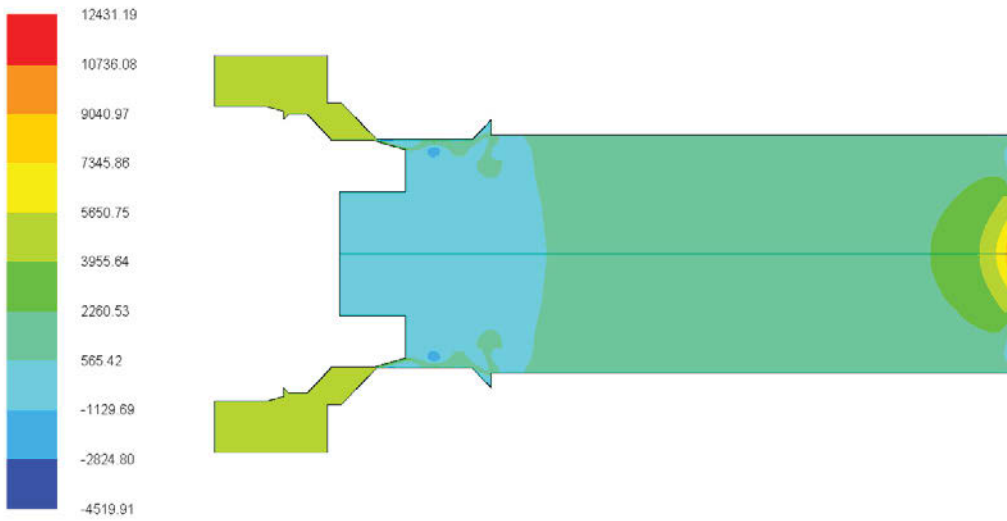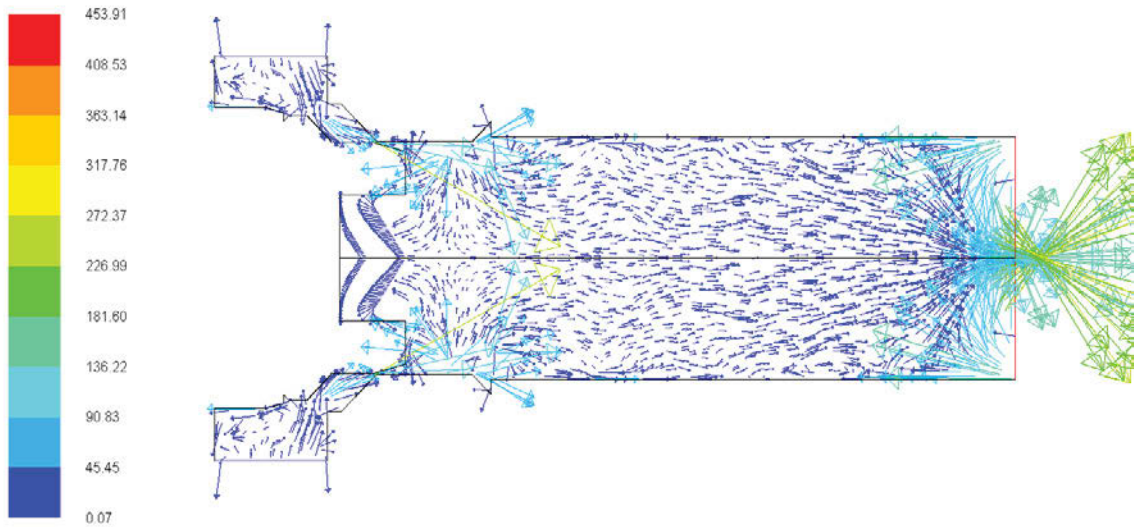
Jun 30, 2013
ANSYS FLUENT 14.0 (axi, dp, pbns, ske)
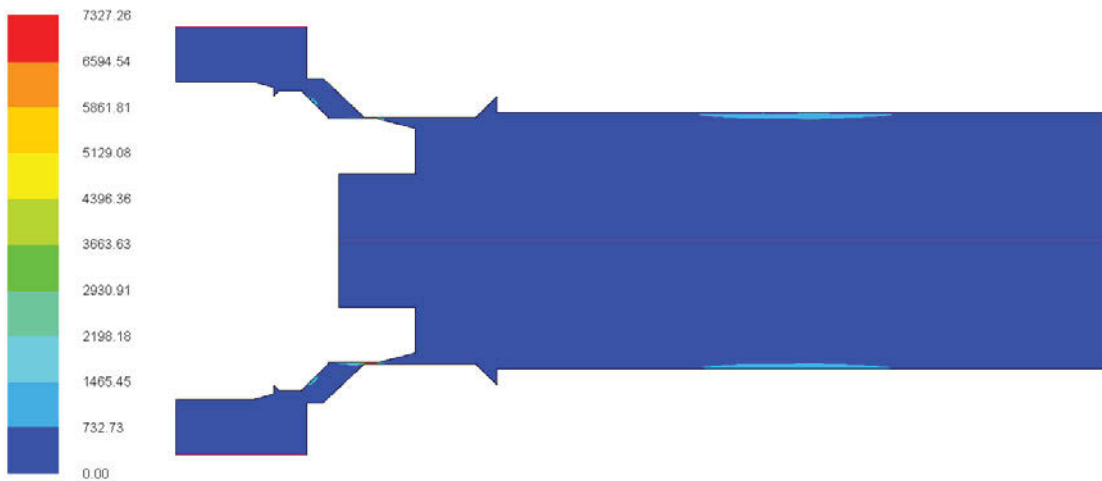
A6 Figure for Velocity vector for 1 inch opening nose to side
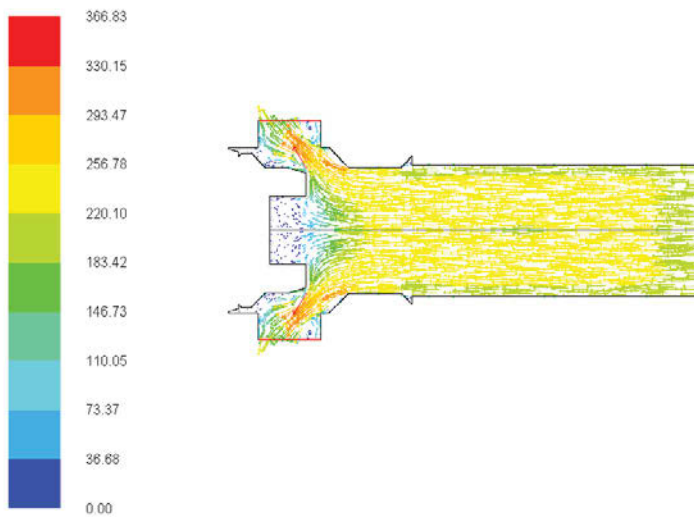
Velocity Vectors Colored By Velocity Magnitude (m/s)

Jun 30, 2013
ANSYS FLUENT 14.0 (axi, dp, pbns, ske)

Side to Nose

A7 Figure Contours of dynamic pressure for 1 inch opening side to nose

Contours of Dynamic Pressure (psi)   Jun 30, 2013
                                    ANSYS FLUENT 14.0 (axi, dp, pbns, ske)

A8 Figure for velocity vector for 1 inch opening side to nose
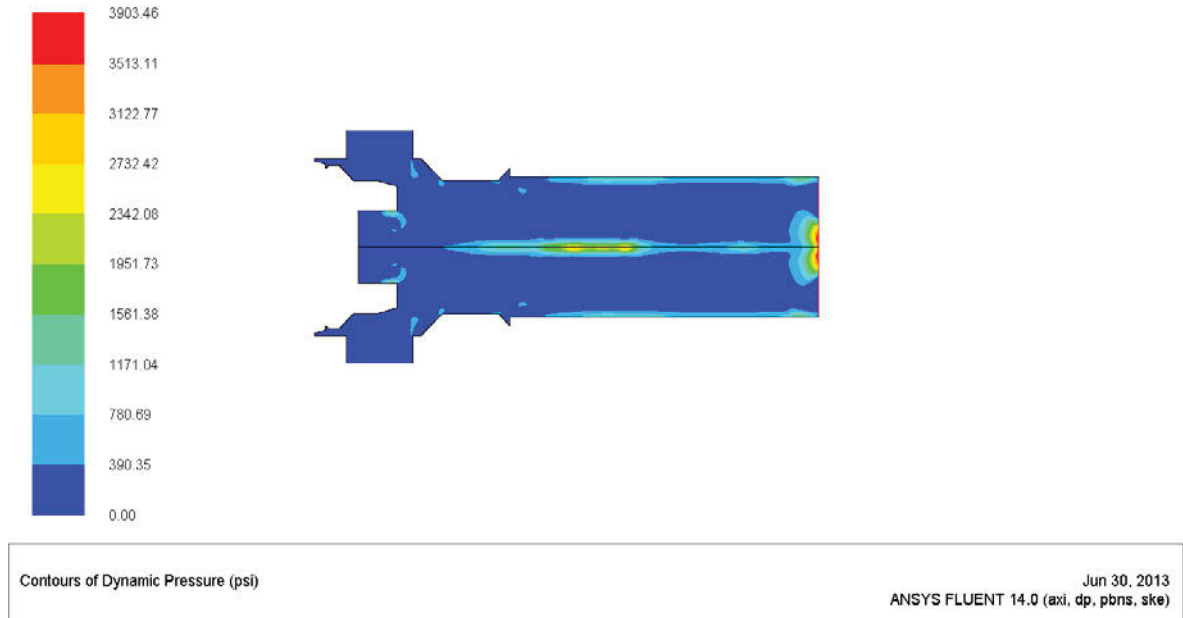
Velocity Vectors Colored By Velocity Magnitude (m/s)   Jun 30, 2013
                                    ANSYS FLUENT 14.0 (axi, dp, pbns, ske)
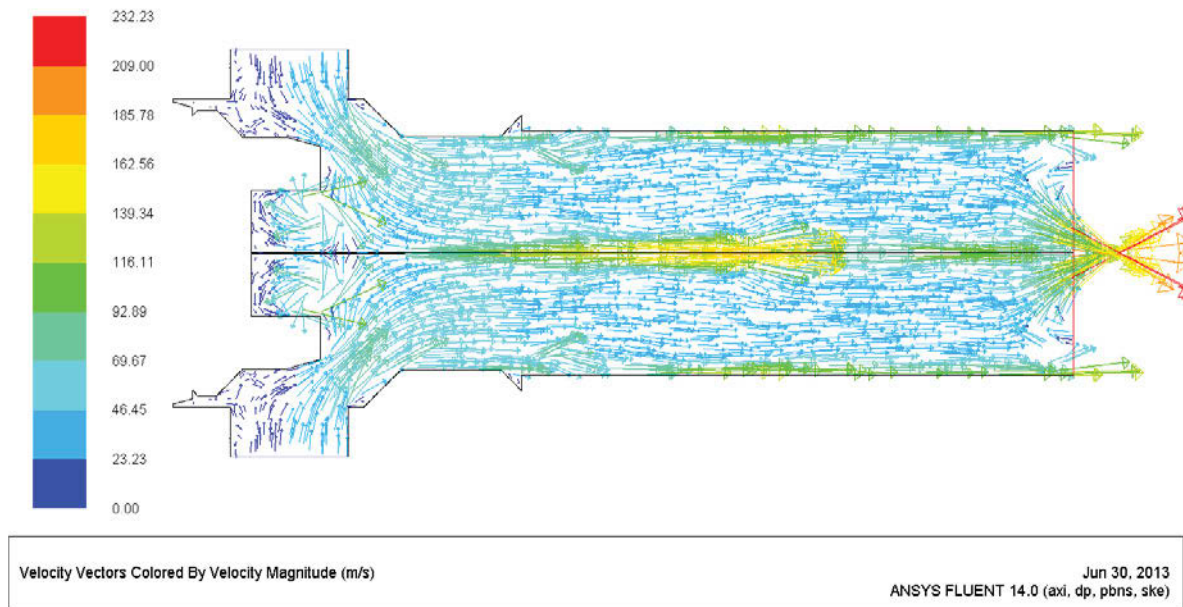
A9 Figure Contours of total pressure for 1 inch opening for side to nose
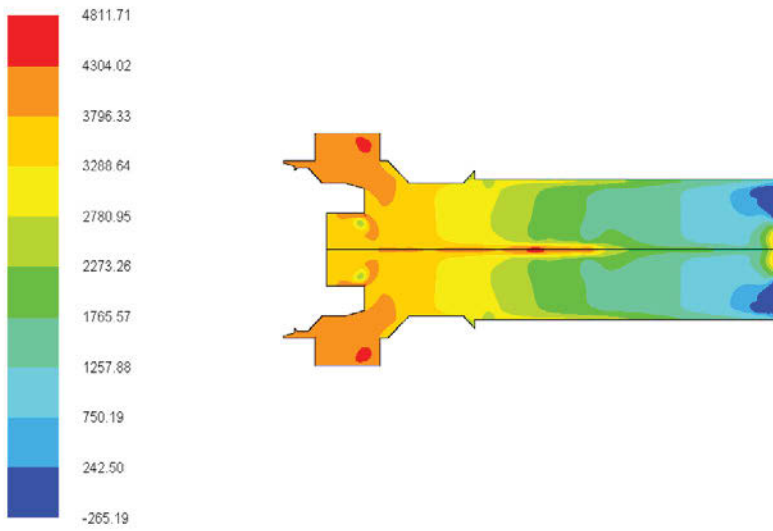
Contours of Total Pressure (psi)
Jun 30, 2013
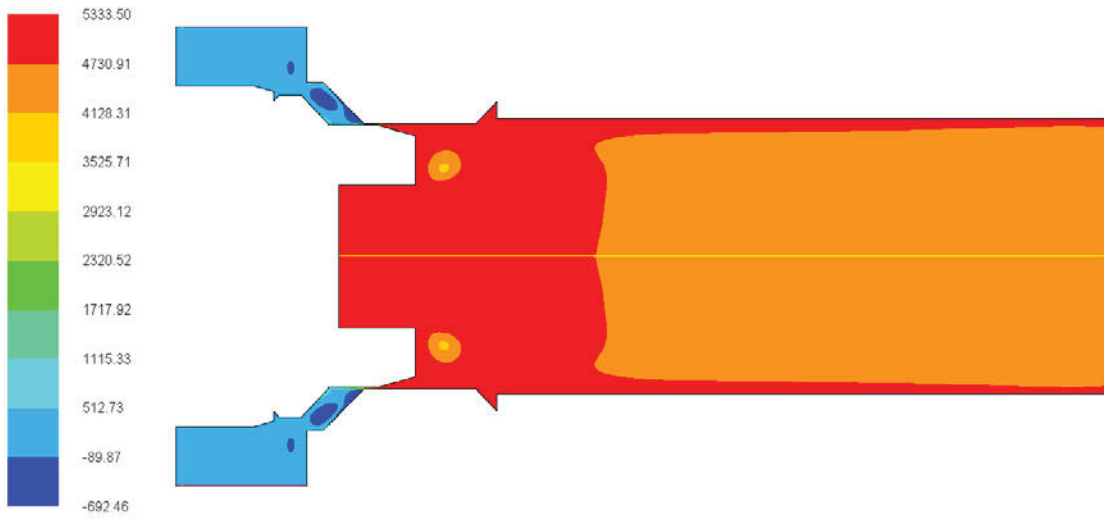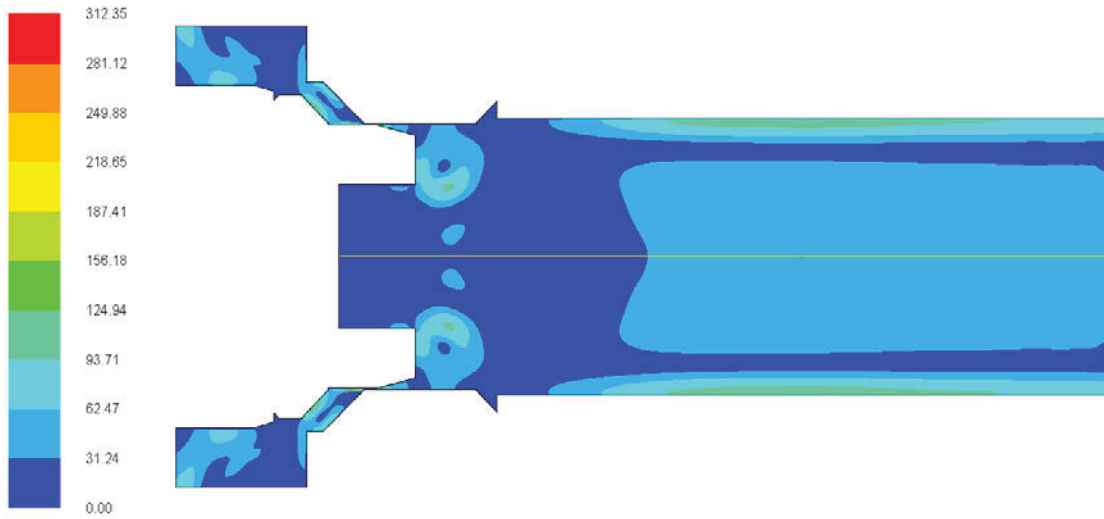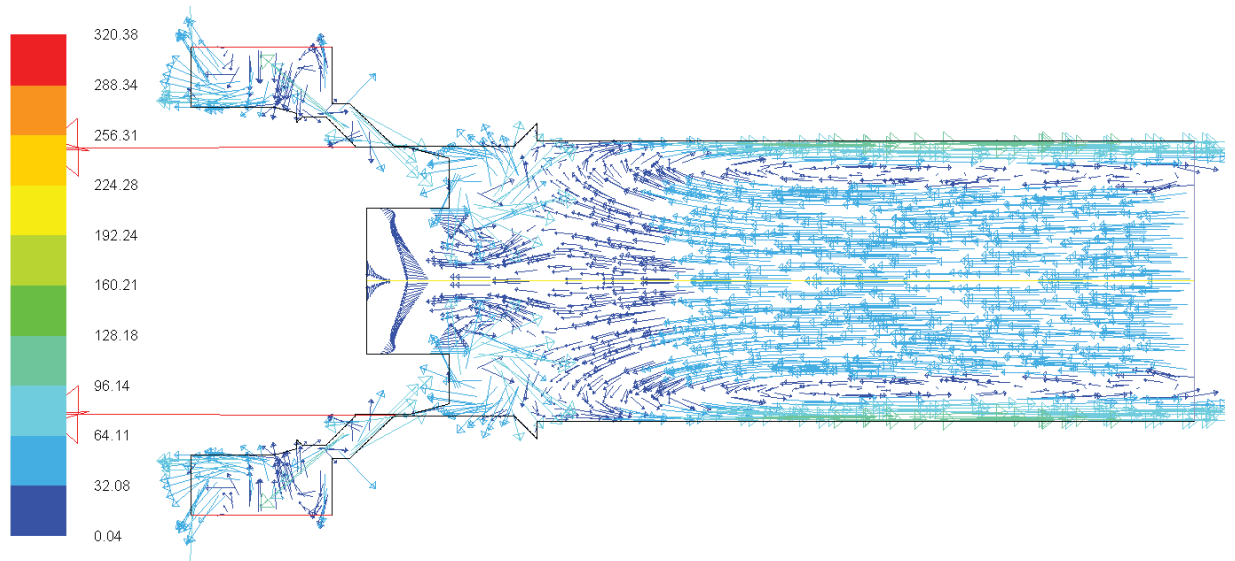ANSYS FLUENT 14.0 (axi, dp, pbns, ske)

Opening 0.3 inch

Nose to Side

A10 Figure Contours of dynamic pressure for 0.3 inch opening nose to side
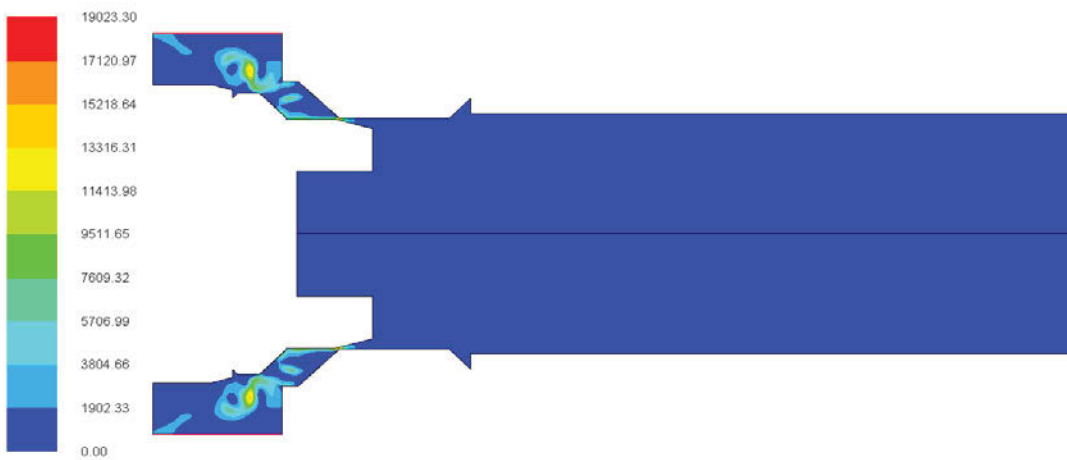
Contours of Dynamic Pressure (psi)
Jun 29, 2013
ANSYS FLUENT 14.0 (axi, dp, pbns, skw)

A11 Figure Contours of total pressure for 0.3 inch opening nose to side
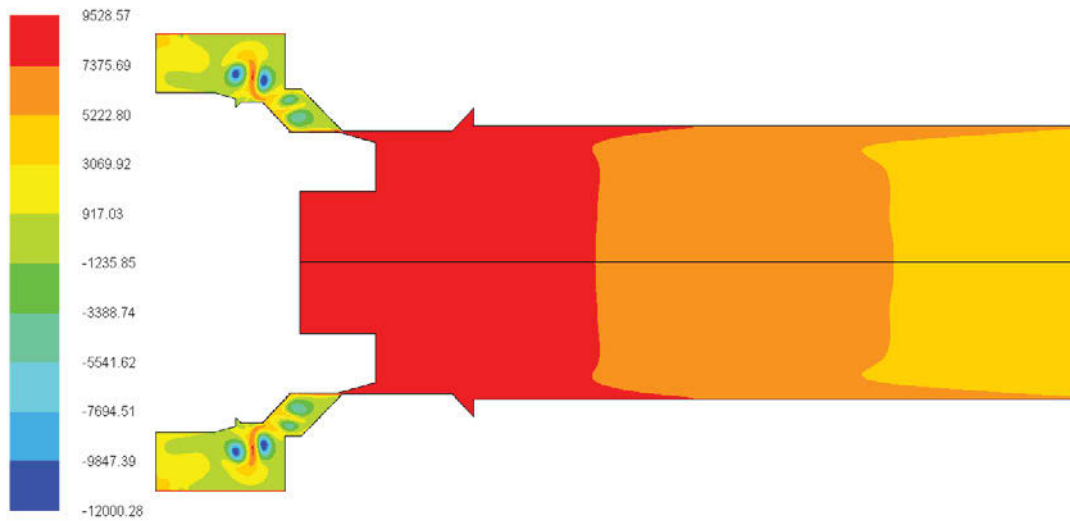
Contours of Total Pressure (psi)

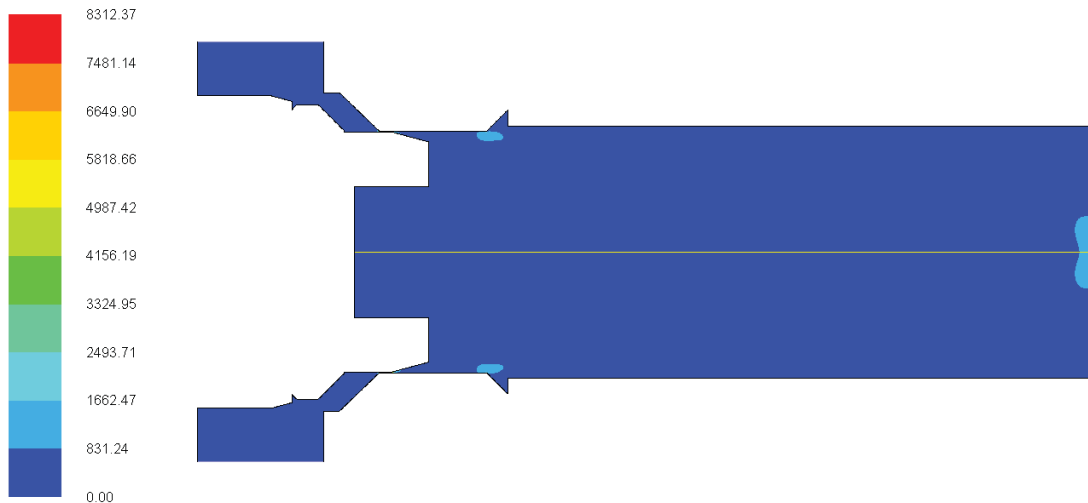Jun 29, 2013
ANSYS FLUENT 14.0 (axi, dp, pbns, skw)

A12 Figure Velocity vector for opening of 0.3 inch nose to side
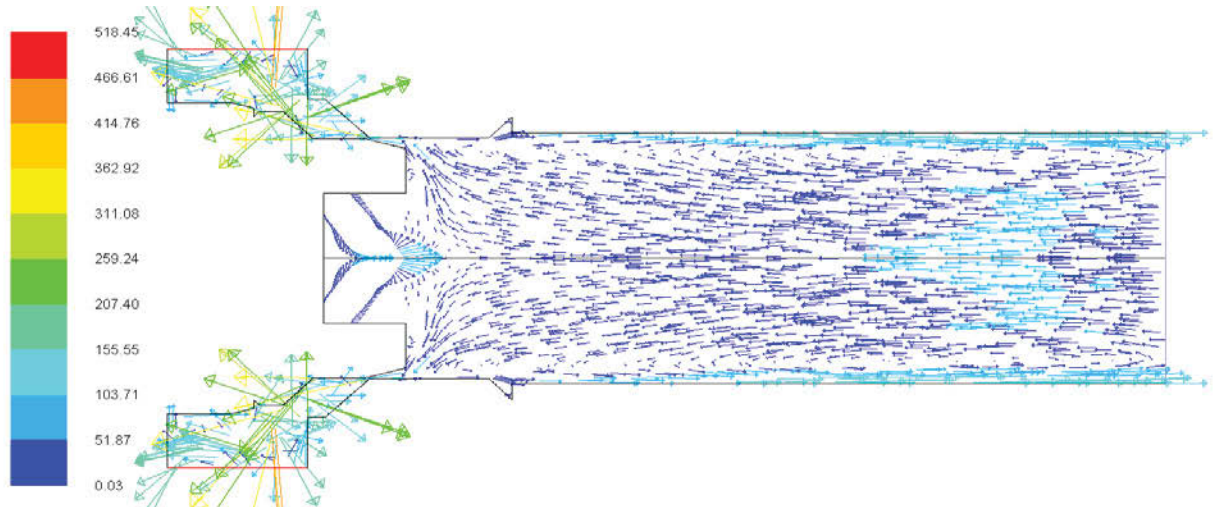
Velocity Vectors Colored By Velocity Magnitude (m/s)

Jun 29, 2013
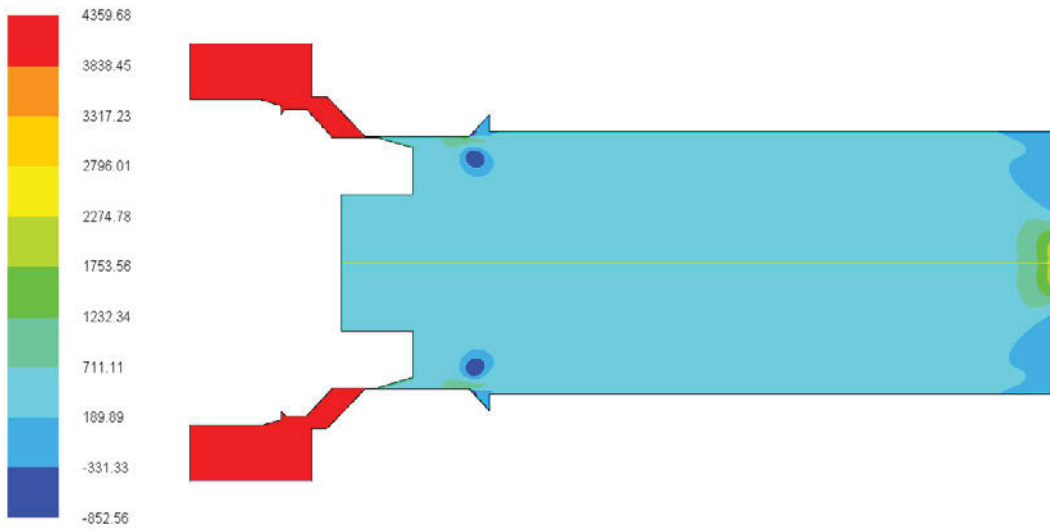ANSYS FLUENT 14.0 (axi, dp, pbns, skw)

A13 Figure Velocity Magnitude for opening 0.3 inch nose to side

Contours of Velocity Magnitude (m/s)
Jun 29, 2013
ANSYS FLUENT 14.0 (axi, dp, pbns, skw)

Side to Nose

A14 Figure Contours of dynamic pressure for 0.3 inch opening side to nose
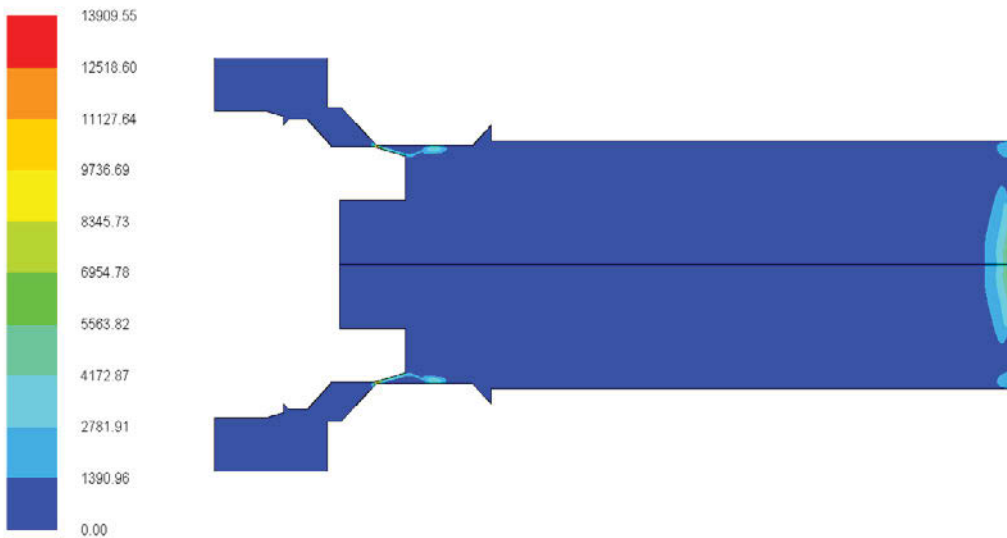
Contours of Dynamic Pressure (psi)
Jun 29, 2013
ANSYS FLUENT 14.0 (axi, dp, pbns, skw)

A15 Figure Contours of total pressure for 0.3 inch opening side to nose

Contours of Total Pressure (psi)

Jun 29, 2013
ANSYS FLUENT 14.0 (axi, dp, pbns, skw)

A16 Figure Contours of Velocity magnitude for 0.3 inch opening side to nose
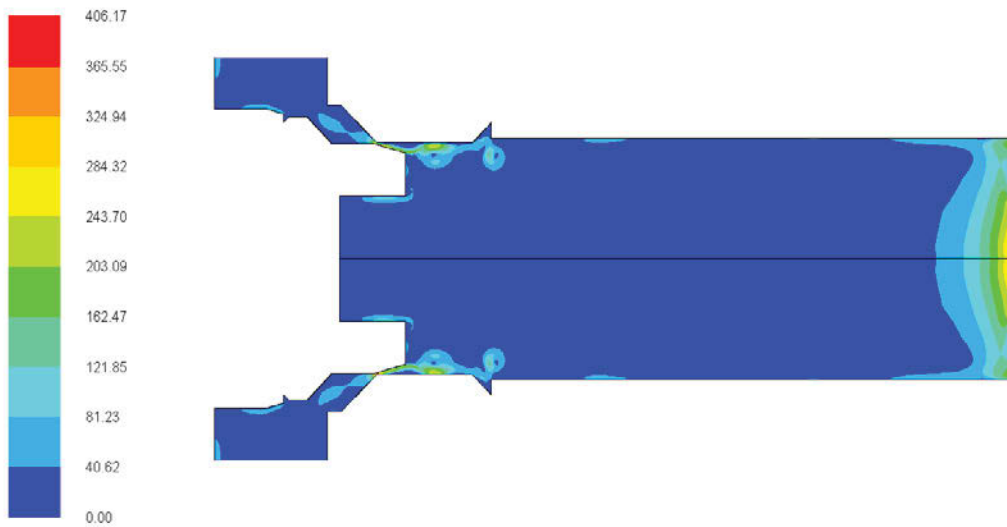
Contours of Velocity Magnitude (m/s)

Jun 29, 2013
ANSYS FLUENT 14.0 (axi, dp, pbns, skw)

A17 Figure Velocity vectors for 0.3 inch opening side to nose

Velocity Vectors Colored By Velocity Magnitude (m/s)

Jun 29, 2013
ANSYS FLUENT 14.0 (axi, dp, pbns, skw)

Opening 0.2 inch

Nose to Side

A18 Figure Contours of dynamic pressure for opening 0.2 inch nose to side

Contours of Dynamic Pressure (psi)
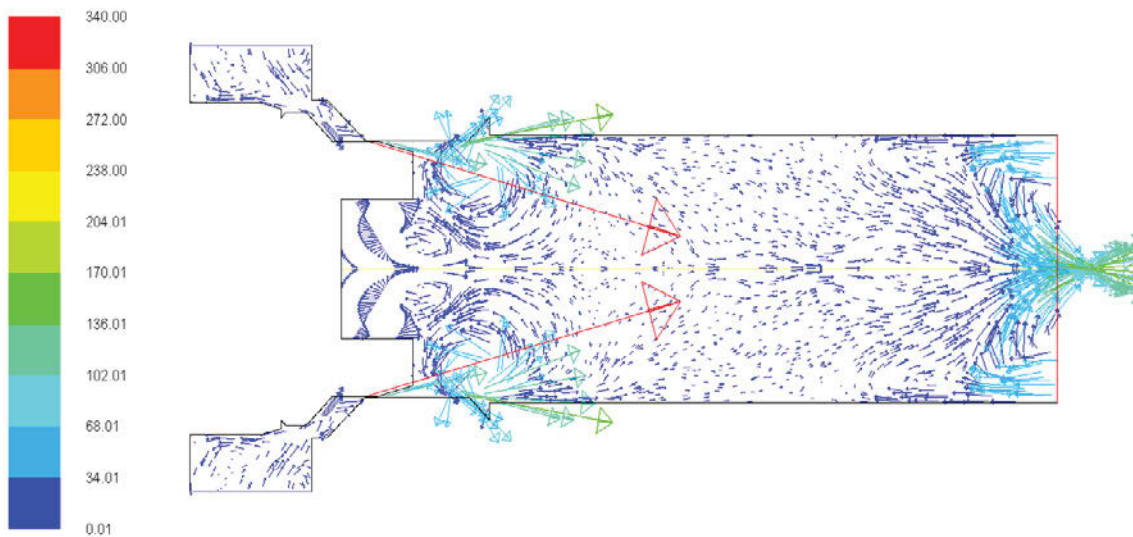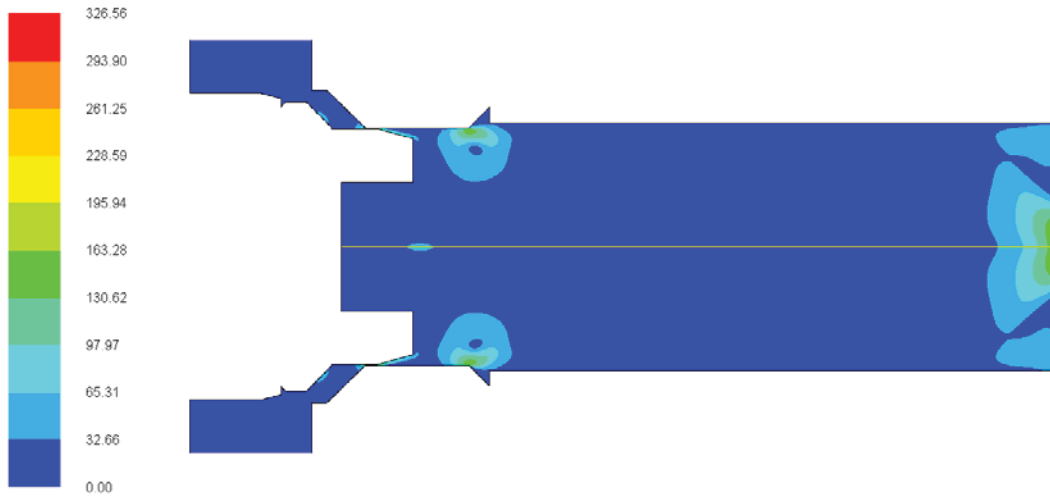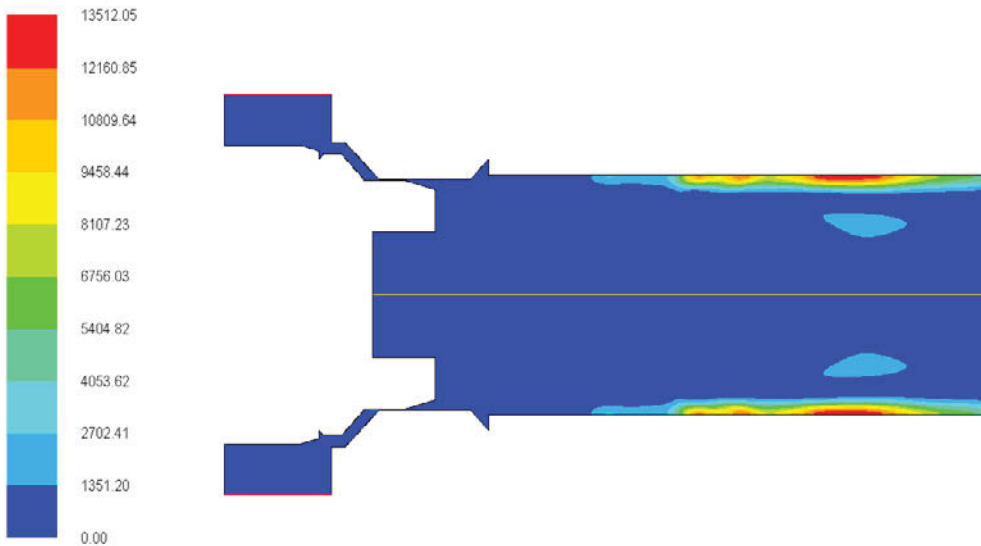
Jun 28, 2013
ANSYS FLUENT 14.0 (axi, dp, pbns, ske)

A19 Figure Contours of total pressure for opening 0.2 inch nose to side

A20 Figure Contours of velocity magnitude for opening 0.2 inch nose to side

A21 Figure Velocity vector for opening of 0.2 inch nose to side

Velocity Vectors Colored By Velocity Magnitude (m/s)

Jun 28, 2013
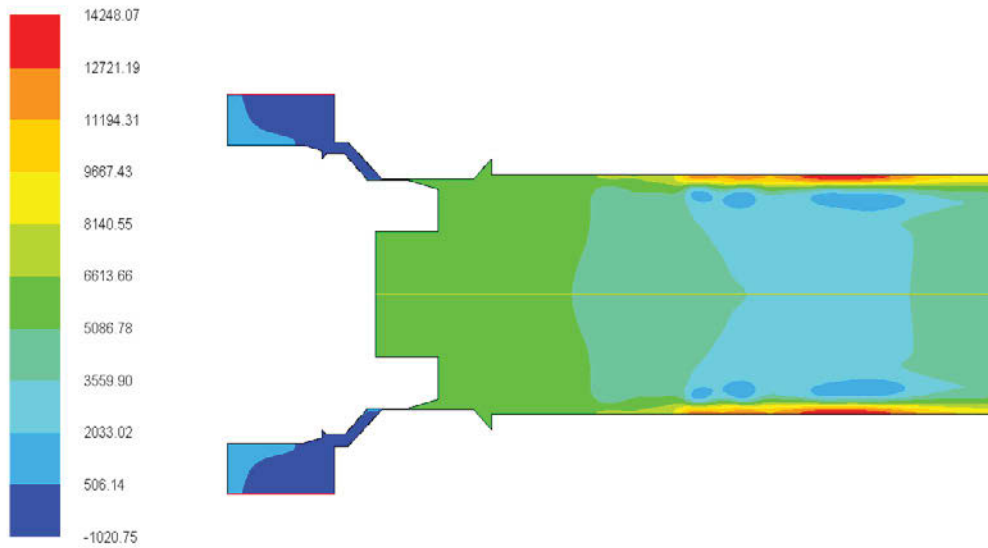ANSYS FLUENT 14.0 (axi, dp, pbns, ske)

Side to Nose

A22 Figure Contours of dynamic pressure for opening 0.2 inch side to nose

Contours of Dynamic Pressure (psi)

Jun 28, 2013
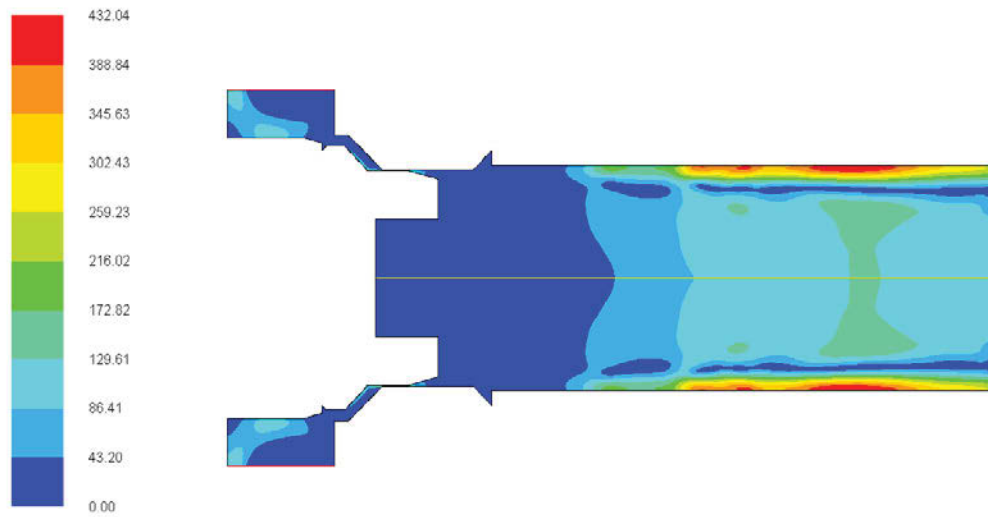ANSYS FLUENT 14.0 (axi, dp, pbns, ske)

A23 Figure Contours of total pressure for opening 0.2 inch side to nose

Contours of Total Pressure (psi)   Jun 28, 2013
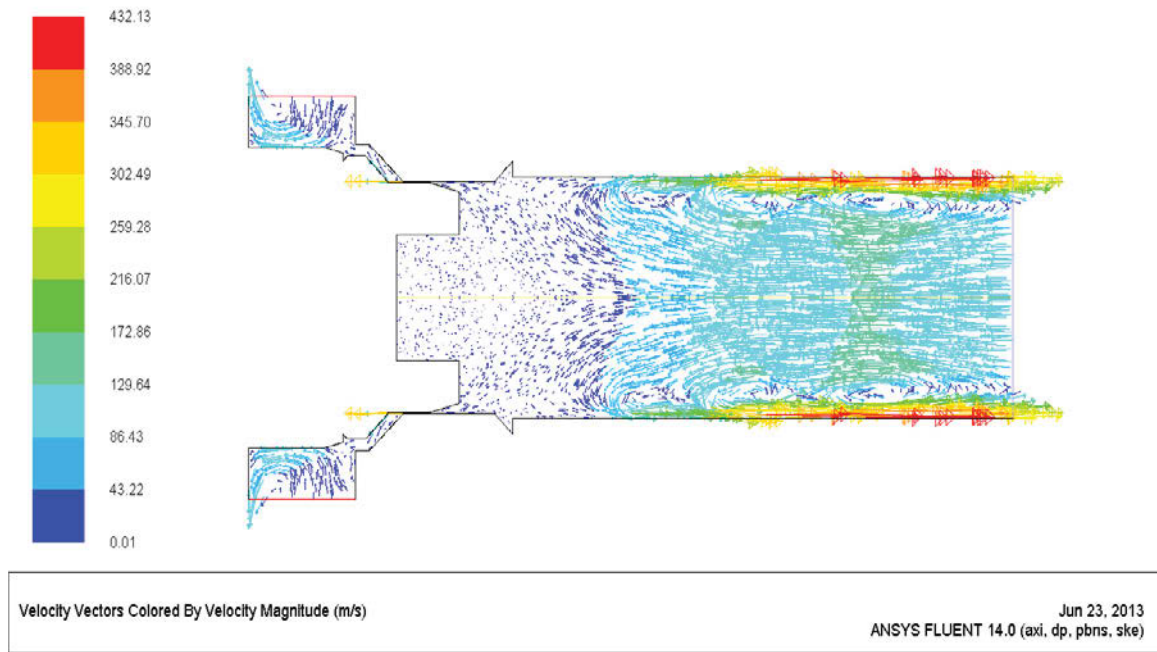   ANSYS FLUENT 14.0 (axi, dp, pbns, ske)

A24 Figure Velocity vector for opening of 0.2 inch side to nose

Velocity Vectors Colored By Velocity Magnitude (m/s)   Jun 28, 2013
                                              ANSYS FLUENT 14.0 (axi, dp, pbns, ske)

A25 Figure Contours of velocity magnitude for opening of 0.2 inch side to nose

Contours of Velocity Magnitude (m/s)   Jun 28, 2013
                                                        ANSYS FLUENT 14.0 (axi, dp, pbns, ske)

Opening 0.1 inch

Nose to Side

A26 Figure Contours of dynamic pressure for opening 0.1 inch nose to side

Contours of Dynamic Pressure (psi)   Jun 23, 2013
                                                        ANSYS FLUENT 14.0 (axi, dp, pbns, ske)

A27 Figure Contours of total pressure for opening 0.1 inch nose to side

Contours of Total Pressure (psi)
Jun 23, 2013
ANSYS FLUENT 14.0 (axi, dp, pbns, ske)

A 28 Figure Contours of velocity magnitude for opening 0.1 inch nose to side

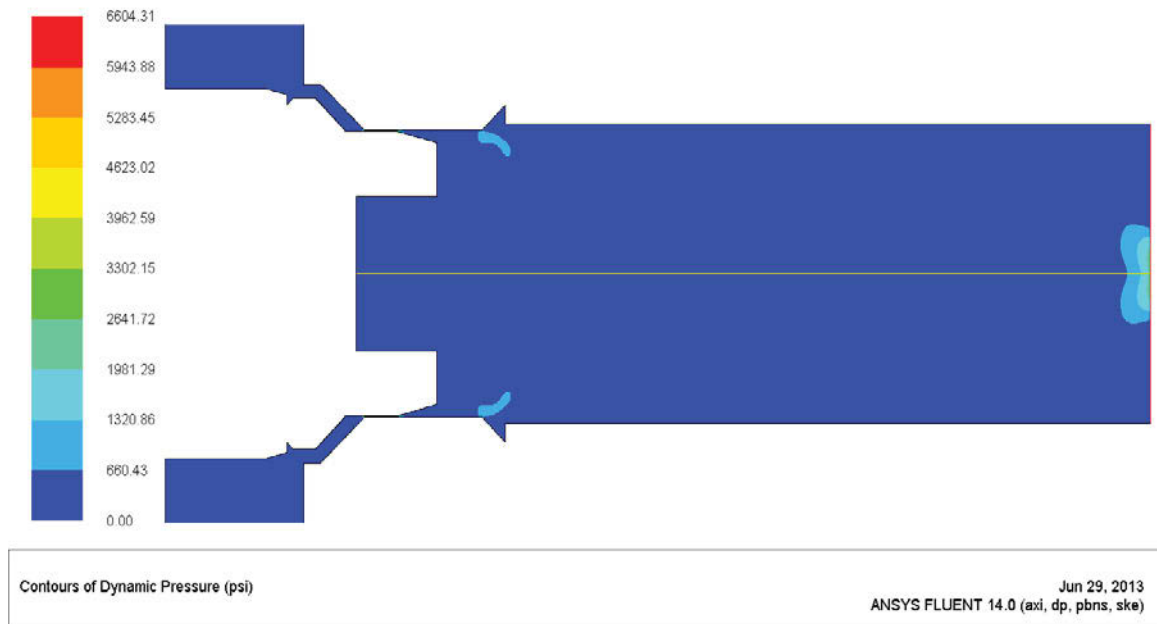Contours of Velocity Magnitude (m/s)
Jun 23, 2013
ANSYS FLUENT 14.0 (axi, dp, pbns, ske)

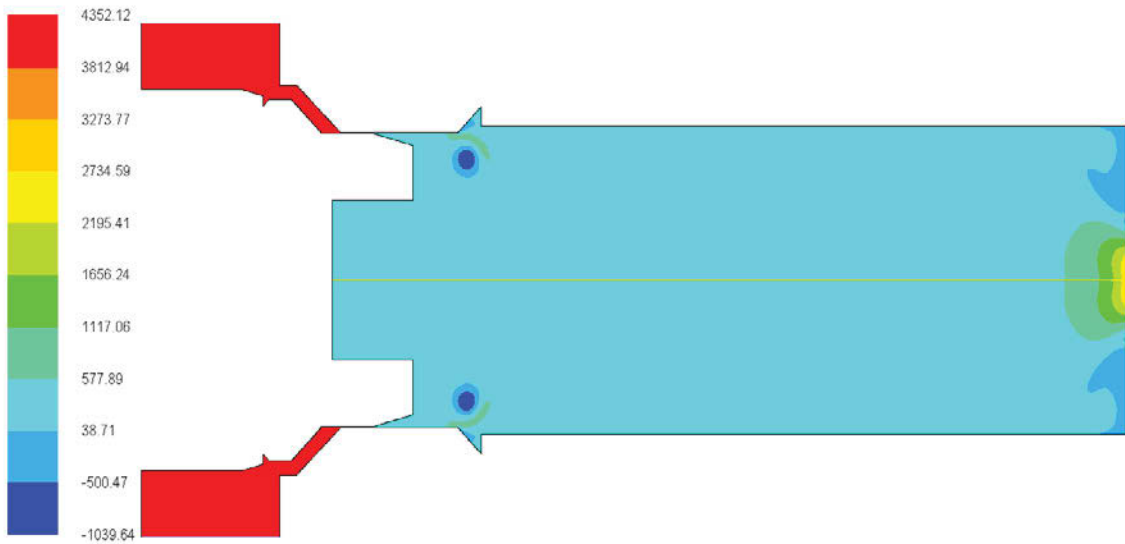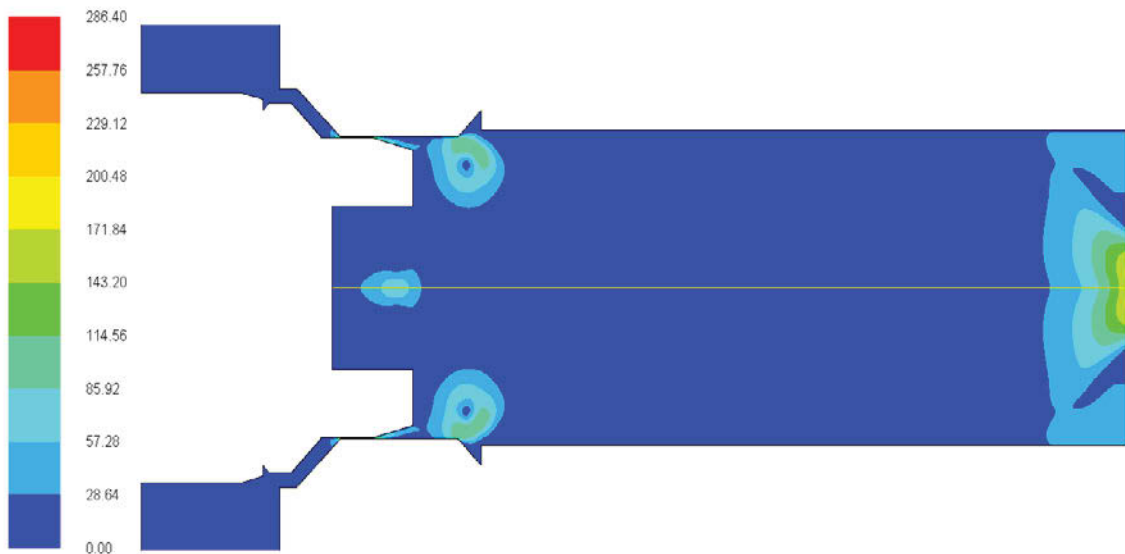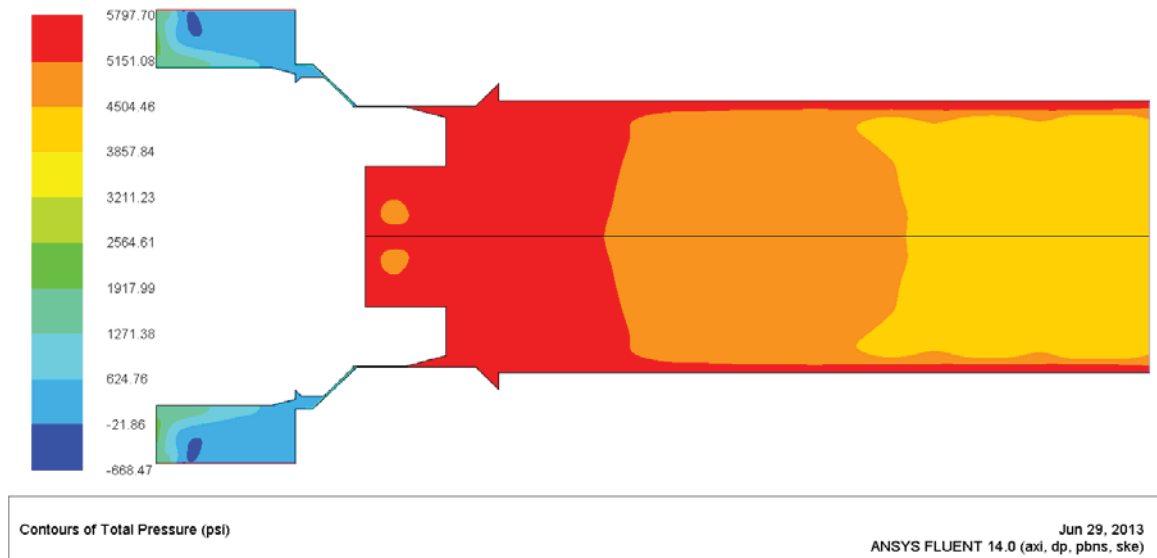A29 Figure velocity vectors for opening 0.1 inch nose to side

Velocity Vectors Colored By Velocity Magnitude (m/s)

Jun 23, 2013
ANSYS FLUENT 14.0 (axi, dp, pbns, ske)

Side to Nose

A30 Figure Contours of dynamic pressure for opening 0.1 inch side to nose

Contours of Dynamic Pressure (psi)

Jun 29, 2013
ANSYS FLUENT 14.0 (axi, dp, pbns, ske)

A31 Figure Contours of total pressure for opening 0.1 inch side to nose

Contours of Total Pressure (psi)

A32 Figure Contours of velocity magnitude for opening 0.1 inch side to nose

Contours of Velocity Magnitude (m/s)

A 33 Figure Velocity vector for opening 0.1 inch side to nose

Velocity Vectors Colored By Velocity Magnitude (m/s)   Jun 29, 2013
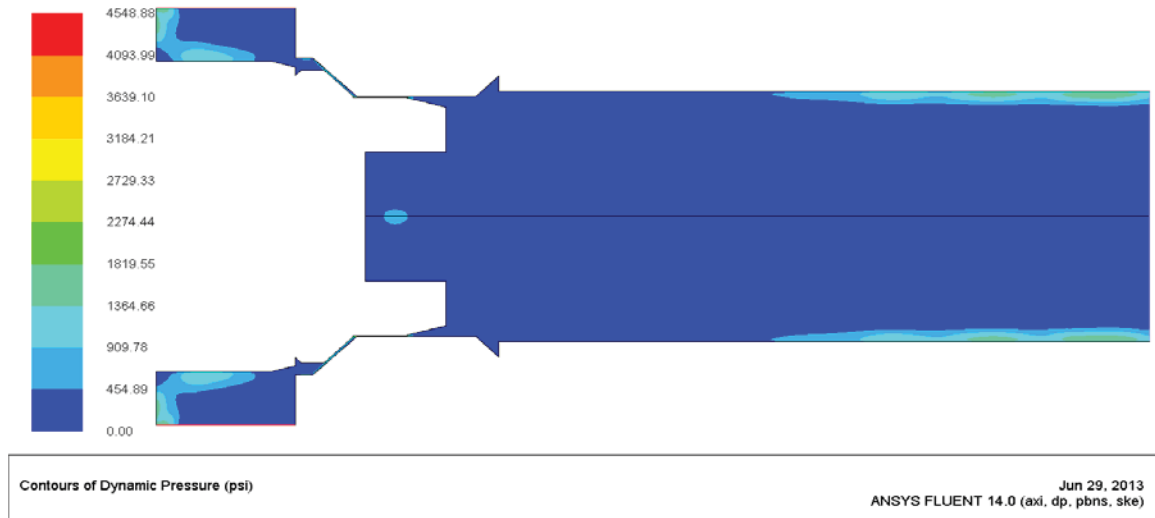ANSYS FLUENT 14.0 (axi, dp, pbns, ske)
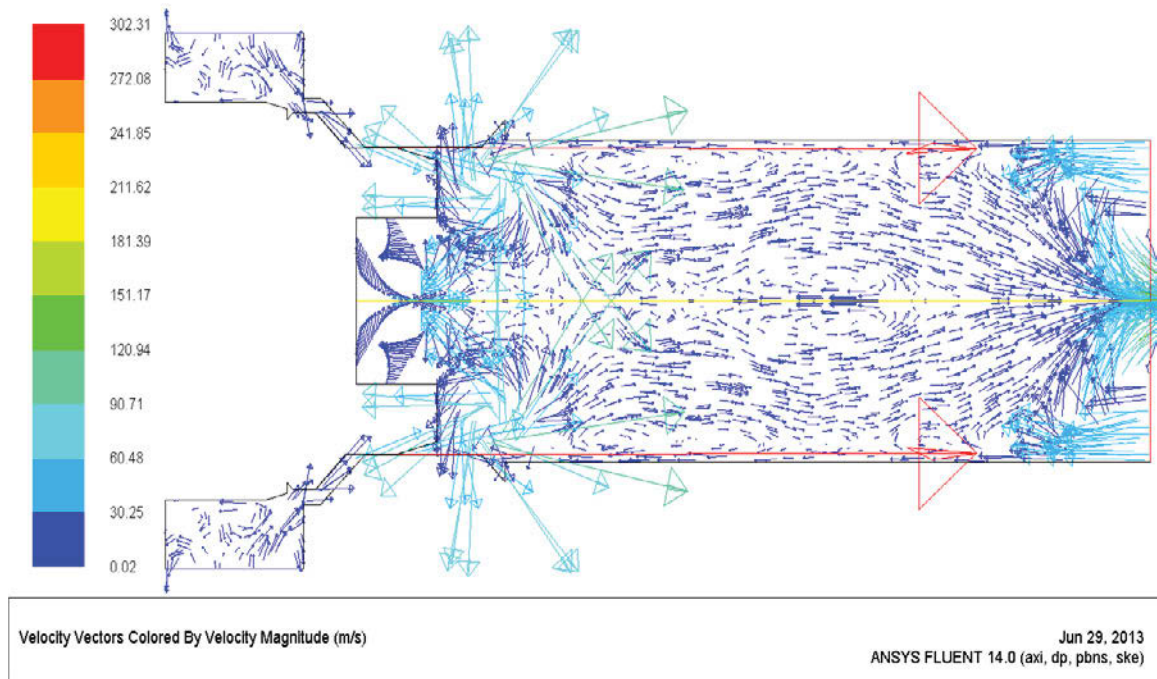
Opening 0.0125 inch

Nose to side

A34 Figure Contours of dynamic pressure for opening 0.0125 inch nose to side

Contours of Total Pressure (psi)   Jun 29, 2013
ANSYS FLUENT 14.0 (axi, dp, pbns, ske)

A35 Figure Contours of total pressure for opening 0.0125 incg nose to side

Contours of Dynamic Pressure (psi)

Jun 29, 2013
ANSYS FLUENT 14.0 (axi, dp, pbns, ske)

A36 Figure Contours of velocity magnitude for opening 0.0125 inch nose to side

Contours of Velocity Magnitude (m/s)

Jun 29, 2013
ANSYS FLUENT 14.0 (axi, dp, pbns, ske)

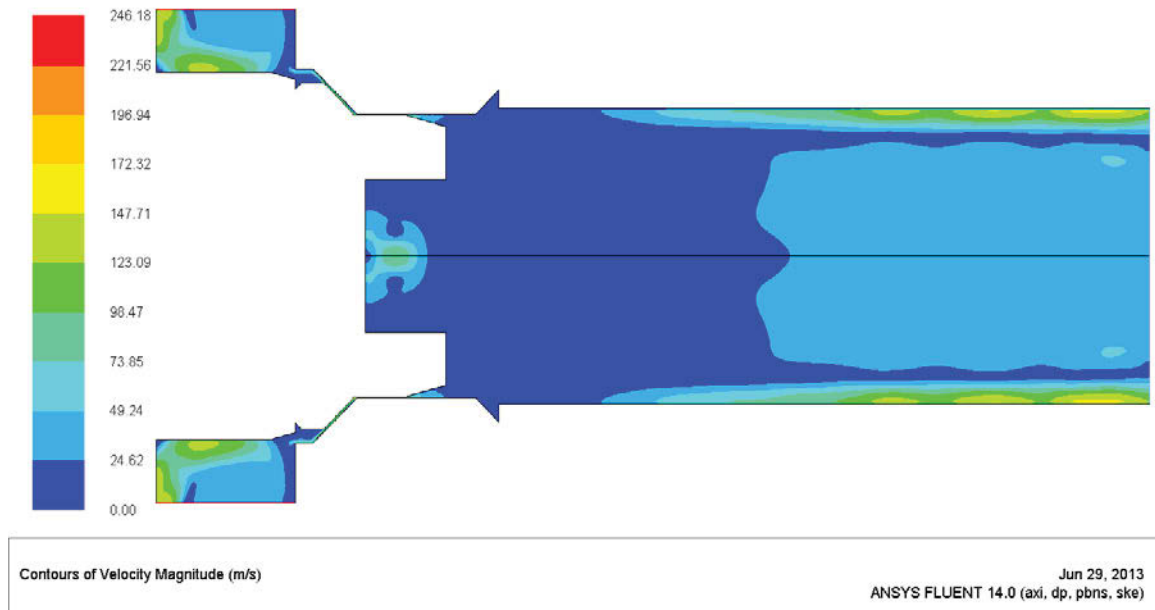A37 Figure Velocity vectors for opening 0.0125 inch nose to side

Velocity Vectors Colored By Velocity Magnitude (m/s)

Jun 29, 2013
ANSYS FLUENT 14.0 (axi, dp, pbns, ske)
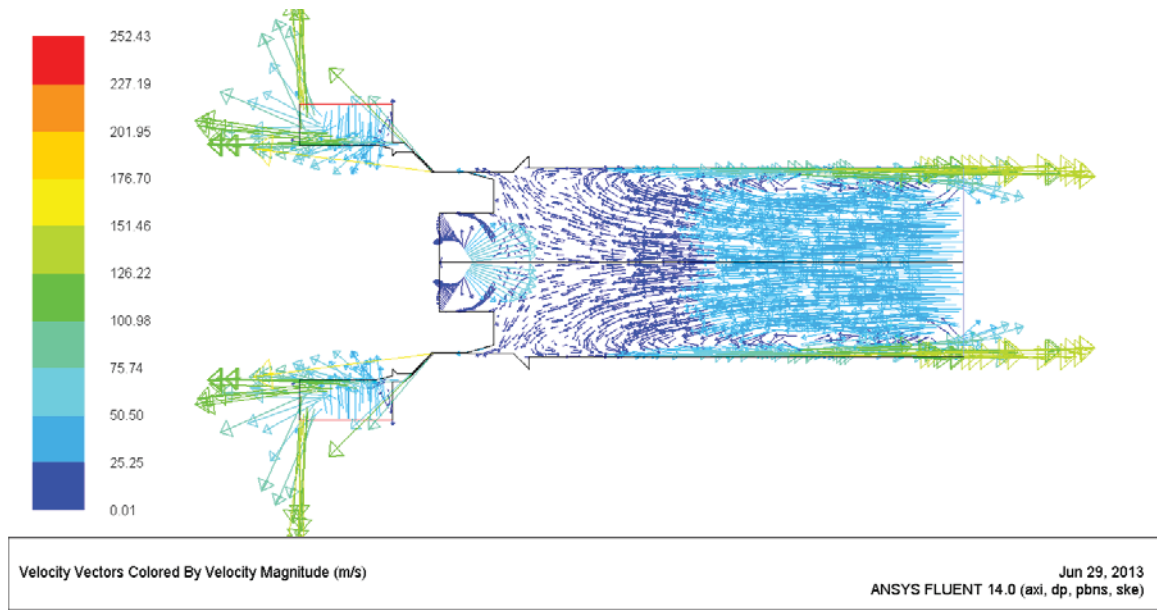
Side to Nose

A38 Figure Contours of dynamic pressure for opening 0.0125 inch side to nose
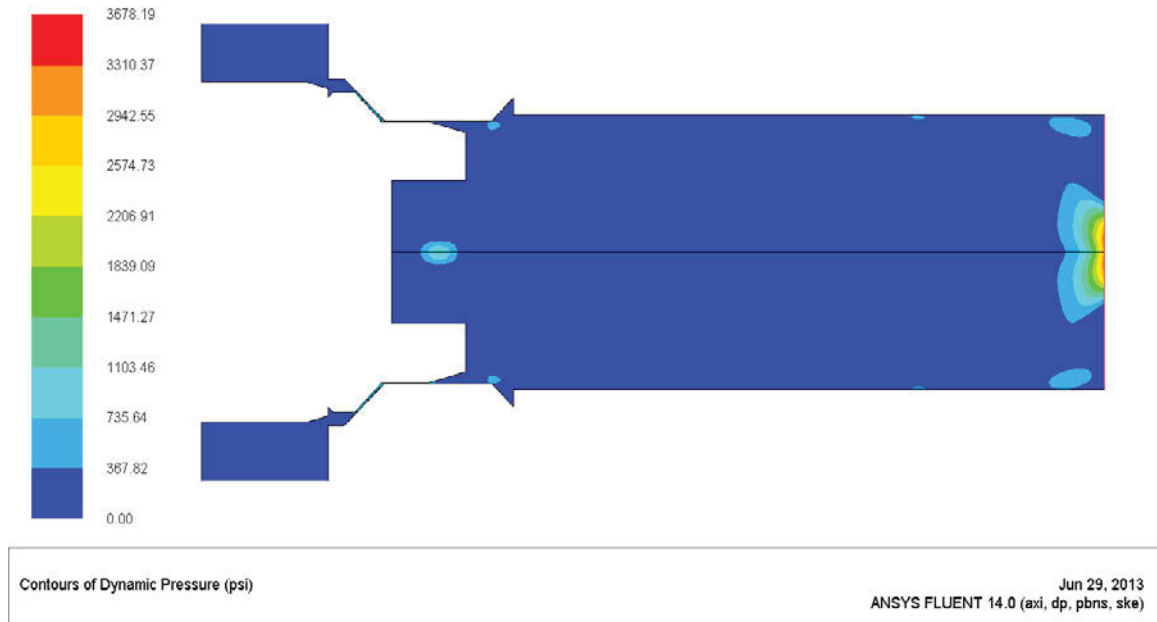
Contours of Dynamic Pressure (psi)

Jun 29, 2013
ANSYS FLUENT 14.0 (axi, dp, pbns, ske)

A39 Figure Contours of total pressure for opening 0.0125 inch side to nose

Contours of Total Pressure (psi)   Jun 29, 2013
                                                     ANSYS FLUENT 14.0 (axl, dp, pbns, ske)

A40 Figure Contours of velocity magnitude for opeing 0.0125 inch side to nose
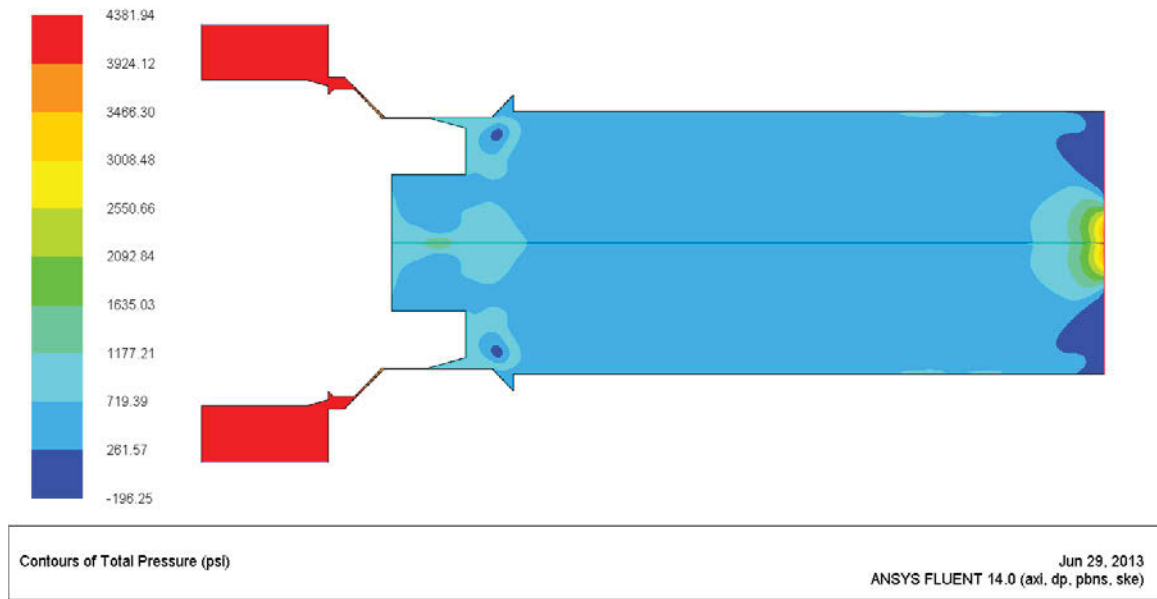
Contours of Velocity Magnitude (m/s)   Jun 29, 2013
                                                     ANSYS FLUENT 14.0 (axi, dp, pbns, ske)
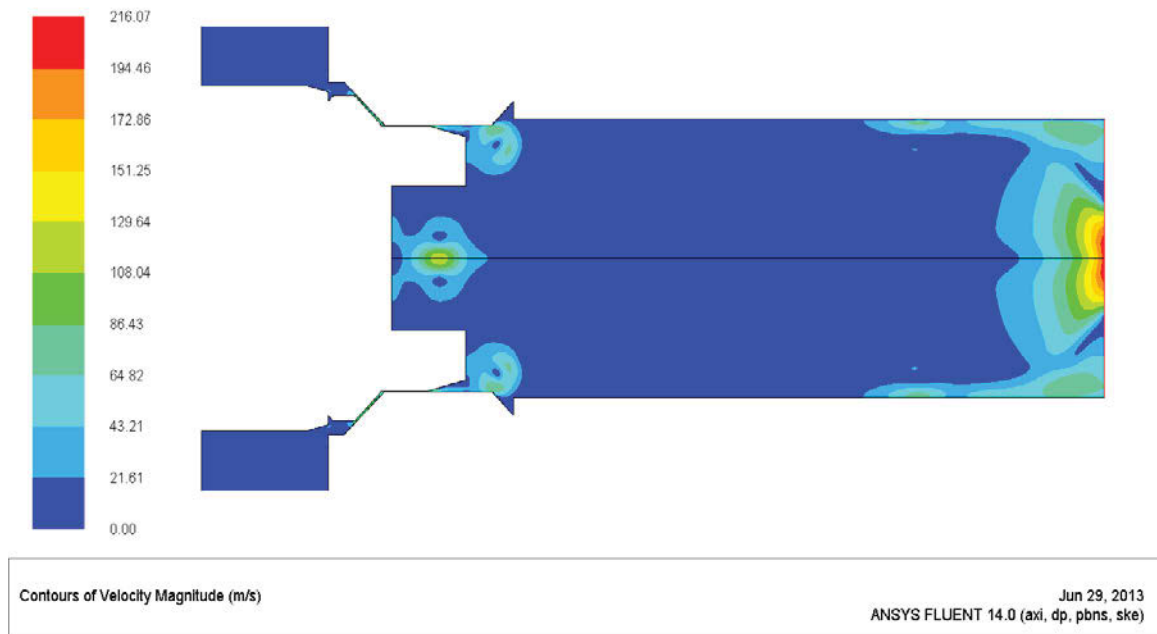
A41 Figure Velocity vector for opening 0.0125 inch side to nose

Velocity Vectors Colored By Velocity Magnitude (m/s)   Jun 29, 2013
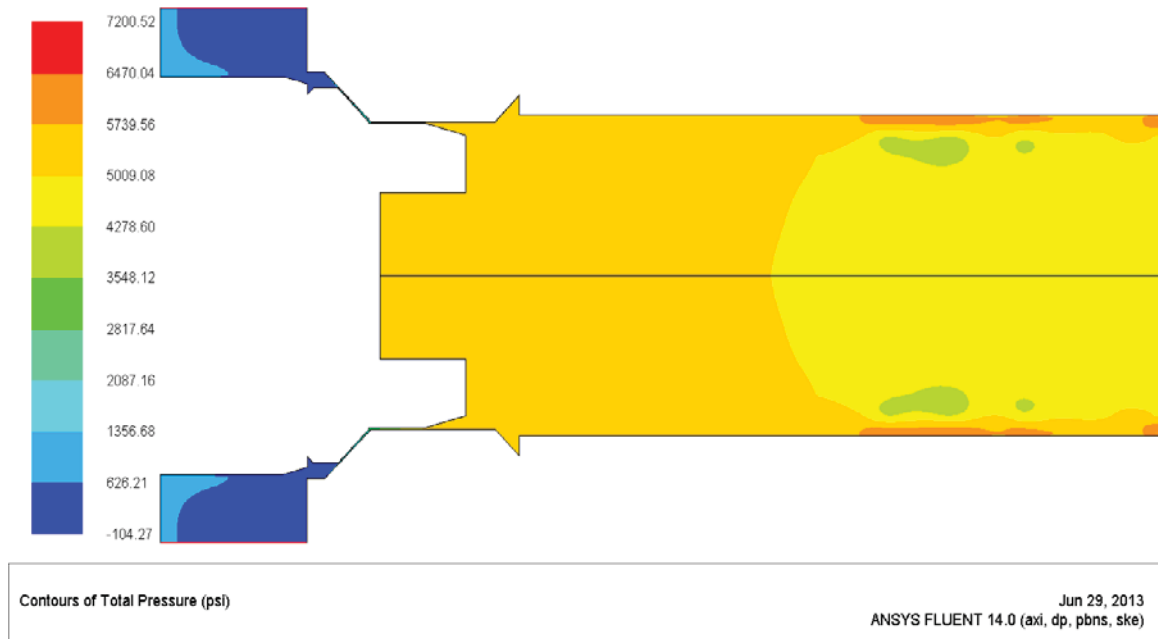   ANSYS FLUENT 14.0 (axl, dp, pbns, ske)
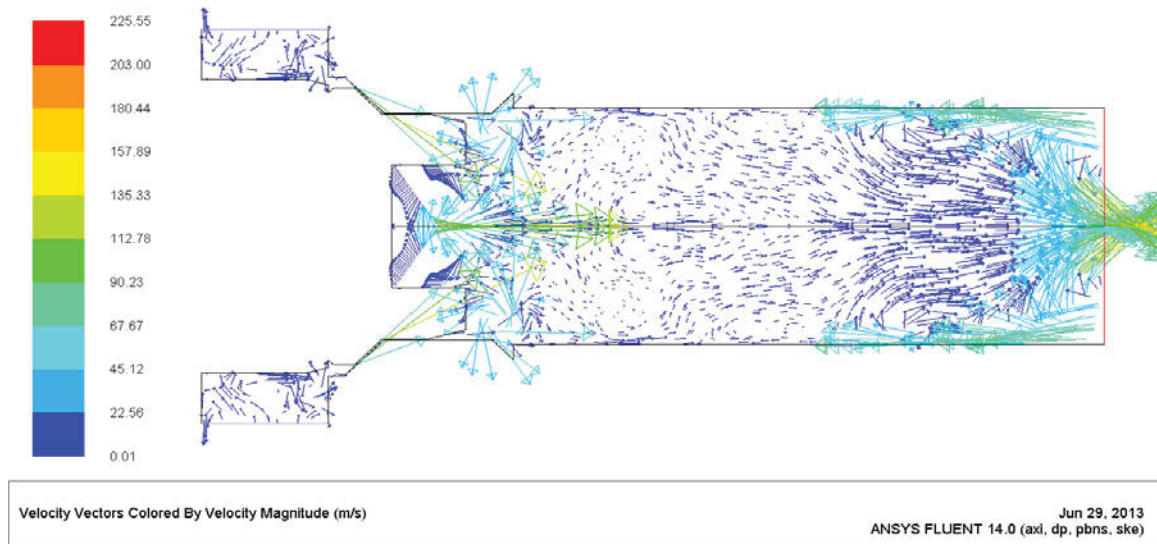
Opening 0.00625 inch

Nose to side

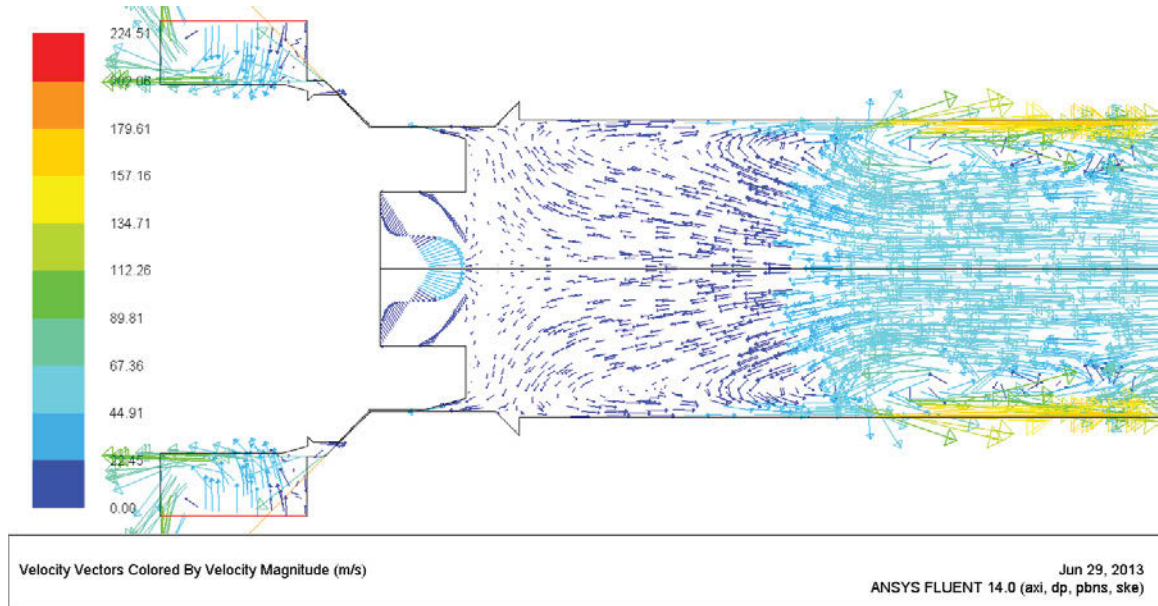A42 Figure Contours of dynamic pressure for opening 0.00625 inch nose to side
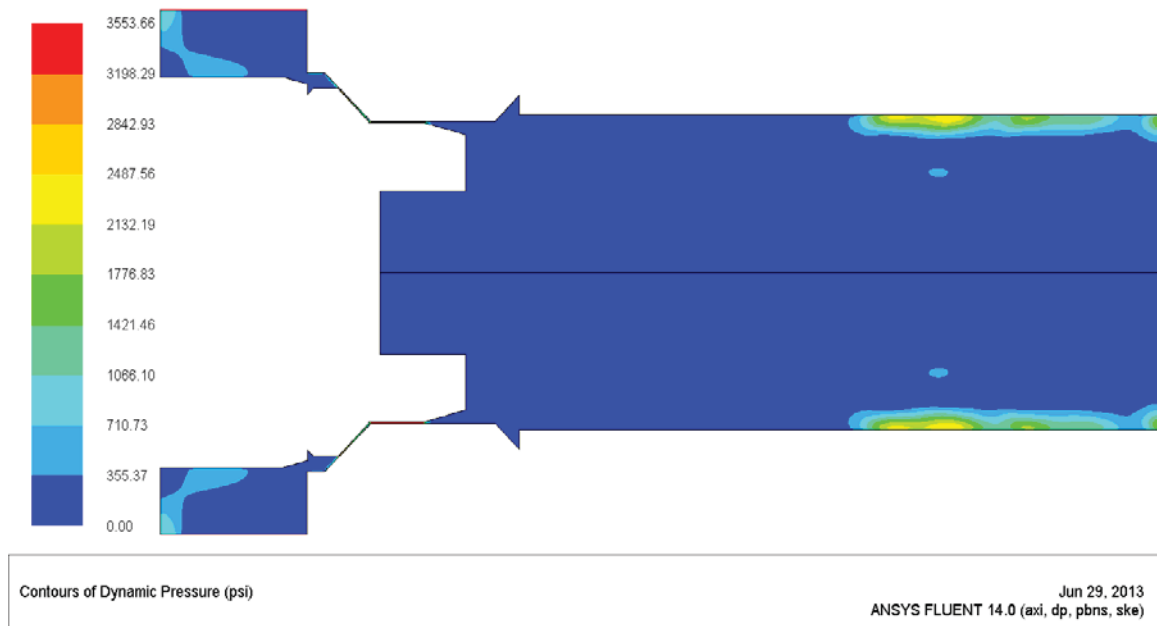
Contours of Dynamic Pressure (psi)   Jun 29, 2013
                                                                       ANSYS FLUENT 14.0 (axl, dp, pbns, ske)

A43 Figure Contours of total pressure for opening 0.00625 inch nose to side

Contours of Total Pressure (psi)

Jun 29, 2013
ANSYS FLUENT 14.0 (axi, dp, pbns, ske)

A44 Figure Contours of velocity magnitude for opening 0.00625 inch nose to side

Contours of Velocity Magnitude (m/s)

Jun 29, 2013
ANSYS FLUENT 14.0 (axi, dp, pbns, ske)
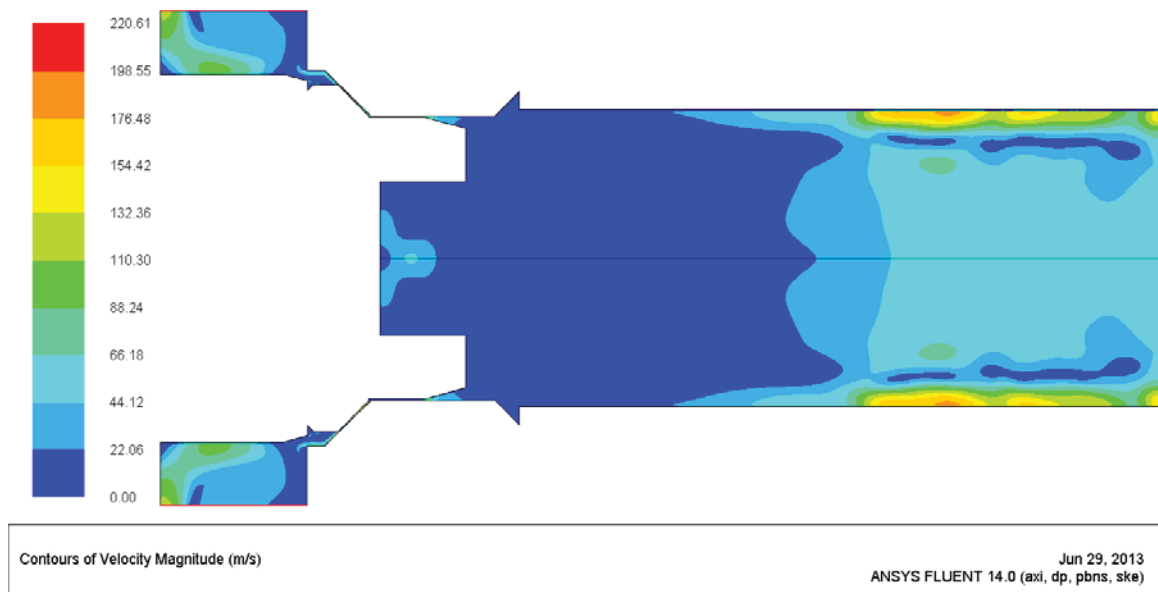
A45 Figure Velocity vectors for opening 0.00625 inch nose to side

Velocity Vectors Colored By Velocity Magnitude (m/s)

Jun 29, 2013
ANSYS FLUENT 14.0 (axi, dp, pbns, ske)

Side to Nose

A46 Figure Contours of dynamic pressure for opening 0.00625 inch side to nose
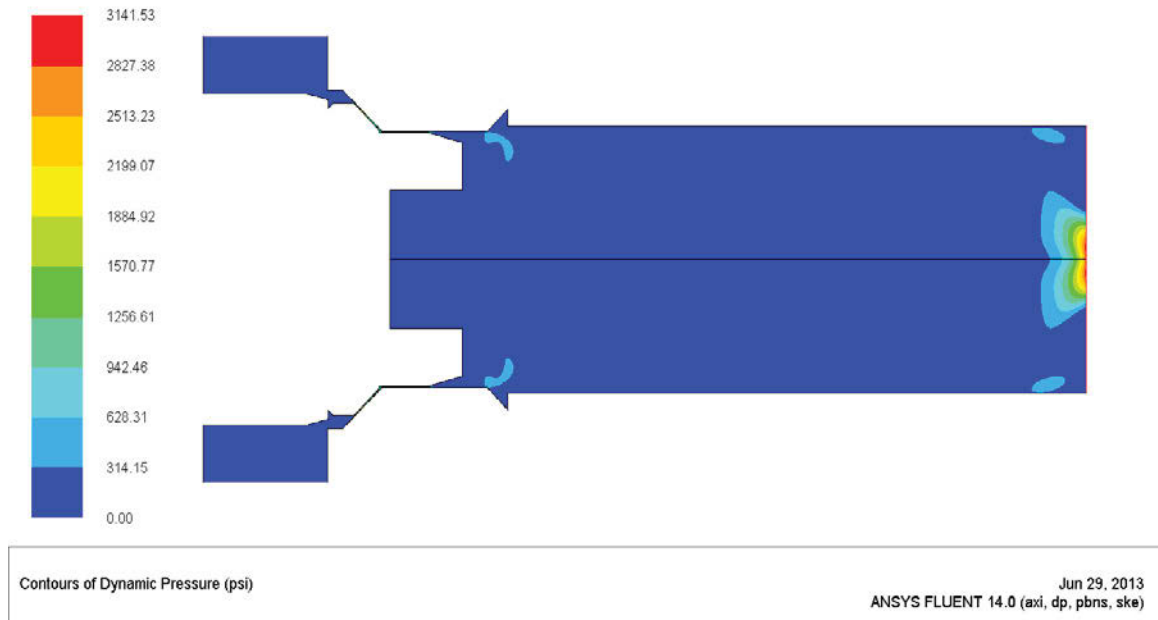
Contours of Dynamic Pressure (psi)

Jun 29, 2013
ANSYS FLUENT 14.0 (axi, dp, pbns, ske)

A47 Figure Contours of total pressure for opening 0.00625 inch side to nose

Contours of Total Pressure (psi)

Jun 29, 2013
ANSYS FLUENT 14.0 (axi, dp, pbns, ske)

A48 Figure Contours of velocity magnitude for opening 0.00625 inch side to nose
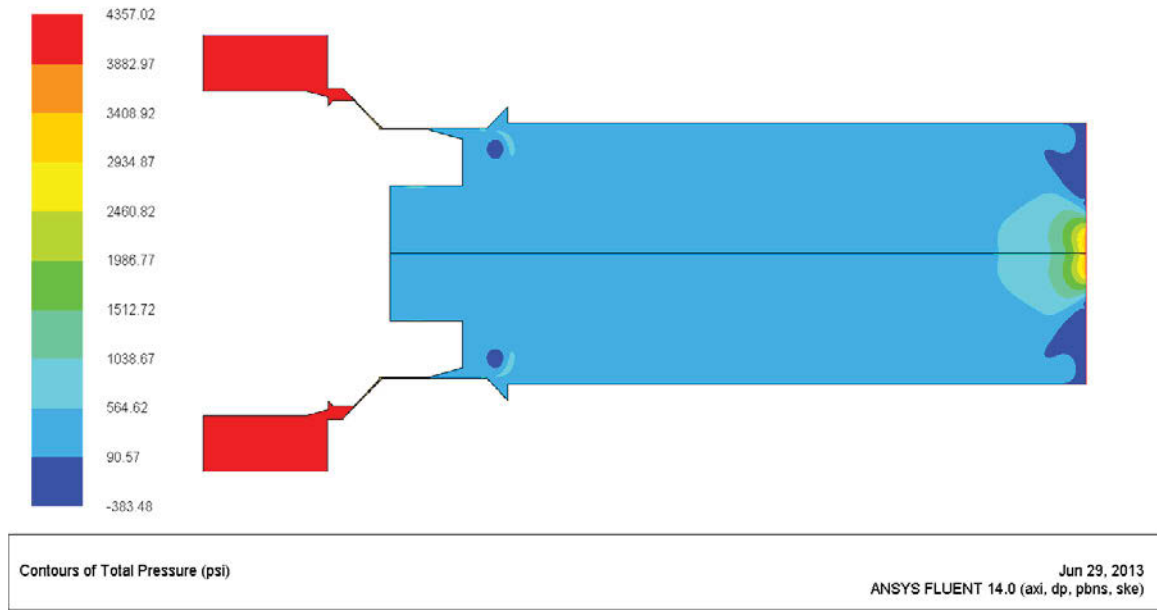
Contours of Velocity Magnitude (m/s)

Jun 29, 2013
ANSYS FLUENT 14.0 (axi, dp, pbns, ske)

A49 Figure Velocity vector for opening 0.00625 inch side to nose

Velocity Vectors Colored By Velocity Magnitude (m/s)

Jun 29, 2013
ANSYS FLUENT 14.0 (axl, dp, pbns, ske)